Development of Photonic Integrated Microchip-Based Flow Cytometers: Device Fabrication

Development of Photonic Integrated Microchip-Based Flow Cytometers: Device Fabrication

By

Thomas M. Kowpak, B.Eng

A Thesis

Submitted to the School of Graduate Studies

In Partial Fulfillment of the Requirements

for the Degree

Master of Applied Science

McMaster University

MASTER OF APPLIED SCIENCE (2009) **McMaster University**

(Chemical Engineering) **Hamilton, Ontario**

TITLE: **Development of Photonic Integrated Microchip-Based Flow Cytometers: Device Fabrication**

AUTHOR: **Thomas M. Kowpak, B.Eng (McMaster University)**

SUPERVISORS: **Professor Shiping Zhu, Professor Chang-Qing Xu, Dr. Zhiyi Zhang**

NUMBER OF PAGES: **xvii, 109**

ABSTRACT

Microchip-based flow cytometry holds promise in replacing conventional flow cytometers, thus providing less expensive point of care alternatives. Although final products are far off, a strong step towards these goals involves developing easy, reliable processes and improved functionality. This study is part of a larger project to develop a photonic integrated microchip-based flow cytometer using optical designs and simulations to imposed stringent requirements in device fabrication. Thus the goal of this work was to perform material selection, process development and device fabrication to meet the stringent optical requirements with an overview of device testing to demonstrate the achievements.

Materials needed careful selection and include an SU-8 2025 structural layer, Pyrex substrate and a polydimethylsiloxane (PDMS) sealing layer. Mismatched properties of SU-8 and Pyrex have previously provided poor bonding, namely due to surface chemistry and thermal expansion differences. To overcome this, a thin intermediate layer of polymer was introduced relaxing stresses and allowing for chemical linkages. A rough range of 186-600nm was effective and limited optical deterioration.

Sealing SU-8 devices with PDMS was previously accomplished using mechanical means or low pressure reversible bonding. Strong irreversible bonding was achieved by coating oxygen plasma treated PDMS with 3-aminopropyltrimethoxysilane (APTMS) and bonding the amino groups to residual epoxy molecules on SU-8 surfaces via polycondensation reactions. Bonding could not be broken through rigorous pressure

testing, with devices withstanding on average 0.6-0.7MPa and up to 2.2MPa before failing at the inlet fluidic connection.

Post processing procedures required a rough dicing saw compromising the SU-8 structural layer. Reversibly sealed PDMS helped reduce chipping and protect against debris. An intermediate layer thickness of 186nm was efficient and 600nm provided no further improvement.

These developed processes met the optical constraints imposed and quality devices were fabricated, capable of coupling high power light through on-chip waveguides, exciting fluorescence in microchannels and providing beam shaping.

ACKNOWLEDGEMENTS

I would like to extend great thanks to Dr. Shiping Zhu, Dr. Chang-Qing Xu and Dr. Zhiyi Zhang for their supervision of this work. They were always available to provide direction and words of encouragement whenever needed, helping keep me focused on my goal. A special thanks to Dr. Zhiyi Zhang for making time to listen, discuss and edit my work whenever needed. Thank you.

I am grateful for the help received from the staff at the National Research Council of Canada including among many others, Ping Zhao, Christophe Py, Fencheng Lin and Phil Waldron.

Thank you to Benjamin Watts for his discussions and support.

I am grateful for the financial support provided by Canadian Photonics Fabrication Research.

Thank you to my parents for their continued support and love in everything I do, consistently taking an interest and providing encouragement every step of the way. Nothing I've done would have been possible without you. I would also like to extend thanks to my sisters for their love and support.

Finally I would like to thank my fiancée, Dorothy Belina, for all her love and encouragement, helping me stay positive through thick and thin. Thank you for always being there for me, and I will happily return the favour whenever needed.

TABLE OF CONTENTS

TITLE PAGE i

DESCRIPTIVE NOTE ii

ABSTRACT iii

ACKNOWLEDGEMENTS v

TABLE OF CONTENTS vi

LIST OF FIGURES x

LIST OF TABLES xvi

1 INTRODUCTION 1

1.1 Microfluidics 1

1.1.1 Brief History 1

1.1.2 Microfluidic Technology 2

1.1.2.1 Device Fabrication Techniques 2

1.1.2.1.1 Open Microfluidic Channel Fabrication 3

1.1.2.1.2 Channel Sealing 7

1.1.2.1.3 Device Packaging 9

1.1.2.2 Microfluidic Control 10

1.1.2.3 Applications and Detection Technology 13

1.1.3 Integrated Flow Cytometry 16

1.1.3.1 Conventional Flow Cytometry 16

1.1.3.1.1 Brief History 17

1.1.3.1.2 Flow Cell 18

1.1.3.1.3 Light Source 19

1.1.3.1.4 Optics and Detection 19

1.1.3.1.5 Data Analysis 22

1.1.3.1.6 Cell Sorting 22

1.1.3.1.7 Current Flow Cytometers 23

1.1.3.2 Microchip-Based Flow Cytometry 23

1.1.3.2.1 Microchip-Based Flow Cells 24

1.1.3.2.2 Microchip-Based Light Sources 26

1.1.3.2.3 Microchip-Based Optics and Detection 27

1.2 Research Objectives 31

1.2.1 Proposal 31

1.2.2 Focus 32

1.3 Contents of Thesis 32

2 EXPERIMENTAL 34

2.1 Materials 34

2.1.1 Substrate 34

2.1.2 Waveguide and Microfluidic Channels 34

2.1.3 Channel Sealing and Device Packaging 34

2.1.4 Device Testing 35

2.2 Device Fabrication 35

2.2.1 Substrate Preparation 35

2.2.2 Waveguide and Microfluidic Channel Construction 35

2.2.3 Channel Sealing 38

2.2.4 Device Packaging 40

2.3 Device Testing 44

3 RESULTS AND DISCUSSION 46

3.1 Device Fabrication 46

3.1.1 Fabrication of Waveguides and Open Microfluidic Channels on Glass 48

3.1.1.1 Bond Improvement Through Processing Conditions 51

3.1.1.2 Bond Improvement Through Surface Modifications 55

3.1.1.3 Bond Improvements Through Stress Reduction 58

3.1.2 Device Sealing 69

3.1.2.1 Mechanism 70

3.1.2.2 Processing 73

3.1.2.3 Performance 78

3.1.3 Device Packaging 83

3.1.3.1 Dicing 83

3.1.3.2 Fluidic Connections 89

3.2 Device Performance 90

4 CONCLUSION 95

4.1 Achievements 95

4.2 Recommendations 98

5 REFERENCES **100**

LIST OF FIGURES

1.1 Main components of a flow cytometer; Flow Cell, Light Source, Optics, Detectors, Electronics [37] **17**

1.2 Emission peaks of common light sources used in flow cytometry [1] **19**

1.3 Optics for side scatter and fluorescence light collection and detection [37] **21**

1.4a Waveguide construction using the concept of total internal reflection where all light propagating at an angle from the normal above the critical angle will be totally reflected within the medium **29**

1.4b Waveguide construction showing the material requirements necessary to fabricate an integrated waveguide on a microchip-based device **29**

2.1 Fabrication of waveguides and microfluidic channels by patterning an SU-8 2025 layer on a thin SU-8 3000 intermediate layer using a one-shot process in a single layer on a Pyrex substrate **37**

2.2 Sealing of microfluidic channels and device structures using a PDMS cover layer **39**

2.3a Photomask used to create 10 devices on one 4" wafer showing guidelines used for dicing **41**

2.3b Zoomed image of a single device showing waveguides, microfluidic reservoirs and microfluidic channels **41**

2.4 Diagram of dicing procedures to expose waveguide ends for optical connections **42**

2.5 Diagram outlining the attachment of buffer layers for fluidic connections and insertion of fluidic connecting pins **43**

2.6 Optical testing setup used to couple light into waveguides and excite fluorescence within device microchannels **45**

3.1 Three main steps involved in fabricating a quality microfluidic device are; i) construction of open microfluidic channels, ii) sealing of open microfluidic channels and iii) packaging of the device **47**

3.2 Waveguides and open microfluidic channels fabricated in a single layer using a one-shot process **49**

3.3 SU-8 layer having largely peeled away from the Pyrex substrate with almost all structures deformed and destroyed using standard baking and an exposure dose of 225mJ/cm^2 **51**

3.4a SEM images of a device created using an exposure dose of 900mJ/cm^2 showing high amounts of residual material remaining between waveguides **52**

3.4b SEM image of a device created using an exposure dose of 900mJ/cm^2 showing greatly increased waveguide core width **52**

3.5 High level of cracking found throughout SU-8 layer with high baking temperature **53**

3.6a Slightly improved bonding obtained using standard processing conditions with surface modifiers of HMDS, GPTMS and Omnicoat shoing a large section of SU-8 film peeled away from the Pyrex substrate **56**

3.6b Slightly improved bonding obtained using standard processing conditions with surface modifiers of HMDS, GPTMS and Omnicoat showing a piece of the peeled away SU-8 film **56**

3.6c Slightly improved bonding obtained using standard processing conditions with surface modifiers of HMDS, GPTMS and Omnicoat showing a device with deformed microchannels and waveguide cores **56**

3.6d Slightly improved bonding obtained using standard processing conditions with surface modifiers of HMDS, GPTMS and Omnicoat showing a device with low residual material but a large air-bubble and deformed microchannel **56**

3.7 Theoretical maximum stress within the patterned SU-8 layer using different intermediate layer thicknesses over varying intermediate layer shear moduli calculated using equations 3.1 and 3.2 **60**

3.8a Cracks and dislocated waveguide cores around a microchannel with regions of debonded SU-8 in a device fabricated with an 18nm intermediate layer **63**

3.8b Waveguide cores and cladding wall region broken and pushed over top of a microchannel and lensing system, seen out of focus in the background, on a device fabricated with a 33nm intermediate layer **63**

3.9 Device fabricated with an intermediate layer thickness of 80nm showing low residual material and sufficient bonding but a high degree of cracking and stress fractures, specifically at corners **64**

3.10a Device fabricated using a 600nm intermediate layer taken with a microscope showing a horizontal microchannel intersecting vertical waveguides with low residual material, strong bonding and low cracking **65**

3.10b Device fabricated using a 600nm intermediate layer an SEM image showing a diced curved waveguide end with sharp sidewalls **65**

3.11a Simulated results showing relative power density of light at the end of a 1cm waveguide without an intermediate layer **66**

3.11b Simulated results showing relative power density of light at the end of a 1cm waveguide with a 600nm intermediate layer **66**

3.11c Simulated results showing relative power density of light at the end of a 1cm waveguide with a 3000nm intermcdiate layer **66**

3.12 Plot of simulated relative power density through a 1 cm-long waveguide on glass without an intermediate layer, with a 600nm intermediate layer and with a 3000nm intermediate layer **68**

3.13 Reaction and bonding of APTMS to surface-oxidized PDMS **71**

3.14 Confirmation of APTMS attachment to PDMS surface by XPS analysis, where the coated PDMS sample was heated to 100°C for 30 minutes and washed with ethanol **72**

3.15a Bonding of APTMS treated PDMS to residual epoxy molecules on the surface of the SU-8 layer and **73**

3.15b A bonded device using the sealing process **73**

3.16a Scratch test results of SU-8 bonded to PDMS treated with 1wt% APTMS in ethanol solution **75**

3.16b Scratch test results of SU-8 bonded to PDMS treated with 1wt% APTMS in hexane solution **75**

3.16c Scratch test results of SU-8 bonded to PDMS treated with 1wt% APTMS in toluene solution **75**

3.17 APTMS treated PDMS mold with 15 channels ranging from 20-160mm with a depth of 27mm bonded to an SU-8 layer on a Pyrex substrate to be used in pressure testing **80**

3.18a Fluorescence in device with sheath flow that hasn't been polished **84**

3.18b Fluorescence in device with sheath flow that has been polished **84**

3.19 Chipping along diced end of a device and high degree of dirt and grit covering the edge of a device that had no protection during dicing **85**

3.20 Rough PDMS after having been cut with the dicing saw with grit jammed in the side cladding channels **86**

3.21a Diced device using a reversibly bonded PDMS cover prior to cleaning **87**

3.21b Diced device using a reversibly bonded PDMS cover after cleaning **87**

3.22a Well cut low damage device with no chipping prior to the bonding of a PDMS sealing layer showing two designs on a strip cut from a 4 inch wafer taken with a camera **87**

3.22b Well cut low damage device with no chipping prior to the bonding of a PDMS sealing layer showing a side view of a waveguide end after being cut and

cleaned with low amounts of grit in the side cladding channels viewed under a microscope **87**

3.23 Cross-section of diced and sealed device showing an exposed waveguide end and cleanly cut PDMS sealing layer **88**

3.24 Excited fluorescent dye in microchannel excited with a 628nm HeNe laser coupled into the on-chip waveguide. The image is seen through a 660nm bandpass filter with the device structures having been drawn on for perspective **92**

3.25a Lens systems implemented to achieve a spot size in the middle of the microchannel of 35μm **93**

3.25b Lens systems implemented to achieve a spot size in the middle of the microchannel of 50μm **93**

3.26 Beam focusing down to about 10μm width at the centre of the microchannel **94**

LIST OF TABLES

3.1 Degree of bonding and residual material determined qualitatively and converted to percentages through inspection with the naked eye and microscope **54**

3.2 Poor improvement of bonding of SU-8 to glass utilizing HMDS, GPTMS and Omnicoat separately as surface modifiers using standard processing conditions **55**

3.3 Solutions necessary for the application of GPTMS on glass **56**

3.4 Properties of different device layers to be used in equations 1 and 2. **59**

3.5 Evaluation of different intermediate layer thicknesses based upon the amount of residual material within the developed area and the bonding of the SU-8 **62**

3.6 Average effect of solvent choice on the bonding of APTMS treated PDMS to SU-8 determined using the scratch test **76**

3.7 Average effect of APTMS/toluene weight percent concentration on the bonding of APTMS treated PDMS to SU-8 using the scratch test **76**

3.8 Average effect of drying time on the bonding of APTMS treated PDMS to SU-8, using the scratch test and 3 different concentrations of APTMS/toluene solutions **78**

3.9 Effect of water on the bonding of APTMS treated PDMS to SU-8, using the scratch test and three different concentrations of APTMS in toluene **79**

3.10 Results of pressure testing in 3 different devices with channels of varying width with the point of failure and maximum pressure reached in each case **81**

3.11 Analysis of SU-8 layer bonding during post processing procedures with intermediate layer thicknesses that provided sufficient bonding and low residual material before post processing procedures **89**

3.12 Summary of each materials use in device construction and function as well as their refractive indices. **91**

1 INTRODUCTION

1.1 Microfluidics

Microfluidics is a science dealing with the manipulation of fluids on the scale of 10^{-6} to 10^{-18} litres in microchannels with cross sections of tens to hundreds of microns in systems primarily used in chemical and biological analysis[1]. The term microfluidics is also encompassed in the terms lab-on-a-chip or micrototal analysis systems (μTAS), which encompass a larger area of devices and microtechnologies, but are sometimes used in reference to the term[2,3]. Microfluidics analysis takes advantage of its small size and microscale fluid characteristics, primarily laminar flow, to provide unique processing characteristics such as concentration and molecular control, reduced size requirements of solvents, reagents and samples, high throughput, short reaction times, portability, low cost, low power requirements, design versatility and the potential for integration with other microsized systems[1,2,4]. All of these advantages combine to provide microfluidics with the unique opportunity to revolutionize the world of analysis allowing us to take a great step towards point of care systems.

1.1.1 Brief History

The first microfluidic device fabricated for analytical purposes was a gas chromatograph able to separate a simple compound mixture in a matter of seconds. It was fabricated on a silicon wafer in 1979 by Terry et al. at Stanford University[5]. Technology such as photolithography and etching procedures were borrowed from the semiconductor industry where they were well established, and used to develop the device. Unfortunately the device did not work very well and the field of microfluidics did not

begin to take off until the early 1990's with the proposition of the idea of μTAS by Manz et al.[6]. The objective of a μTAS was to simplify the job of an analytical chemist by providing more automated systems where samples were transported via microfluid streams rather than hands. With this paper came the first few devices that initiated increased research, performing capillary electrophoresis to separate fluorescent dyes or labeled amino acids[7,8]. These devices were produced independently by the research groups of Manz (1992) and Ramsey (1994). Since then different materials and production methods have been incorporated to produce highly integrated multifunctional devices performing procedures such as immunoassays, DNA and protein separation and analysis, PCR and cell sorting and analysis[2,3,4]. Future study holds great promise for further developing these devices and integrating different components and procedures as groups work towards the production of a true μTAS system.

1.1.2 Microfluidic Technology

Today microfluidic technology has found its niche in the biomedical and chemical analysis field. Attractive benefits including small size and weight, potential for low unit cost, high reaction rates, smaller consumption of reagents and their ability to be much less invasive provides great advantages in these fields[2,9,10]. The following sections provide an overview of microfluidic technology, as it exists today.

1.1.2.1 Device Fabrication Techniques

There are traditionally three basic steps required when fabricating a microfluidic device; (i) structure and open microfluidic channel fabrication, (ii) channel sealing and (iii) device packaging. Open microfluidic channel fabrication consists of creating walls

and structures to contain and manipulate the fluid within a device. They can be fabricated using many different methods depending on the device application. Next, the channels must be sealed to protect them, their contents and other device structures from the surrounding environment, as dust particles in particular can clog microchannels. Channel sealing can be obtained using numerous methods depending on the channel materials used and device function. Finally the device requires packaging, which deals with any necessary connections to external pieces of equipment to allow the device to be fully functional. These can include fluidic or electrical connections allowing for fluid flow or sensor activity. The following sections outline the main techniques involved in each of these fabrication steps.

1.1.2.1.1 Open Microfluidic Channel Fabrication

As mentioned earlier, preliminary microfabrication methods used for microfluidics were borrowed from the semi-conductor industry, and structures were traditionally fabricated on silicon or glass substrates[2,6,11]. Structures were fabricated in clean room conditions using wet or dry etching procedures by chemical reactions or physical methods respectively. Some of the most useful dry etching methods utilized a combination of both chemical and physical methods[2,3,12,13].

Wet etching generally focused on liquid etchants to eat away at the substrate or a film on the substrate to form microchannels and other structures. Chemical etchants were generally isotropic, meaning the chemical would etch away the substrate quickly and equally in all directions as opposed to anisotropic, meaning etching would occur in only one direction, but at a much slower rate[3,12,13]. Anisotropic etching was found to be a

much more attractive and controllable method to fabricate microchannels and structures, achieved primarily through physical sputtering where energetic ions strike the wafer surface. These techniques that do not include liquid chemicals are known as dry etching, and generally employ a combination of chemical isotropic and physical anisotropic etching allowing for fast, accurate etching.

Typical dry etching technologies for fabricating microfluidic channels are plasma etching, ion milling and reactive ion etching[13]. Similar to wet etching, plasma etching utilizes a chemical reaction in gas state, creating only volatile byproducts which could be vacuumed away. However the product is isotropic and not very useful for microfluidic channel construction and more utilized in cleaning or stripping of materials[13]. Ion milling utilizes a high energy inert ion beam, such as Argon, under high pressure to physically remove material. It is a much more accurate anisotropic etching method but does cause damage extending horizontally about 100nm and these areas must be cleaned with a wet etch after[13].

Combining both physical and chemical etching methods, one can achieve high rate anisotropic etching using a method known as reactive ion etching. Charged ions bombard the material to be removed, but also react with it forming volatile compounds, providing higher selectivity and faster etching rates. Reactive ion etching has become a widely used and popular microfabrication technique[3,13]. In some cases, to effectively etch a design into the substrate a polymer resist must be spun or applied as a film over the surface and patterned, exposing only the regions to be etched and protecting the rest of the wafer.

It soon became apparent that the polymers could be used to fabricate microfluidic walls and structures themselves and were more efficient because of lower costs and ease of fabrication, while still providing acceptable chemical and mechanical properties depending on the application. Thus there was a large shift towards polymeric microfluidic devices[2,9,14]. Traditionally the three main polymer types used were thermoplastics, thermosets and an important subgroup, elastomers consisting mainly of thermoset polymers[9].

Thermoplastics are polymer chains that interact via Van der Waals forces, hydrogen bonding and dipole-dipole interactions. They can be formed, melted and reformed with small amounts of thermal degradation in each turn, making them very versatile materials. Microfluidic channel fabrication technologies using thermoplastics include injection molding, hot embossing, thermoforming and laser ablation, which take advantage of their melting properties[9]. Injection molding is one of the most widespread methods for mass polymer processing, where the polymer is heated and injected into a mold, where it is cooled and removed[9,14]. Hot embossing is another effective fabrication method utilizing a master structure that is heated and pressed onto the similarly heated polymer stamping the design into the polymer before being cooled and separated[9,14]. Thermoforming is similar to hot embossing in that it uses pressure to force the polymer over a mold, however in this case a polymer sheet is forced over a mold using compressed gas[9,14]. These methods are primarily used for mass production and not currently cost effective for research purposes. Laser ablation is a more appropriate method for the production of research microfluidic devices and may also be used with

thermoset polymers and elastomers. A high intensity laser is used in pulses to vapourize material at its focal point to create well-defined channels and structures. Designs can be easily programmed into a computer and a machine completes the process[9,14].

Thermoset polymers differ from thermoplastics by forming strong 3D-networks that cannot be melted and reformed once cured. Typical microfluidic channel fabrication technologies using thermosets include the previously discussed laser ablation and etching techniques as well as lithographic techniques[9]. In particular, photolithography is widely used in semi-conductor and microfluidic channel fabrication. Resins, known as photoresists, are dissolved in a solvent and spun onto wafers at different thicknesses depending on their viscosities and spin speeds. Evaporation of the solvent forms a solid resin film, which is activated by exposure to UV light through a photomask. Depending on the photoresist type, positive or negative, the UV light degrades the already cured polymer or initiates and cures the uncured polymer respectively in only the regions exposed to the light. Uncured polymer is then developed away and the pattern is transferred into the resist. This method can be used to directly produce microfluidic channels or to create a master mold from which numerous elastomer devices can be fabricated. Thermoset polymers generally produce a high degree of thermal stress and can be hard to process[9]. Elastomers are generally thermoset polymers that consist of long polymer chains that become physically entangled, allowing stretching of the cured material[9]. These polymers have found wide use in microfluidics due to the low cost fabrication method of soft lithography developed by George Whitesides at Harvard[15]. This method begins with the production of a negative master mold, generally a thermoset

polymer such as the negative tone epoxy photoresist SU-8, on a silicon wafer. Monomer is then mixed with the initiator and placed in the mold and left to set. When the elastomer is cured and peeled off, it contains the indentations from the master mold forming microfluidic channels and structures[15].

1.1.2.1.2 Channel Sealing

Many microfluidic applications require sealed channels and structures allowing for confined flow and protecting any structures or device surfaces. Furthermore, sealing prevents any contamination to fluids added to the system during device use. In choosing a sealing method, special care must be taken ensure the procedure does not damage the device in any away, specifically by clogging microchannels or damaging structures. Common sealing technologies include reversible adhesion or irreversible adhesion using adhesives, solvent bonding, thermal pressure bonding, laser welding and plasma bonding[9,14].

Reversible adhesion involves a cover slip, such as PDMS, that is placed on top of the channels and structures and held in place via Van der Waals forces. It is an attractive choice in the sense that it can be used with most polymers and is minimally invasive, easily avoiding any channel clogging or structure damage. However, very clean conditions must be maintained and only low channel pressures can be used. With most cases, high channel pressures are required, thus other methods must be employed[9].

The most widely used method of sealing microfluidic devices made of polymer and non-polymer materials is done using adheisves, as there are many available and they can be easily applied. Depending on the materials to be bonded and the adhesive

properties, curing occurs through solvent evaporation, UV irradiation, heat, pressure or a combination of these. This sealing method allows for higher channel pressures, but care must be taken in the adhesive application as it can easily block channels especially if they are shallow[9,16,17].

One bonding method that does not require an external material is thermal or fusion bonding traditionally with thermoplastics. In this method, materials are heated above their glass transition temperature (Tg) and brought together under pressure to provide close contact and allow for sufficient interdiffusion of the polymer chains, where they are allowed to cool providing a strong bond. The method is most effective when two materials have similar Tg's. Combinations of temperature and applied pressure must be carefully controlled as if they are too high they may melt and destroy device structures or cause the material to clog the microchannels, so a narrow range of temperature and pressure must be found[9,17]. Glass wafers can be similarly sealed, but require much higher temperatures, about 650°C, and can encounter problems with thermal stresses. These high temperatures may not be compatible with built in sensors[3].

Solvent bonding is a method similar to thermal or fusion pressure bonding and is generally used with thermoplastics, except it requires an outside solvent material, but no applied heat. A solvent is used to dissolve a thin layer of the polymer materials, which are brought into contact under pressure and intertwine across their boundaries. As the solvent evaporates, the intertwined materials harden forming a strong seal. Again, this process requires precise control and can be very difficult, as the solvent may dissolve and destroy structures or cause flow into microchannels, blocking them[9,17].

Welding of two materials is a method of sealing that does not use adhesives or mechanical forces. It can be achieved using ultrasonic energy, microwave energy or infrared laser welding. These processes induce heat at material interfaces locally melting them and causing their polymer chains to intertwine. They are not commonly employed due to a number of specific conditions for each procedure that must be met in order to allow for efficient bonding[15,17].

Surface modifications or treatments can also be used to seal microfluidic devices. The most common of these is the use of oxygen plasma, commonly used to produce silanol groups on the surface of PDMS providing strong covalent bonding between PDMS-glass and PDMS-PDMS interfaces. After exposure to oxygen plasma, there is very little time for bonding to occur before the silanol groups are replaced on the PDMS surface to the point where bonding is degraded, approximately 30-60 seconds, making alignment difficult, and the bond is not reworkable[9,17].

1.1.2.1.3 Device Packaging

Packaging a microfluidic device is the final step in creating a working device. These procedures are primarily focused on cutting the device to size and making any connections to external equipment, such as fluidic or electrical connections.

Cutting a device to size is necessary when a device is fabricated on a wafer or sheet material. This may be necessary to expose certain structures, such as waveguides, or simply to decrease the bulk of the device. Typical dicing methods employ mechanical saws, water jets or lasers. In order to ensure alignment while cutting, lines or guides should be fabricated into the device[9]. These methods can be rough and destroy films or

small structures while creating large amounts of debris, so one must be careful choosing an appropriate method and taking necessary precautions to protect the device.

Fluidic connections depend upon the type of flow to be used and range from the two most common, pressure driven and electroosmotic flow to less used centrifugal force and capillary action. Depending on the method chosen, the device may need to be hooked up to external equipment such as a syringe pump for pressure driven flow, connected to a voltage source for electroosmotic flow, or a spinner for centrifugal flow. Specific structures may need to be built into the device to accommodate this equipment, such as holes or ports necessary to connect tubing for fluid insertion[2].

Further packaging is necessary for detection purposes. An electrical connection may be necessary with wires connecting to an external chip for use with sensors such as electrochemical detectors, or an optical connection may be necessary for use with external optical fibers, photodiodes or microscopes for fluorescent detection. One must ensure the necessary ports and connections are made accessible during device fabrication so they can be easily hooked up during packaging[2].

All devices and applications have different special needs and may require some creative thinking when packaging the device in preparation for testing, so it is important to keep an open mind.

1.1.2.2 Microfluidic Control

After fluidic connections are made to insert the fluid into the microchannels, there are two main methods from which fluid flow may be generated; pressure driven flow and electroosmotic flow[2,3,4].

Pressure driven flow, or hydrodynamic flow, is generated by an applied pressure drop (ΔP Pa) across the channel and is characterized by equation 1 below, where Q (m^3/s) is the flow rate and R is the channel resistance (Pa·s /m^3)[18].

$$Q = \frac{\Delta P}{R} \tag{1.1}$$

Channel resistance is characterized by equation 2 below for rectangular channels where μ is the fluid viscosity (Pa·s), L is the channel length (m) and w and h are the width (m) and height (m) of the channel respectively for high channel aspect ratios, i.e. w<<h or h<<w[18]. (The equation for rectangular channels for medium to low aspect ratios is much more complicated and can be found in reference 18).

$$R = 12\frac{\mu L}{wh^3} \tag{1.2}$$

Channel width and height are generally on the scale of 10^{-6}m, which means the channel resistance is exceptionally large, and thus the applied pressure must be similarly high to provide acceptable flow rates, generally around 0.1MPa[2,4]. Pressure driven flow produces a parabolic flow profile that may be detrimental in certain applications, however this effect can be minimized with flow focusing by introducing a sheath flow discussed later in more detail[2,3,4].

Electroosmotic flow works by moving charged molecules within an electric field. When the channel wall is negatively charged, cations within the solution congregate close to the walls. When a voltage is applied, the cations migrate towards the negatively charged cathode dragging the bulk fluid with them, creating a sort of plug flow. Electroosmotic flow works for channel diameters ranging from a few hundred

nanometers to a few hundred of microns. The high surface to volume ratio in the channels helps to eliminate heat generated by the process and the voltage controlling the fluid flow can easily be switched on and off. However, the solution must be of appropriate pH and ionic strength to accommodate electroosmotic flow. Further drawbacks include electrolytic bubble formation and solvent evaporation due to heat generation. Electrophoretic separation occurs naturally with electroosmotic flow and may not be favourable in all applications[2,4]. Other methods of driving fluid flow in microchannels have been used in devices such as capillary action, centrifugal force and temperature gradients, but have fewer applications to this point[2,4].

Fluid flow within microchannels is unique in the sense that the small diameter of the microchannels confines the fluid to laminar flow[2,3,4,18]. This can be seen with the Reynolds number (Re) which generally needs to be greater than 2300 to allow turbulence[3,18]. The equation is seen below.

$$\mathrm{Re} = \frac{v D_h \rho}{\mu} \tag{1.3}$$

In the equation v is velocity of the fluid (m/s), D_h is the hydraulic diameter (m), dependent on the cross-sectional geometry of the channel, and ρ and μ are the fluid density (kg/m^3) and viscosity (kg/ms) respectively[18]. Assuming the fluid is water flowing within microchannels on the scale of 10^{-6}m, and for moderate flow rates on the scale of 0.01 m/s, the Reynolds number will rarely rise above 1, meaning laminar flow is observed[3,4].

Due to the constraint of laminar flow, mixing of fluids in microchannels is mainly subject to molecular diffusion, and mechanical methods must be introduced in order to speed up the process for applications such as bioassays. Examples of effective mixing focus on increasing the interfacial area to speed up the rate of diffusion. This has been done by fabricating grooves in the channel floor[4] or by flowing streams between microbeads within the channel[19].

1.1.2.3 Applications and Detection Technology

As microfluidic technology was developed, it became clear that integration of various structures, sensors and functions were key to creating a true μTAS. It is important to keep all fabrication methods and processing conditions in mind when fabricating a device, such that all integrated components can survive the processing and operate as efficiently as possible. The following provides an outline of some of the more important application and detection technological advances to date.

As mentioned earlier, the first application of a microfluidic device was gas chromatography in 1979 with a thermal conductivity detector clamped on to the silicon wafer[2,5,11]. With the moderate performance of this device, applications began to move away from gas separation systems and focused on liquid separation applications with the introduction of liquid chromatography and electrophoresis chips in the early 1990's[2,6]. Miniaturizing liquid chromatography devices had trouble overcoming the high pressures required for flow and has not seen great success to this point. That being said, they are still produced commercially by companies like Nanostream and Eksigent Technologies. Much research has focused on integrating different packing materials such as polymer

beds and sol-gels into the microchannels in an attempt to move away from pressure flow and incorporate electroosmotic flow instead. These devices have been able to provide effective microchip-based chemical analysis[2,20,21].

Microchip electrophoresis (MCE) on the other hand has been widely embraced by the microfluidics industry due to the ease of implementing electroosmotic flow providing a flat flow profile minimizing sample dispersion and improved heat dissipation. This allowed for higher voltages and faster separation times making MCE a superior method to capillary electrophoresis (CE) that worked with similar dimensions but with a much less effective platform[2,4,22]. The electrodes necessary for electroosmotic flow can be integrated into the microchip-based device by patterning and depositing metallic layers on substrates using micromachining methods and can also be used for electrochemical detection in different applications[2,3,23]. Furthermore, disposable polymer devices are being explored using materials such as PDMS, PMMA or PET, but the material properties such as thermal conductivity for heat dissipation and surface charges are ill-suited for electroosmotic flow. Surface modifications may be available to increase surface charges with some polymers. Current electrophoresis research focuses on increasing separation efficiency by increasing channel lengths or introducing sieving matrices, as well as integrating electrophoretic separation with other applications[2,4,22].

Microfluidic benefits have also been realized with chemical reaction engineering as their small size allows for high heat and mass transfer rates. Integration of sensors and detectors such as optical or temperature allows for a high degree of reaction control. Furthermore, microreactors have been shown to be safer when working with explosive

materials due to the high level of heat dissipation. Reactions such as heterocyclic synthesis, catalytic oxidation and photochemical reactions are just some of the reactions that have been explored to date. Scale up procedures provide a problem, however many devices can be set up in parallel to maintain the benefits of the micro scale while simultaneously increasing production[24,25].

One important application utilizing microreactors is the amplification of DNA using polymerase chain reaction (PCR)[2,3,26]. Microchip-based PCR has become widely successful because of decreased reaction times. Devices were outfitted with integrated heaters and temperature sensors to closely control the process within the chips microreactor[27]. Further progress has incorporated optical sensors for fluorescent detection as well as sections allowing separation using MCE of the DNA after PCR for further analysis[28].

Current optical detection primarily uses external equipment such as lasers and microscopes, but some research has focused on incorporating various optical components, such as on chip light emitting diodes (LED's) or lens systems, which will be discussed later in more detail. With the use of optical detectors for fluorescent detection, labeling of the samples is necessary, thus on chip immunoassays have become a popular application[2].

Enzyme assays and mass spectrometry has also been integrated on some devices for the analysis of protein molecules, which are more complex than DNA[2]. Devices focusing on protein digestion, separation and synthesis have taken advantage of increasing device integration and complexity[26]. Microchip-based devices for cellular

analysis was the next step up from protein analysis. Surface modifications and material selection allow for cells to be immobilized on microchannel surfaces and careful monitoring of environment conditions within the channels allowing cells to flourish[2,4]. Devices have been fabricated for studies where cells are deposited on microchannel surfaces and allowed to grow and interact mimicking tumour growth or tissue interaction[2]. Other devices have been used to mimic blood capillaries and explore cellular interactions in this environment[29,30]. One important application for cellular study using microchip-based devices is flow cytometry which will be discussed in great detail in the following sections.

1.1.3 Integrated Flow Cytometry

1.1.3.1 Conventional Flow Cytometry

Flow cytometry is the study of physical and chemical properties of cells within a fluid stream. Current instruments use the interaction of cells with light to analyze different cell properties and are able to detect and analyze between 10^5 to 10^7 cells per second[31]. Common flow cytometers consist of 4 main components as seen in figure 1.1. They are; the flow cell; the light source; the optical and detection systems consisting of lenses, filters, photodiodes and photomultiplier tubes; and the electronics used to convert the photons collected to a voltage signal sent to a computer system for analysis. Most instruments today are also equipped with sorters that allow for the collection and purification of samples for further analysis. The rapid rate of analysis, ability to sort, purify and collect cell populations for further characterization and the ability to collect multiple fluorescence signals in one pass all combine to make flow cytometers an

invaluable instrument, and they are widely used in clinical and research applications today.

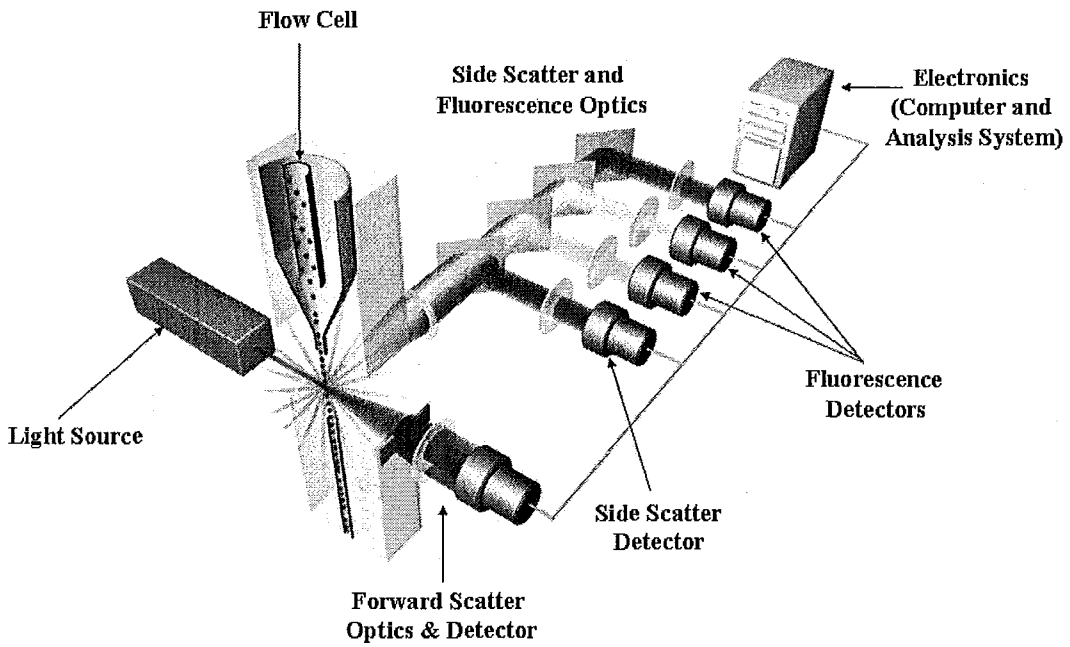

Figure 1.1: Main components of a flow cytometer; Flow Cell, Light Source, Optics and Detectors, Electronics[37]

1.1.3.1.1 Brief History

During World War II, an early flow cytometer was attempted for detecting bacteria in aerosols. The goal was to create a device to rapidly detect airborne bacteria or spores that may be used in biological warfare by employing airflow through an illuminated chamber using a Ford headlamp and an early photomultiplier tube for detection[31,32]. In 1956, Three years after the discussion of laminar sheath flow by P.J. Crossland-Taylor[33], Wallace H. Coulter contrived a device for automatic high speed

counting and analyzing of blood cells, called the Coulter Counter. He used a saline solution containing red blood cells flowing them through a 100μm orifice and exploited the property that the saline solution was a good conductor of electricity whereas the cells lipid membranes were not and measured impedance proportional to the cell volume[31,34]. Cell sorting, introduced in the mid 1960's, greatly increased the usefulness of flow cytometry by allowing for collection and further analysis of cells. In 1969, Herzenberg and his team from Stanford University developed the Fluorescence-activated cell sorter, (FACS), the first commercialized flow cytometer[31,35]. Advancements in other industries including computer technology, laser technology, optics technology and fluorescent labeling technology have also contributed to the evolution of the flow cytometer.

1.1.3.1.2 Flow Cell

The flow cell is used to transport the cells of a sample through the unit while maintaining a stable flow pattern. Flow cells generally employ a curvette, separated into two regions; the conical region and flat-sided region. A sheath stream, traditionally a saline solution or water, is injected in the conical region and the sample stream is injected in the centre. The conical region tapers to a flat-sided region of rectangular dimensions ranging from 100 by 200μm to 200 by 400μm. Trajectories and velocities of each cell are kept as constant as possible through the principle of hydrodynamic focusing, which requires laminar flow. Sheath stream diameter is controlled by the diameter of the curvette as the cross-sectional area of each flow will decrease with decreasing curvette diameter and by the initial velocity of the streams, typically pinching the sample stream to 20μm. This helps ensure a high probability of cells flowing through the system one at

a time as cell sizes roughly range from 1 to 15μm. A larger sample stream results in a higher flow rate and higher throughput of cells, however the higher the throughput, the less time each cell is illuminated resulting in a weaker collection signal, thus a balance must be found[31].

1.1.3.1.3 Light Source

Lasers are the traditional light source of choice in most flow cytometrs because they are monochromatic and easily focused. Monochromatic light allows for specific excitation peaks, thus specific fluorophores with different emission peaks can be chosen for more complex analysis. Some units have even incorporated the use of up to 4 separate lasers. The most common laser used in flow cytometrs are 15-25mW air-cooled Argon ion lasers at 488nm[31]. Figure 1.2 shows a collection of light sources commonly used in flow cytometry and their emission peaks.

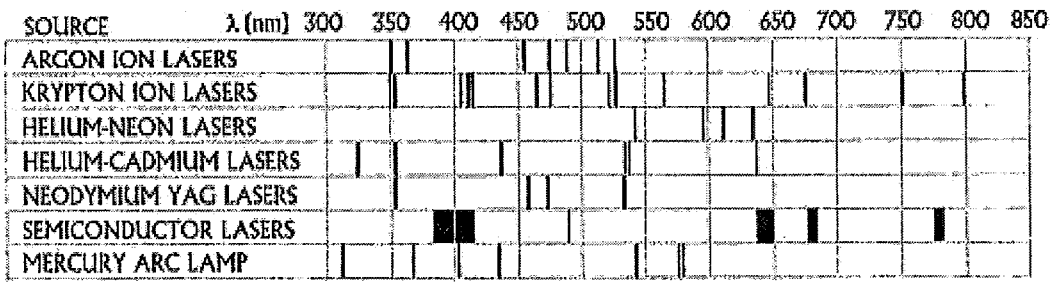

Figure 1.2: Emission peaks of common light sources used in flow cytometry[1]

1.1.3.1.4 Optics and Detection

The optics of a flow cytometer are used to focus the beam from the light source on the observation point, collect and focus forward and side scattered light as well as to

collect, filter and focus the fluorescence emissions. Many flow cytometers incorporate different methods and optical systems to achieve similar goals[31].

Forward scattered light is generated when cells pass through the incident laser beam and the light is scattered at low angles, generally 0.5-5° but can range as high as 19°. A rough estimation of cell size is provided as the larger the cell, the more light is scattered in the forward direction resulting in higher collection peaks. Forward scattered light is detected by a photodiode set up immediately in front of the incident laser beam and uses a small stopper to eliminate non-scattered incident light as seen in figure 1.3. There are numerous factors that effect forward scattered light, including the intensity and wavelength of the incident light, the optical setup of the machine, the presence of absorptive materials on cells and the difference in refractive index between the medium and the cells, thus separate calibration is required for each system[31].

Side scatter and fluorescent light is generally collected in tandem. Lenses are used to collect and collimate the light and numerous filters separate the different wavelengths. Side scattered light is sent to a photodiode and the emitted fluorescent light is sent to photomultiplier tubes because their signals are generally much weaker. A simplified set up is seen in figure 1.3.

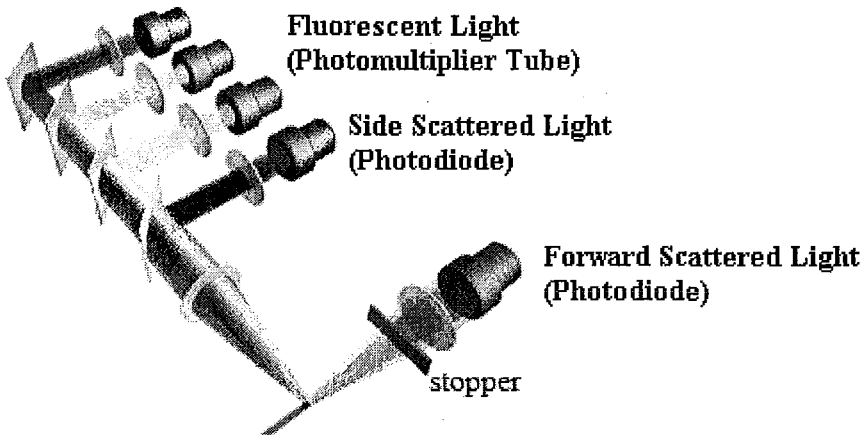

Figure 1.3: Optics for side scatter and fluorescence light collection and detection[37]

Side scatter signals are generally used to determine the granularity of a cell, or the density of matter within it, as the more matter present, the more light that is scattered. This light can be collected at angles ranging from 20° to 90° from the incident beam and it has been shown that light scattered at 20° and 90° provides the same information, irrelevant of number of scattering events per photon. The mechanism has not quite been fully explained, but it has been found useful and reproducible[31].

Fluorescence signals are used to obtain more complex information about cells, providing insight on a wide variety of structural and functional properties depending on the label used. Fluorescence detection is based upon the immunofluorescence technique, where a fluorochrome is attached to an antibody or molecule that will selectively bind to a receptor or area of interest on or within a cell. Emissions are collected and produce a signal peak, where the size of the peak is proportional to the number of fluorochromes attached to the cell, generally requiring a few thousand bound antibodies to be detected. Most machines are capable of effectively filtering and detecting four different

wavelengths of light[31], and some specialized machines can effectively filter and detect up to 12[38]. One must keep in mind that the fluorescence signals are attenuated as they pass through each filter, making light collection and optical design very important to maximize the effectiveness of the machine[31].

Many less common detection methods exist for specific applications, including polarization measurements or absorption measurements.

1.1.3.1.5 Data Analysis

As discussed, data analysis is performed by converting photons into voltage signals and generating plots. The more photons that are collected, the higher the voltage signal and thus the larger the peak recorded. Data collected by the computers is generally presented in two forms; scatter or dot plots and histograms. Traditionally graphs are two dimensional, but many also contain a third dimension. The amount of information extracted can become immense by tailoring your cytometry equipment and employing specially designed software created by yourself or external companies[31,39].

1.1.3.1.6 Cell Sorting

Cell sorting is an important tool for flow cytometers as it allows for the collection and purification of large complex cell populations for further analysis. Cell sorting requires initial cell detection, generally from forward scatter, and further characterization, from side scatter or fluorescence, by the electronic system that then determines where the cell should be sorted. There are two main types of cell sorting used in flow cytometry; charged droplet sorting and mechanical sorting. Charged droplet sorting utilizes adapted ink jet printer technology and works by uniformly breaking down the flow stream into

tiny droplets in such a manner that each droplet has a high probability of containing 1 cell. Droplets are charged and directed to the appropriate container by two deflection plates with separate charges. Mechanical sorting is less popular and harder to employ using valves to change flow paths to sort cells. Specific to ones application, these systems could be tuned to obtain high purity, but with a potential loss of some cells with non-distinct readings, or to ensure that all types of a cell are retained but at reduced purity[31].

1.1.3.1.7 Current Flow Cytometers

Current flow cytometer systems cost about $30000 for the most basic models, but more typically around $100000[36], with highly specialized machines reaching $1 million. On top of the high price tag, flow cytometers are large bench-top units that require a high degree of optical calibration that may need to be changed for each separate analysis. This optical system is generally bulky and very shock sensitive and thus needs to be kept secure. Dedicated technicians are usually required to look after the machine and perform analysis, and use of the machines can cost researchers hundreds of dollars per hour. All this results in long expensive queues, sometimes taking weeks to have ones tests completed[31].

1.1.3.2 Microchip-Based Flow Cytometry

The ultimate goal of integrated microchip-based flow cytometry is to overcome the shortcomings of conventional flow cytometers, by producing a device that is smaller, easier to handle, uses smaller sample sizes at a lower operating cost, requires less investment capital with the potential for mass production and possibly disposable

devices. To achieve these goals, a device requires a simple fabrication method preferably using as few materials as possible with all components integrated in a single plane. With this in mind, current research goals focus on shrinking the main components of conventional cytometers or developing alternative technologies that function similarly and integrating them on a single chip. Thus a basic microchip-based flow cytometer will require a microfluidic flow cell capable of focusing the sample stream to ensure single cell analysis, a light source and an optical region where light is focused to an interrogation point within the microchannel followed by collection reservoirs to retrieve the samples. Future research may also focus on incorporating an on-chip region capable of mixing sample and fluorescent labels before focusing and an on-chip region used to sort the sample for further analysis. Data analysis would require connections to a computer system, but would essentially function the same as conventional flow cytometery. The following sections will discuss technological advancements focused on the main components necessary for a microchip-based flow cytometer; the microfluidic flow cell, a short discussion on light sources and most importantly, the optical system for detection and collection[36,40].

1.1.3.2.1 Microchip-Based Flow Cells

The goals of a microfluidic flow cell is the same as a conventional cytometer flow cell; to focus the sample stream such that the velocity and location of cells is precisely known and that there is a high probability of cells flowing past the interrogation point one at a time. This ensures that all particles or cells pass the interrogation point at the same spot and speed and thus are exposed to the same intensity of light to maintain consistent

analysis[36,40]. As discussed previously, flow in microchannels is inherently laminar and generally implemented using pressure driven or electroosmotic means. In the case of microchip-based flow cytometry, pressure driven flow is more easily applied as the sample streams may not have the necessary charges for electroosmotic flow and heat generation may adversely affect sample cells[36,40].

Sample focusing was first achieved simply by manufacturing microchannels of sufficiently small sizes, typically with a 5-20μm cross sectional area[41]. However, these microchannels were designed for specific cells and could not be used for a wide variety of cell sizes. Furthermore, these systems were prone to clogging and fouling due to cell interaction with the microchannel walls[40]. The parabolic profile of pressure driven flow also contributed to velocity differences in cells or particles that could lead to inconsistent analysis[36,40]. Thus a more appropriate method of sample focusing must be found.

Using the sheath flow principle described above, sample streams have been two-dimensionally (2D) focused to minimize the problems associated with small channel particle focusing. To employ this technology, three microchannels converge to form a single microchannel, with the sample stream in the middle of two sheath fluids, pinching the sample stream into a vertical plane[42,43]. The thickness of this focused stream can be controlled as in conventional flow cytometry by varying the velocities of the three inlet streams but is also affected by channel dimensions[44]. This 2D focusing minimized sample interaction with the microchannel walls greatly reducing fouling and channel clogging as well as reducing the size of the parabolic profile, helping maintain a consistent cell velocity within the channel. 2D focusing can easily be implemented in a

single plane and is the most common method of sample focusing currently used in research applications today. However, the particle location within the vertical plane cannot be controlled, and some variation still exists. This variation must be eliminated if microchip-based flow cytometry is going to match the efficiency of conventional cytometers[36,40].

Three-dimensional (3D) focusing is the ultimate goal in microfluidic flow cell technology, and necessary for more complicated flow cytometer systems. This would completely eliminate sample interaction with microchannel walls and allow for the precise control of cell or particle velocity and location within the microchannel allowing for consistent analysis. 3D focusing has been implemented using complicated 3D microfabrication techniques that are very difficult to implement and do not lend effectively to the goals discussed above[45,46]. More recently, a novel method for 3D focusing has been implemented hydrodynamically in an easily fabricated single plane that is much more accommodating for mass production[47]. However the current planar design remains complicated and requires further research into material construction to allow for integration with other microchip-based systems.

1.1.3.2.2 Microchip-based Light Sources

Most research in microchip-based flow cytometry currently employs the same external lasers as those used in conventional flow cytometry. Light is coupled into devices using lenses or optical fibers and focused within the microchannels. A few works have experimented with generating on-chip lasers using small light-emitting diodes and dye lasers, but the technology requires further refinement before the powers

achieved can match external sources. On-chip lasers with a high enough intensity to provide a sufficiently high signal to noise (S/N) ratio would be a great step towards a fully integrated device[36,40,48,49].

1.1.3.2.3 Microchip-based Optics and Detection

Free space optics traditionally incorporated in flow cytometer systems are bulky, expensive and require precise calibration to operate correctly. In order to fully realize a small, inexpensive, easily operable microchip-based flow cytometer, the free space optics must be replaced. Ideally the optical system should be able to be integrated on-chip in the same plan with as much of it as possible fabricated directly with the microfluidic system. The main difficulty in switching away from free space optics is being able to collect enough light such that a sufficiently high signal to noise (S/N) ratio could be obtained in order to distinguish the signal from the background noise. This is especially true when working with fluorescence signals[36,40]. Because of this many researchers currently working with microchip-based flow cytometers continue to use the free space optical systems to test integrated features using microfluidic channels[45,47,50,51,52]. One way to replace these bulk optical systems in microchip-based devices was with the use of optical fibers, a method that was even considered with conventional flow cytometers[31,53]. Optical fibers were first used to transport light from laser sources directly to the interrogation point eliminating the free space optics traditionally used for this function but sacrificed the degree to which light was focused within the channel. Many of these devices continued to use free space optics for detection purposes as well. It was shown that signals could be detected, but the devices did not operate as well as

conventional units[54,55,56]. Further elimination of the free space optical systems on microchip-based devices came by replacing the collection optics with optical fibers as well. Again it was demonstrated that detection with sufficiently high S/N ratios was possible but still not comparable to the capabilities of conventional flow cytometers[57,58,59,60]. Methods used to integrate these optical fibers include clamping the fibers in place before molding a polymer directly over top of them[61], or more successfully by fabricating a groove in the microchannel plane and inserting the optical fiber after curing of the device and using an adhesive to bond it in place[58]. Microchip-based devices using optical fibers, although a great improvement from free space optics, can be bulky especially with smaller devices and do not lend well to more complicated microsystem designs with multiple detection sources. They also require alignment steps that can become complicated, as well as additional procedures to bond them in place. Furthermore the fibers are of specific dimensions and thus place design constraints on the devices, requiring microchannel walls to be of specific height or requiring extra processing steps[36,40].

A more practical method of eliminating the bulky free space optical systems while maintaining ease of fabrication in microchip-based devices has been to fabricate waveguides directly on-chip in the same plane as the microfluidic channels. Waveguides operate via total internal reflection, where light propagating above the critical angle (θ_c) from the normal, determined by the refractive index of the core material (n_1) and the cladding material (n_2) will totally reflect within the waveguide core instead of refracting from one medium to another as seen in figure 1.4 (a). The critical angle is determined

using equation 1.1 below, where n_1 must be greater than n_2, or the equation is undefined[62].

$$\theta_c = \arcsin\left(\frac{n_2}{n_1}\right) \tag{1.4}$$

Thus waveguides require the refractive index of the waveguide core to be greater than that of the surrounding cladding material, which can be different, as seen in figure 1.4 (b), requiring careful selection. The closer the cladding index matches the core index, the more specific the waveguide is, only propagating light that is coupled almost directly into it. However a bigger index difference means more photons may be collected by the waveguide providing a better S/N ratio. Thus a balance must be found such that as many photons as possible are collected while ensuring outside non-scattered light collection is limited.

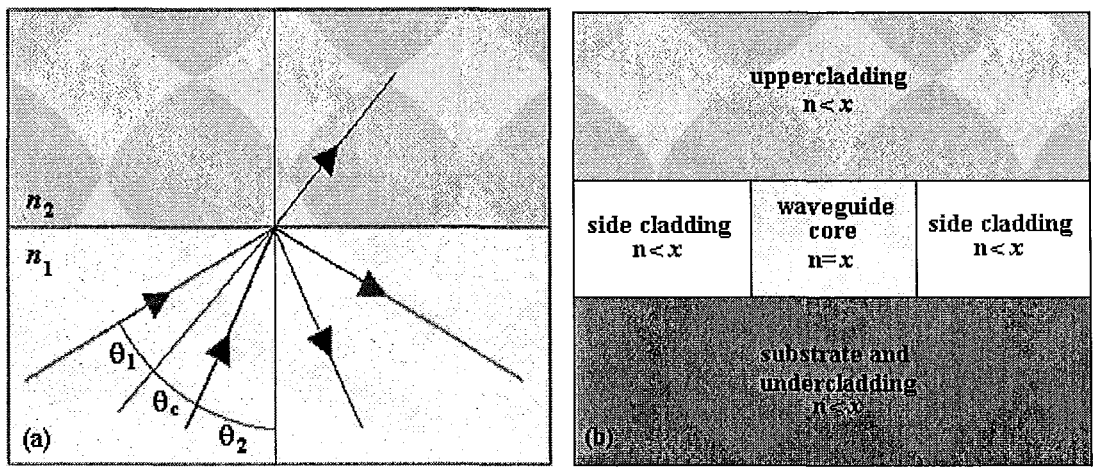

Figure 1.4: Waveguide construction (a) using the concept of total internal reflection, where all light propagating at an angle from the normal above the critical angle will be totally reflected within the medium and (b) showing the material requirements necessary to fabricate an integrated waveguide on a microchip-based device

These waveguides can be tailored to the size of the microchannels for the best possible channel illumination and allowing for easy fabrication and integration of complex detection and microfluidic systems[36,40]. However, as just discussed, the waveguide use imposes a number of restrictions on materials selection for effective total internal reflection. Many devices incorporate waveguides by fabricating channels within the structural layer that can be filled with a separate waveguide core material, generally a polymer such as PDMS or a UV curable adhesive[40,63]. Other groups have also looked at creating liquid core waveguides that allow for changing of the core material and cleaning[64,65]. The process can be further simplified by fabricating all device structures, including microfluidic channels and waveguide cores, out of a single material[66,67]. This has been most successfully implemented using the photoresist SU-8 and photolithography[66]. To date SU-8 provides the most feasible method to fabricate a simple microchip-based flow cytometer for optical detection, as the structural and optical components can be created using a single exposure step in a single plane.

Eliminating the expensive and bulky free space optical systems when shrinking to microchip-based flow cytometers is absolutely necessary to bring the technology to the masses, but current research faces many roadblocks. To date processing has been unable to produce quality microchip-based devices capable of achieving the high signal to noise (S/N) ratio of conventional flow cytometers and is far from practical use, primarily due to the small areas from which scattered or fluoresced light can be collected. Some research has focused on incorporating lensing systems to help focus light at the interrogation point increasing the number of photons interacting with particles or cells to help increase the

S/N ratio[55,59,68]. However, such lensing systems are essentially useless without effective integrated waveguide systems. Furthermore, current microchip-based devices are unable to collect multiple signals, as most research focuses on single detection, collecting only fluorescence or scattering signals. Achieving high S/N ratios with multi-detection capabilities using a simple fabrication process to integrate the necessary components of a microchip-based flow cytometer into a single layered device results in many restrictions to material selection and processing. Most important of these issues are poor material compatibility resulting in poor bonding of substrates, structural layers and sealing layers, making reproducible device fabrication very difficult. To eliminate the above-mentioned shortcomings, careful material selection and better device production quality must be imposed such that devices can be easily, quickly and reproducibly fabricated.

1.2 Research Objectives

1.2.1 Proposal

The objective of this research is to design, fabricate and test a planar photonic integrated microchip-based flow cytometer on a chip using one shot processing of the structural layer. Integrated waveguides and lens systems will be capable of propagating and focusing light at the interrogation point where the integrated optics intersect the microfluidic channel, and additional waveguides will collect both fluorescent and scattering signals of labeled particles. Design of these components will be completed and implemented in a simple fabrication procedure to achieve an inexpensive compact device requiring no optical alignment.

1.2.2 Focus

The project will be completed in collaboration with Benjamin Watts who shall focus on the optical design, simulation and testing of the fabricated quality devices. Material selection, process development and device fabrication will be the main focus of this thesis, with an overview of device testing to demonstrate the achievement of the fabrication goals. All materials will be carefully selected based upon the requirements generated by the optical design goals and simulations, ensuring efficient optical performance while maintaining strong and robust structural components. Process development and device fabrication will be performed in tandem to ensure a simple process capable of integrating all designed components including waveguide structures, lensing systems and microfluidic channels. Final devices will be compact and durable so that they may undergo rigorous testing to demonstrate their ability to produce fluorescent and scattering signals as well as demonstrate signal collection.

1.3 Contents of Thesis

This thesis contains 4 chapters; an introduction, experimental section, results and discussion and a conclusion chapter. Chapter 1 introduces the field of microfluidics with a brief history and an overview of the fabrication and governing technologies as well as current applications. This will be followed by an overview of flow cytometry and a detailed discussion on converting this technology to microchip-based devices. Chapter 2 outlines the processes and experimental design followed in this work along with the chemicals and equipment used. Chapter 3 presents the experimental work performed in the fabrication of a quality photonic integrated microchip-based flow cytometer and

discusses the results obtained. Finally chapter 4 summarizes the conclusions of the work presented and discusses future recommendations on the direction of the technology.

2 EXPERIMENTAL

2.1 Materials

2.1.1 Substrate

Pyrex 7740 4" wafers from University Wafers were the substrates used for the quality integrated photonic microchip-based devices fabricated and tested. Four-inch silicon wafers from University Wafers were used for master molds for replica PDMS covers as well as for process testing of the PDMS to SU-8 bonding. Substrates were pretreated in a piranha etch consisting of sulfuric acid (H_2SO_4) and hydrogen peroxide (H_2O_2) purchased from Sigma Aldrich.

2.1.2 Waveguide and Microfluidic Channels

Waveguides, microfluidic channels and structures were fabricated from the photoepoxy SU-8 2025, developed using SU-8 developer (propylene glycol monomethyl ether acetate, or PGMEA) from Microchem Corporation, and rinsed with isopropyl alcohol from Sigma Aldrich. Surface treatment materials included hexamethyldisilizane (HMDS) and 3-glycidoxypropyltrimethoxysilane (GPTMS) from Sigma Aldrich and Omnicoat from Microchem Corporation. Tests involving intermediate layers used SU-8 3000 from Microchem Corporation.

2.1.3 Channel Sealing and Device Packaging

All materials used to seal the device were purchased from Sigma Aldrich. They include the following; PDMS monomer and initiator, 3-aminopropyltrimethoxysilane (APTMS) and anhydrous toluene. PDMS buffer pieces to reinforce fluidic connecting

pins were glued to the PDMS covers using Loctite, silicon adhesive sealant from Henkel Loctite Corp. Rockliffe Connecticut.

2.1.4 Device Testing

Fluorescent dye for device testing was Nile Blue 690 Perchlorate purchased from Exciton Inc. Dayton, Ohio, and fluorescent micro-beads for device testing were 7-9μm polymer beads labeled with Far-Out Red Reference Standard purchased from Bangs Laboratories Inc., Fishers, Indiana.

2.2 Device Fabrication

2.2.1 Substrate Preparation

Substrate preparation was performed in cleanroom conditions. Using a wet bench, substrates were subjected to a piranha etch of H_2SO_4:H_2O_2 in a 4:1 ratio for 2 hours at room temperature to remove any organic material. Deionized water was used to rinse the wafers, which were then left to air dry. Next the wafers were baked on a hotplate at 265°C for 3 hours to remove any residual water molecules. The wafers were removed from the hotplate and left to cool for 30 seconds to a minute before SU-8 processing was continued.

2.2.2 Waveguide and Microfluidic Channel Construction

All fabrication procedures were carried out in cleanroom conditions. A summary of the overall process can be seen in figure 2.1 on page 37. SU-8 2025 was poured upon the treated wafers and spun using a Model WS-400A-6NPP/LITE from Laurell Tehnologies Corporation in a slow stepwise process to obtain a uniform film of 27μm. Soft baking took place on a hot plate to ensure solvent was evaporated from the bottom

up to provide a firm film that would not stick to the glass mask during exposure. The wafers were heated to 65°C and 95°C and held for 1 and 3 minutes respectively followed by a natural cooldown in air to room temperature. Exposure to UV light through a glass photomask from HTA Photomask, San Jose, California using an ABM High Performance Mask Aligner and Exposure System from ABM Inc., San Jose, California, with an I-line filter was performed to initiate crosslinking in the exposed regions of the SU-8. A dose of 150mJ/cm^2 was initially used and a range up to 900mJ/cm^2 was implemented for quality improvement. Post baking was performed at 65°C and 95°C for 2 and 5 minutes respectively followed by a natural cooldown in air to room temperature. Wafers were developed in SU-8 developer with agitation for 5 to 7 minutes to remove all unexposed material followed by a rinse in isopropyl alcohol and dried using a nitrogen gun.

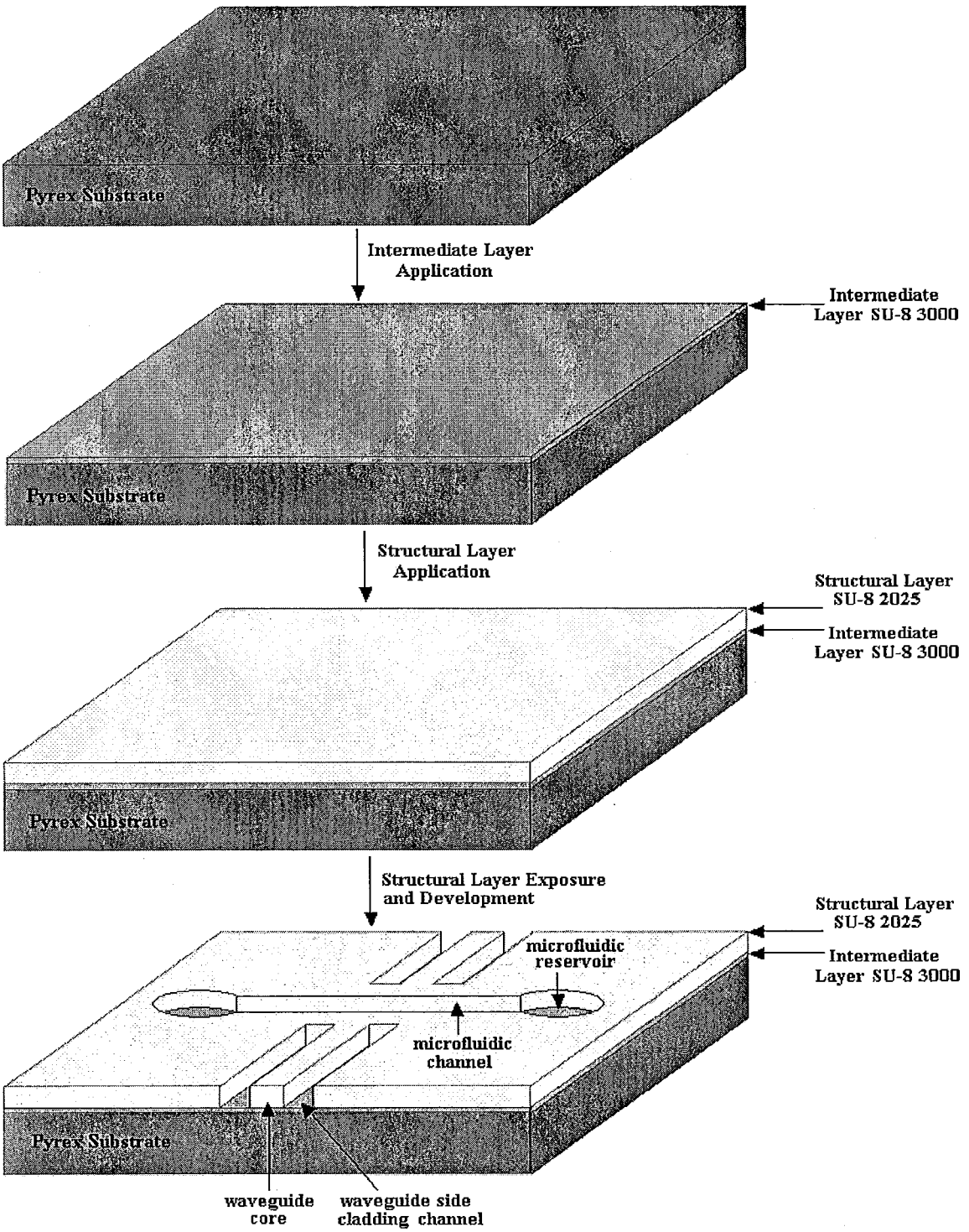

Figure 2.1: Fabrication of waveguides and microfluidic channels by patterning an SU-8 2025 layer on a thin SU-8 3000 intermediate layer using a one-shot process in a single layer on a Pyrex substrate

2.2.3 Channel Sealing

All sealing procedures were performed in cleanroom conditions. A summary of the channel sealing can be seen in figure 2.2 on the next page. Master molds were created by fabricating SU-8 on silicon wafers instead of Pyrex in the same manner as above except that the wafers were subjected to an addition hard bake on a hotplate at 100°C for 1 hour. Heptane was used to coat the SU-8 and wafer to facilitate easy removal of PDMS replicas. A metal ring was placed around the master to create a reservoir to hold the PDMS replica. PDMS monomer and initiator were combined in a 10:1 ratio and mixed for 5 minutes, poured into the master mold, covered and left overnight to ensure all air bubbles escaped. Baking at 100°C for 1 hour fully cured the PDMS which was left to cool naturally to room temperature before being removed from the mold using a scalpel then cut to the appropriate device size. The PDMS covers were placed bonding side up in Extended Plasma Cleaner/Sterilizer 110V from Harrick Plasma Inc., Ithaca, New York, and exposed for 10 seconds at 600mTorr before being removed. It should be noted that these conditions vary depending on the machine and should be optimized separately. In this case, PDMS was exposed to oxygen plasma at pressures ranging from 50-2000 mTorr for times ranging from 5-180 seconds and placed directly on glass microscope slides. The samples were then heated to 100°C for 30 minutes, cooled natrually and the degree of bonding determined. The bonding side of the PDMS covers was immediately coated with an APTMS/toluene solution, created by adding APTMS drop wise to anhydrous toluene to create the appropriate weight percent concentration, ensuring the entire surface was covered before immediate drying in an air

stream. Cover slips were then left briefly to allow the toluene solvent to evaporate from the swollen PDMS allowing it to return to its natural shape before being aligned and placed on the SU-8 surface. The covered device was then baked at 100°C for 1 hour and left to cool naturally.

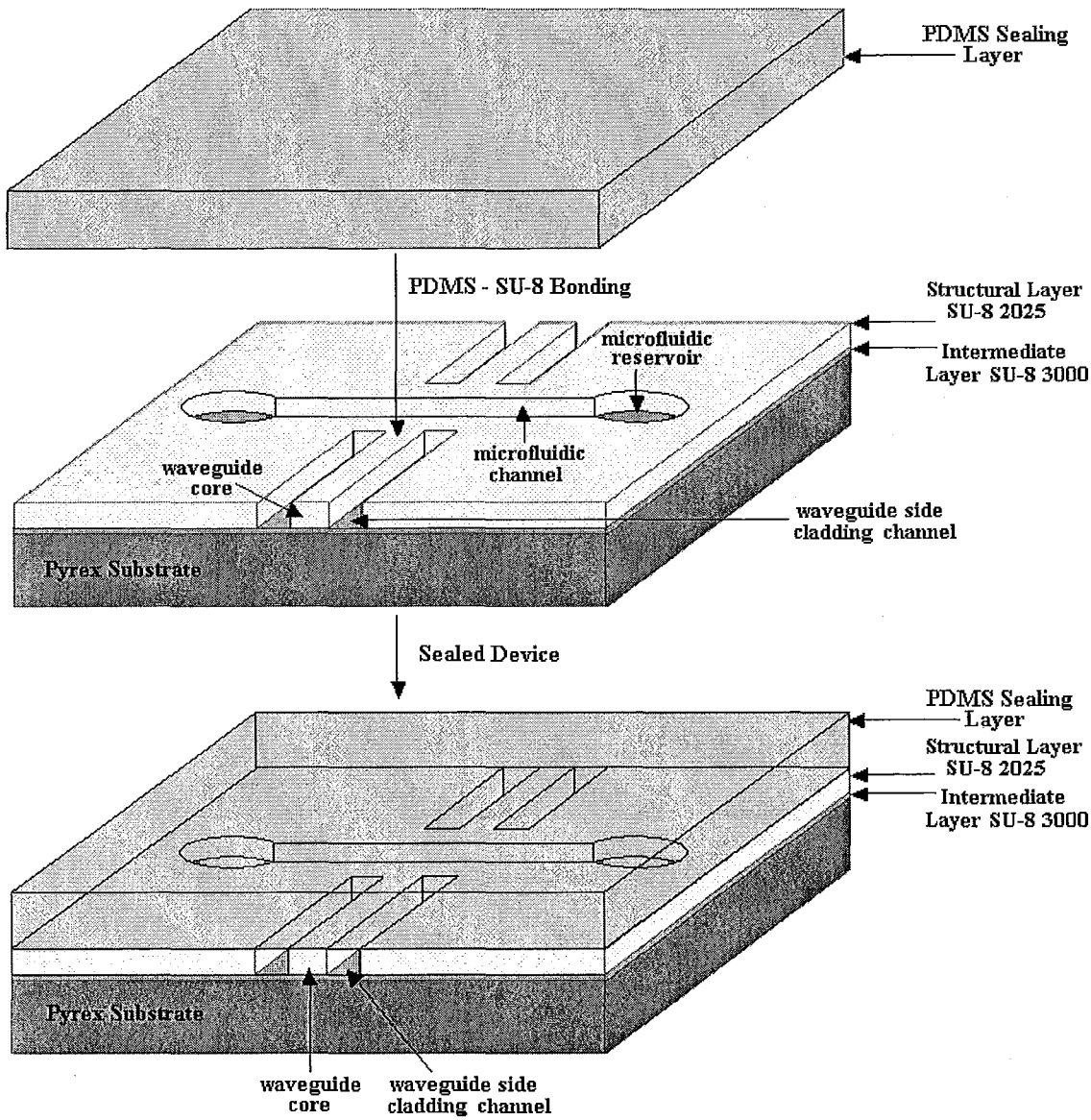

Figure 2.2: Sealing of microfluidic channels and device structures using a PDMS cover layer

2.2.4 Device Packaging

After the SU-8 had been patterned and cured on the wafers, devices were cut to size using a Precision Dicing System made by Kulicke & Soffa, Model 780 with a 1mm thick PDMS layer placed on top with reversible bonding to help protect the SU-8 layer from chipping and dirt. Figure 2(a) shows the photomask used in the exposure step and the dicing guidelines used to cut the devices to size and figure 2(b) shows how the waveguide ends would be exposed as the dicing occurs right next to the waveguide end. Figure 2.4 further demonstrates this showing the removal of diced pieces from a single uncovered device. Diced devices were cleaned using deionized water and ethanol to remove as much grit and particles as possible. Waveguide ends were then inspected and polished using aluminum oxide polishing discs with 1μm grit then 0.3μm grit from Buehler, Lake Bluff Illinois. Before the PDMS cover layer for irreversible sealing was applied as described above, 1mm thick buffer pieces of PDMS were attached to the cover using a silicon adhesive to reinforce the device for fluidic connection. After the adhesive was cured, holes were punched through the PDMS layer using a cut and sharpened syringe tip similar to the size of the fluidic connecting pins. After device sealing, the connecting pins were inserted into the punched holes and connected to rubber tubes attached to a Harvard Apparatus syringe pump, Pump 33, Holliston, Massachusetts. The fluidic connection packaging is outlined in figure 2.5.

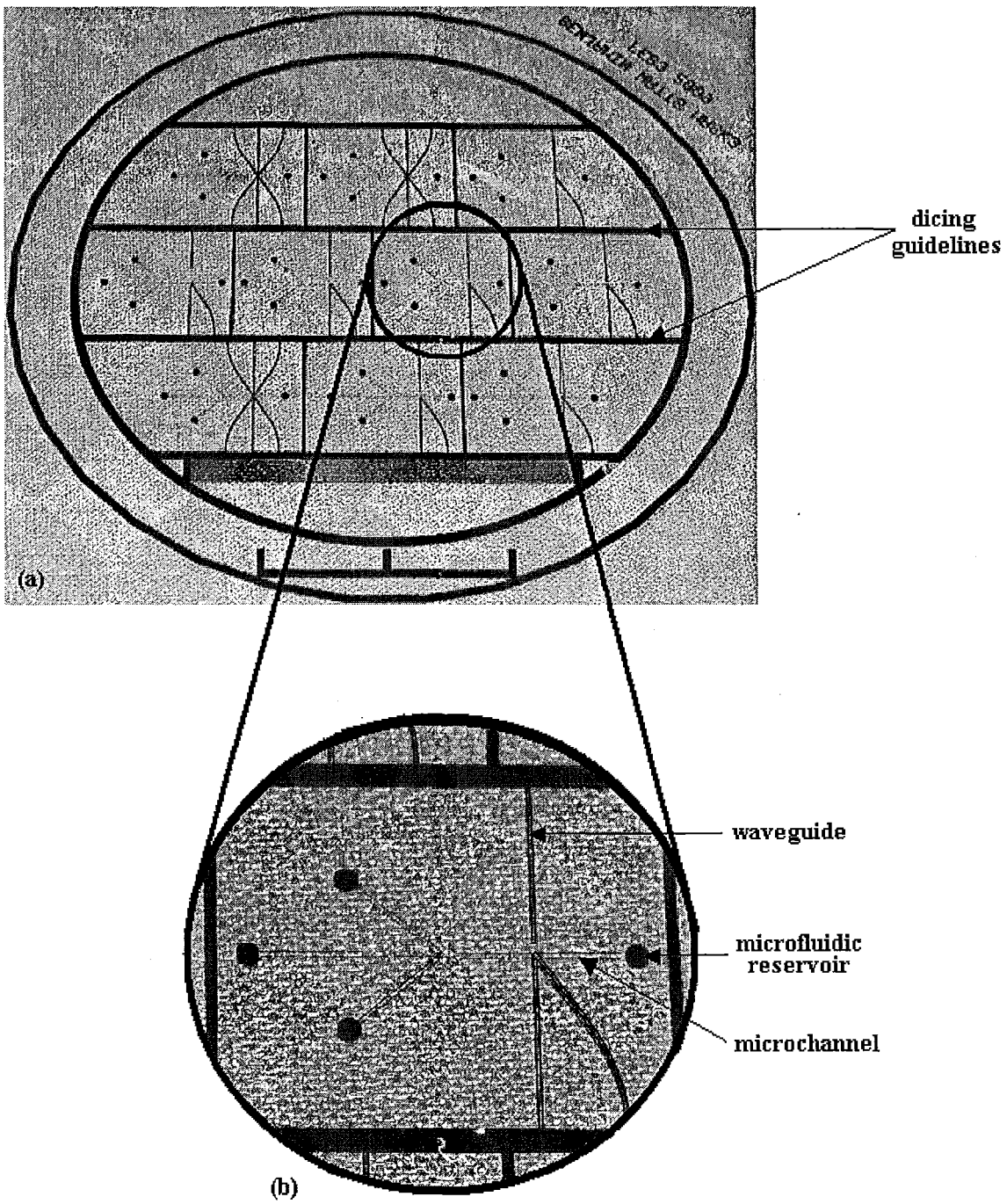

Figure 2.3: (a) photomask used to create 10 devices on one 4" wafer showing guidelines used for dicing and (b) zoomed image of a single device showing waveguides, microfluidic reservoirs and microfluidic channels

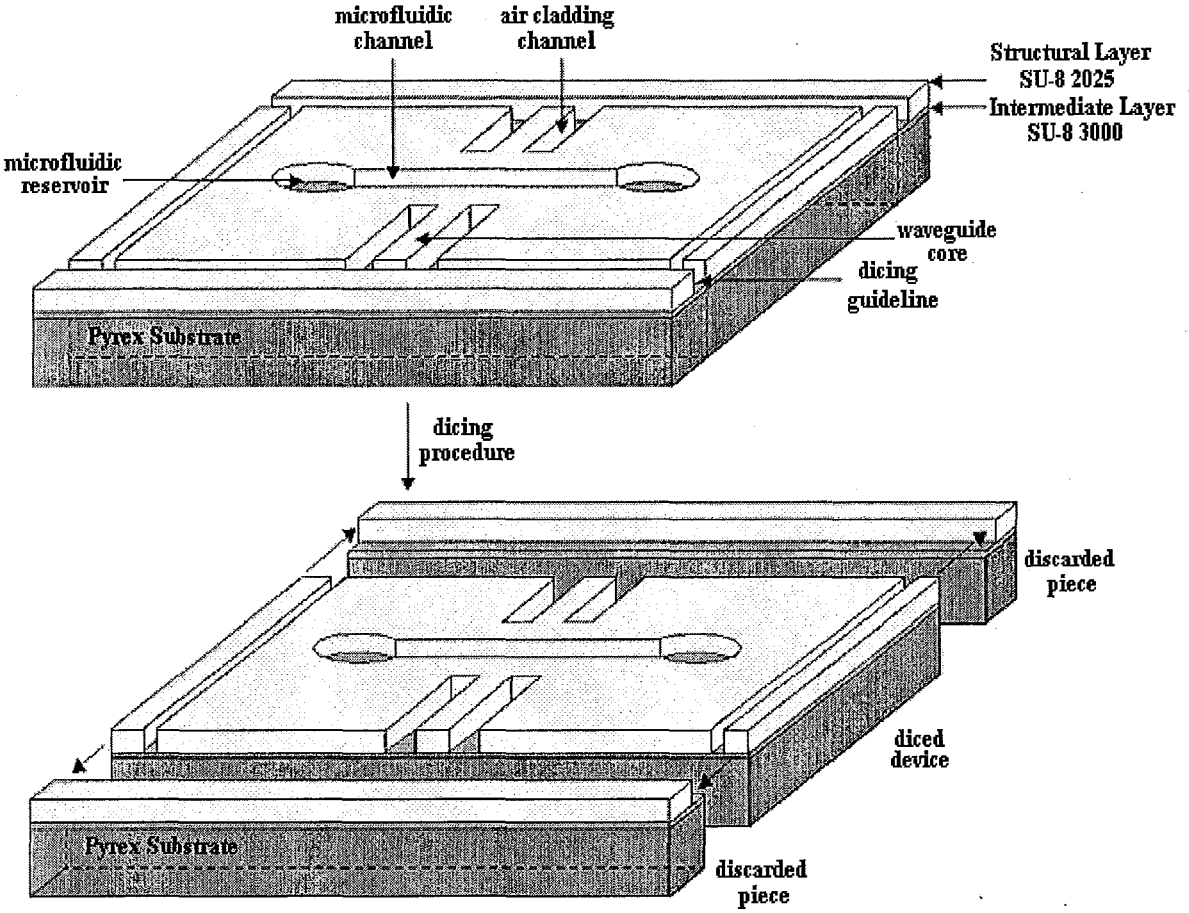

Figure 2.4: Diagram of dicing procedures to expose waveguide ends for optical connections

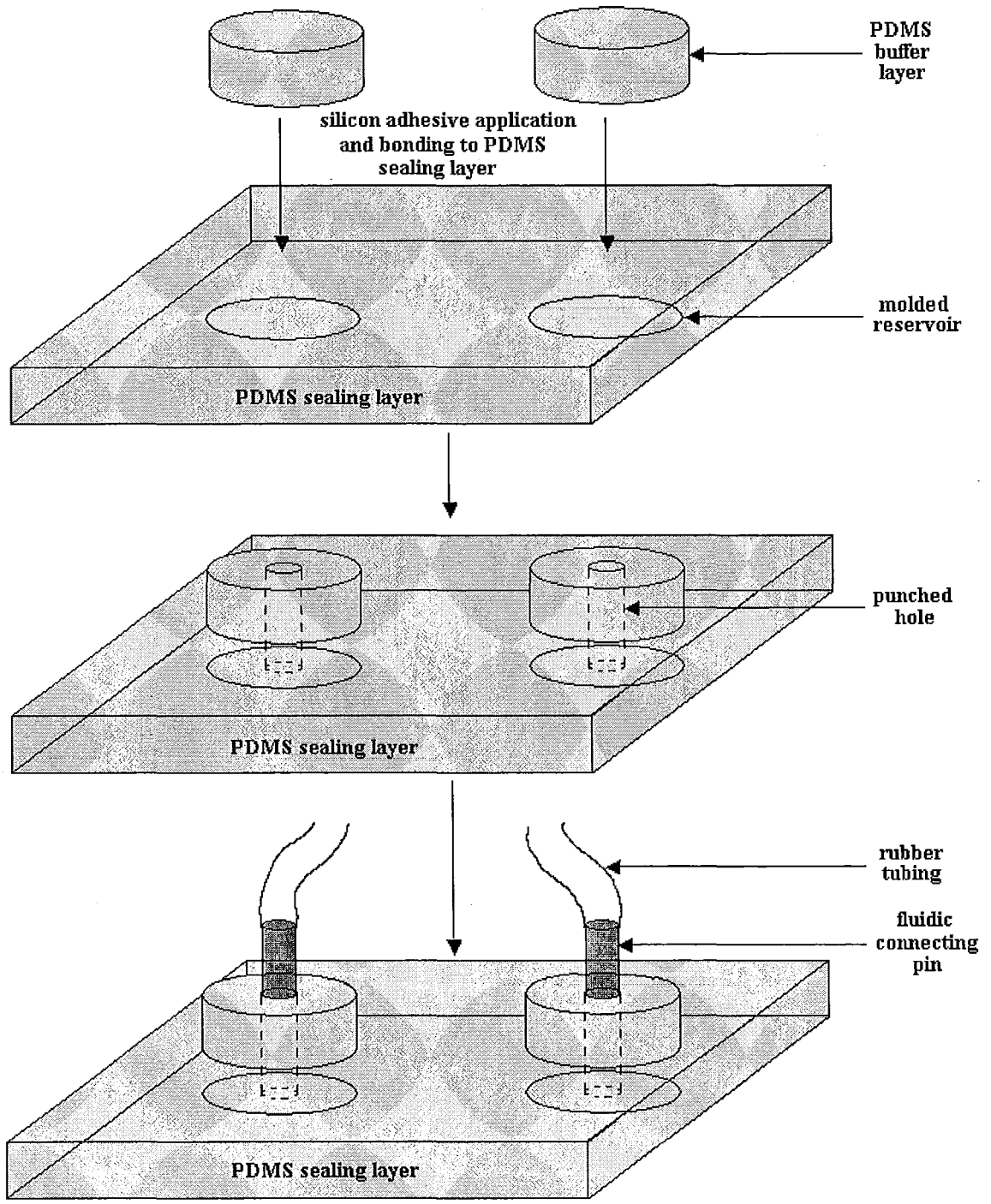

Figure 2.5: Diagram outlining the attachment of buffer layers for fluidic connections and insertion of fluidic connecting pins

2.3 Device Testing

The microchannels were flushed with DI water for 10 minutes to ensure there was no clogging and to help remove any tiny residual particles. Connections to inject fluorescent dye or microbeads were made next depending on the type of testing to be performed and sheath flow was established using the sheath channels and the appropriate sheathing fluid, either deionized water or ethanol, if necessary. Devices were placed on the optical stage and held by a vacuum pump, and the setup can be seen in figure 2.6. The 633nm laser was aligned with the waveguide facet and the light was coupled into the input waveguide. Fluorescence images were detected using a microscope camera with an attached 660nm bandpass filter made by Newport, Irvine, California, to eliminate the incident light. Pictures were taken with an Infinity 2-3 3.3 megapixel CCD camera from Lumenera Corporation, Ottawa, Ontario, connected to a computer to analyze fluorescence excitation within the channel and the ability of different lens designs to focus light within the channel and determine the differing intensities.

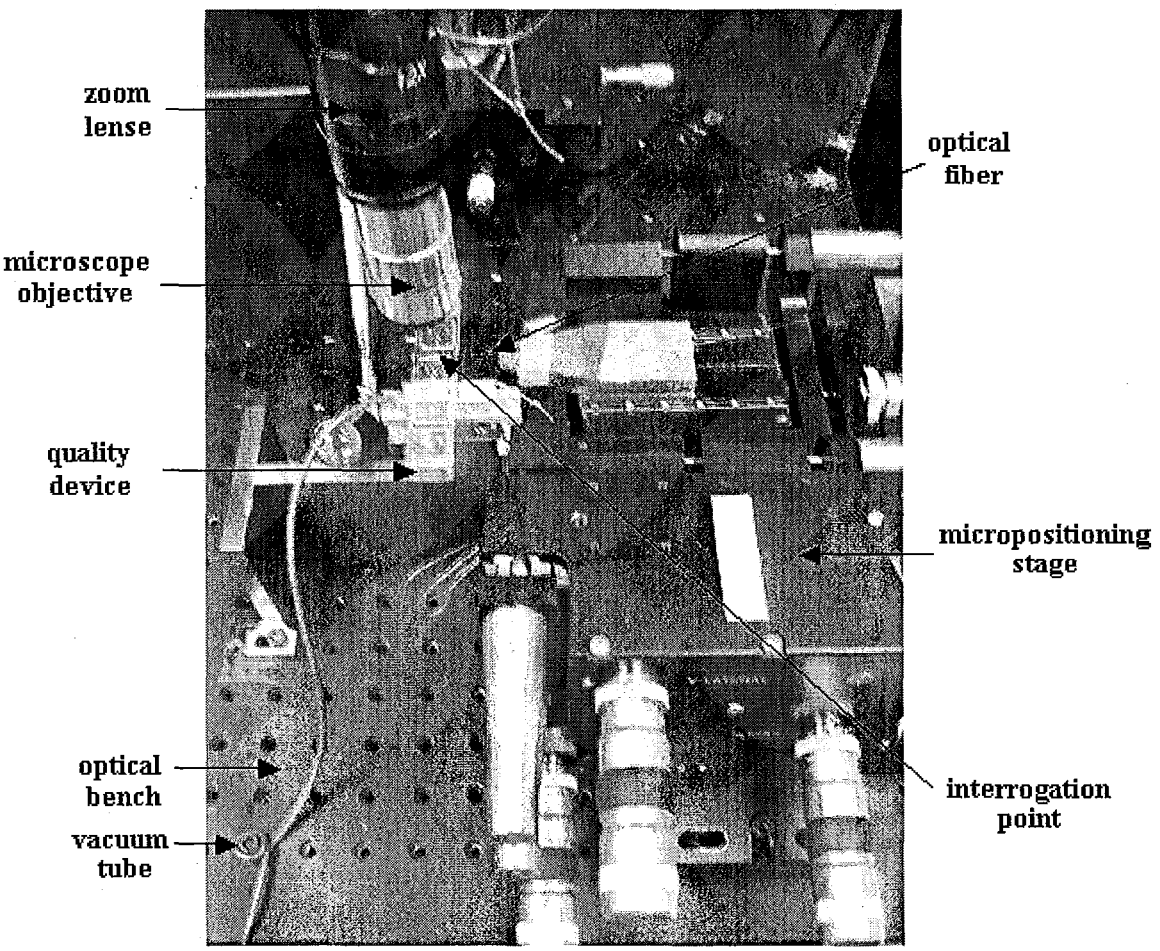

Figure 2.6: Optical testing setup used to couple light into waveguides and excite fluorescence within device microchannels

3 RESULTS AND DISCUSSION

3.1 Device Fabrication

There are three main steps involved in fabricating a quality microchip-based device outlined in figure 3.1, using any of the fabrication methods discussed in the introduction, depending on the materials selected. The first step is to create the open microfluidic channels to contain the fluids used or house any reactions or sensors. A sealing process must follow, protecting the open channels from any contamination once outside of the cleanroom. Finally the device must be prepared by making any connections to external equipment for flow, sensing or detecting. Depending on the specific use of a fabricated device, many other functions exist that could be incorporated at different stages, such as integrated waveguides or sensors fabricated in the structural layer or other external connections that may need to be made during the packaging step. The following sections discuss the challenges faced during the three main fabrication steps for our photonic integrated microchip-based devices.

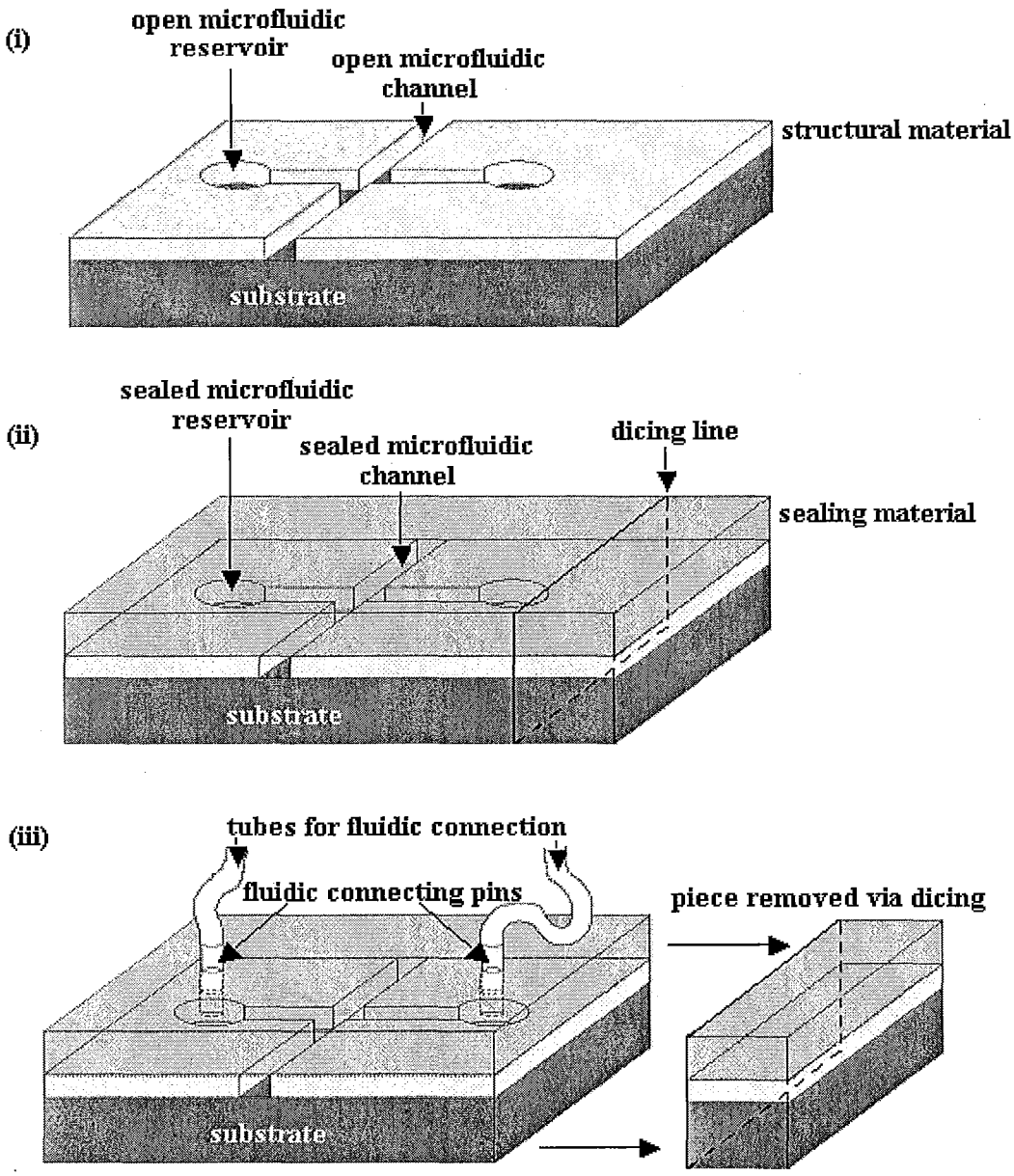

Figure 3.1: Three main steps involved in fabricating a quality microfluidic device are; (i) construction of open microfluidic channels, (ii) sealing of open microfluidic channels and (iii) packaging of the device

3.1.1 Fabrication of Waveguides and Open Microfluidic Channels on Glass

As discussed earlier it is advantageous when working with microfluidic devices to move away from bulky external equipment and integrate as many functions as possible on-chip and attempts at producing photonic integrated microchip-based devices have utilized challenging and complicated procedures. Thus we followed an approach suggested by Mogensen et al.[66] in fabricating open microfluidic channels and waveguides in a single structural layer using a one-shot process. To do this a suitable material must be chosen to provide sufficient wall structures for microfluidic channels and waveguides, as seen in figure 3.2, and the material must also have acceptable properties for use as a waveguide core as discussed previously in the introduction and shown in figure 1.4 (b). With this in mind, a suitable substrate material must not only have a sufficiently low refractive index, but it must also be transparent for light collection and scattering requirements.

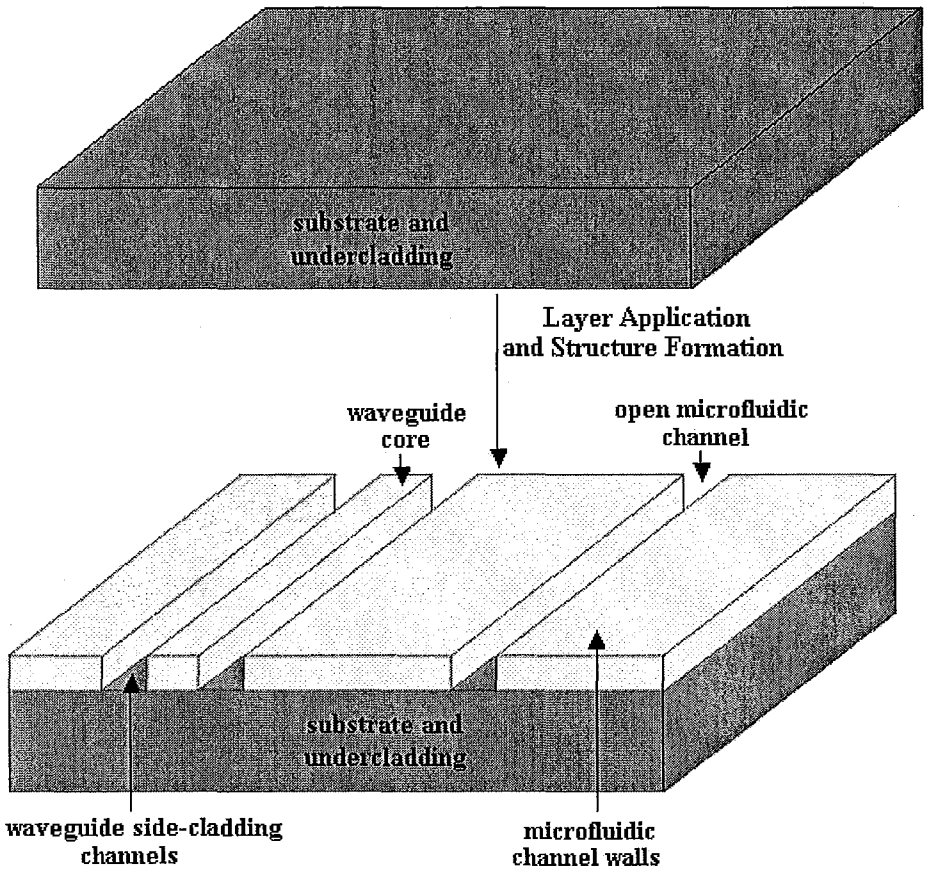

Figure 3.2: Waveguides and open microfluidic channels fabricated in a single layer using a one-shot process

The epoxy based photoresist SU-8 was determined to be the most appropriate material from which to fabricate both waveguide cores and microchannel walls as it has been widely used in the construction of microchip-based devices[52,66,69]. As a structural material, SU-8 provides strong mechanical strength as well as high thermal and chemical resistance. It can be fabricated with a high aspect ratio in thicknesses ranging from 0.5 to 200μm, however the structures are generally limited to rectangular. As a waveguide core, SU-8 provides advantageous optical properties, including low optical losses and a sufficiently high refractive index of 1.59 at 628nm. Air (n=1 at 628nm) was chosen for

side-cladding of the waveguide because of the simplicity in fabricating open channels on either side of the waveguides. SU-8 has traditionally been fabricated on silicon wafers (n=3.59 at 628nm), however due to the optical requirements of the on-chip waveguides and the necessity for a transparent device for analysis purposes, a glass substrate (n=1.45 at 628nm) was more appropriate. However glass substrates differ from silicon substrates in many ways. One issue is the necessary transparency of glass, which allowed the UV light during exposure to pass through and be absorbed by the black platform of the exposure machine. With silicon, this light was usually reflected, thus a higher exposure dose was required when working with glass. Primarily glass is a more hydrophilic surface than silicon, and SU-8 is highly hydrophobic, resulting in poor compatibility between SU-8 and glass. These main differences meant that following the standard SU-8 processing procedures provided by the manufacturer were unacceptable for use with glass. When they were used, the patterned SU-8 layer failed to remain bonded to the glass surface during development. Further trials showed strong bonding but a high degree of residual material remaining between structures. Literature suggested a processing window should exist where the post expose baking time and temperature and exposure dose could be manipulated such that strong bonding and low residual material between structures could be obtained on glass substrates[66]. Thus a progression of methods were implemented in order to combat this poor bonding, starting with the manipulation of processing conditions, followed by improvement through surface modification and finally achieving our goal by reducing stresses involved in device processing.

3.1.1.1 Bond Improvement Through Processing Conditions

Our first attempt to improve the bonding of SU-8 to the glass substrate was through the manipulation of the post expose baking times and temperatures and the exposure dose. The first attempt was to vary the exposure dose, ranging from 100mJ/cm^2 to 900mJ/cm^2 where about 200mJ/cm^2 was suggested by the manufacturer. A low exposure dose resulted in poor bonding as expected and much of the SU-8 layer peeled off the Pyrex during development and could be completely removed with little effort afterwards, as seen in figure 3.3.

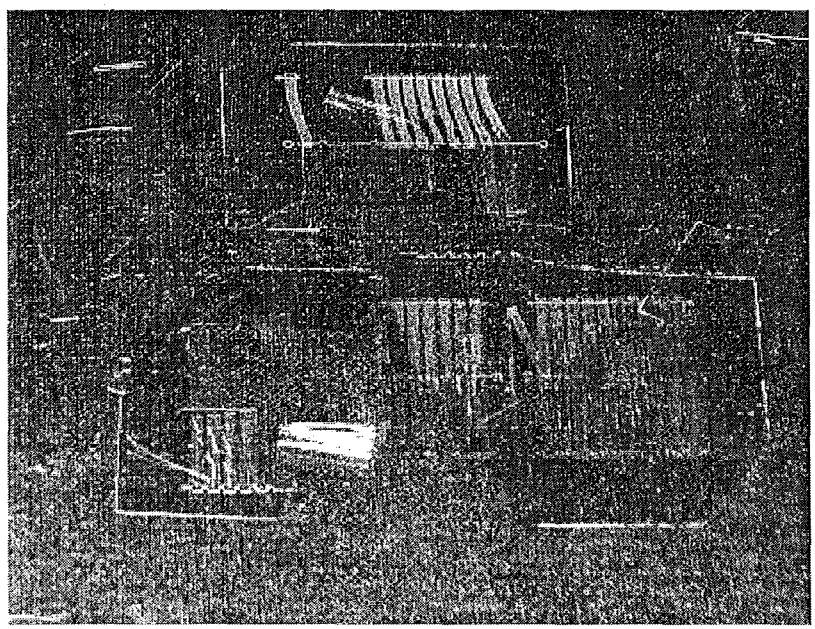

Figure 3.3: SU-8 layer having largely peeled away from the Pyrex substrate with almost all structures deformed and destroyed using standard baking and an exposure dose of 225mJ/cm^2

It was hoped a higher exposure dose would increase crosslinking and provide stronger bonding. This was the result, however all structures were thicker and misshapen as a high degree of residual material was able to polymerize between structures as seen in

figures 3.4 (a) and (b), and it could not be removed even with increased development time. The waveguide core width should be 50μm as denoted by the Exposed Region label in figure 3.4 (b), with 75μm between them, however they are much thicker. This was primarily due to the excessive exposure dose used in order to achieve effective bonding on glass, demonstrating that a low exposure dose is necessary, thus a more effective method of improving SU-8 bonding must be found.

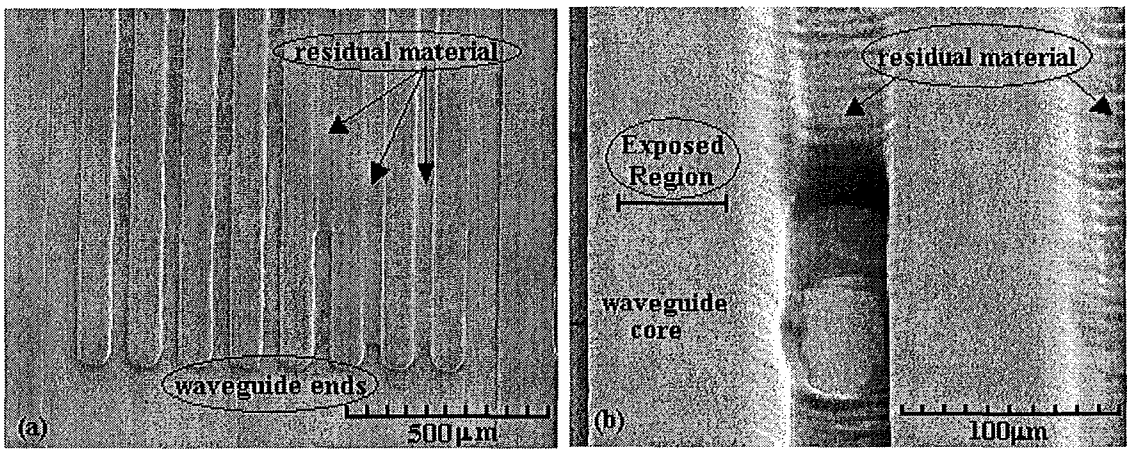

Figure 3.4: SEM images of a device created using an exposure dose of 900mJ/cm^2 showing (a) high amounts of residual material remaining between waveguides and (b) greatly increased width of waveguide core

The next step was to vary the temperature, using a range of 65°C and 200°C for maximum temperatures. It was found that lower temperatures provided no improvement to bonding due to decreased polymerization while high temperatures provided slightly improved bonding from increased polymerization, but again left a high degree of residual material between structures and lots of cracking of the SU-8 layer which can be seen in figure 3.5.

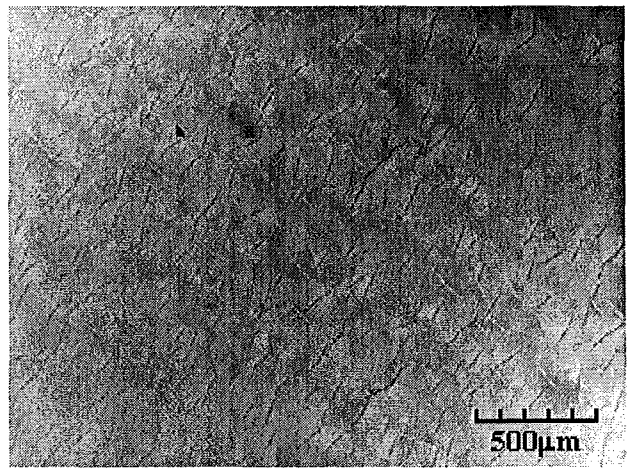

Figure 3.5: High level of cracking found throughout SU-8 layer with high baking temperature

While keeping the maximum temperature at the suggested 95°C, the heating and cooling rates were varied between 20°C/hr and 500°C/hr. Fast heating and cooling rates resulted in the entire SU-8 layer peeling away during development. Slow heating and cooling resulted in much less cracking throughout the SU-8 layer and seemed to provide a slight improvement to bonding while maintaining a low level of residual material between structures. However, the improvements were still not acceptable for producing quality devices and thus other methods of obtaining the appropriate processing window were explored. In all cases, increased development time and agitation were unable to remove the residual material from unexposed areas. Table 3.1 summarizes the results.

Table 3.1: Degree of bonding and residual material determined qualitatively and converted to percentages through inspection with the naked eye and microscope

Exposure Dose (mJ/cm^2)	Max Temperature (^oC)	Heating and Cooling Rate ($^oC/hr$)	Residual Material (% of developed area)	Bonding		
				Air bubbles (% of film)	Displaced Structures (% of total structures)	Cracking (% of film)
100	95	100	Complete Delamination of SU-8 Layer			
200	95	100	Complete Delamination of SU-8 Layer			
300	95	100	0-5	80-100	80-100	50
400	95	100	5-10	60-80	60-80	50
500	95	100	5-10	30-50	30-50	40
600	95	100	5-10	10-25	10-25	40
700	95	100	10-15	5-15	5-15	30
800	95	100	15-20	0-5	0-5	20
900	95	100	20-25	0	0	10
200	65	100	Complete Delamination of SU-8 Layer			
200	125	100	5-10	60-80	60-80	50
200	150	100	5-10	30-50	30-50	75
200	175	100	10-15	20-40	20-40	75
200	200	100	15-20	10-20	10-20	75
200	95	20	0-5	60-80	60-80	40
200	95	50	0-5	60-80	60-80	50
200	95	100	Complete Delamination of SU-8 Layer			
200	95	250	5-10	80-100	80-100	75
200	95	500	5-10	80-100	80-100	75

As can be seen, it was very difficult to find the processing window allowing for strong bonding and low residual material if it even existed. This was due to the fact that wherever a gain was made in one condition, improved bonding or low residual material, it was accompanied with a loss in the other. From these tests, it was determined that in order to provide an acceptably low level of residual material, the exposure dose must be kept below $300mJ/cm^2$, ideally around $225mJ/cm^2$, while utilizing slow heating and cooling between 20-50°C/hr and a maximum temperature of 95°C. These will be known

as the standard processing conditions throughout the rest of the paper. Thus another method to provide sufficient bonding at these processing conditions must be found.

3.1.1.2 Bond Improvement Through Surface Modification

Surface modifications were applied to the Pyrex substrate as the next attempt to provide improved bonding with low residual material. Literature suggested the use of HMDS in an attempt to reduce the hydrophilic nature of the glass substrates and match it more closely with hydrophobic SU-8[70]. HMDS was applied to the glass substrates after baking at 265°C for 3 hours using a LP-III Vacuum Bake Vapour Prime System from Yield Engineering Systems Inc., San Jose, California, followed by the SU-8 processing using the standard processing conditions determined in the previous section. Although the HMDS did provide a small improvement to bonding, it was not able to prevent all air bubbles and structure displacement from occurring. Results of bonding using HMDS and other surface modifications can be seen in table 3.2 as well as figures 3.6 (a), (b), (c) and (d) depicting the moderate improvement provided by all three surface modifiers, as it was quite similar in each case.

Table 3.2: Results on the improvement of bonding of SU-8 to glass utilizing HMDS, GPTMS and Omnicoat separately as surface modifiers using standard processing conditions

Surface Treatment	Residual Material (% of developed area)	Bonding		
		Air bubbles (% of film)	Displaced Structures (% of total structures)	Cracking (% of film)
HMDS	0-5	30-50	30-50	50
GPTMS	0-5	30-50	30-50	50
Omnicoat	0-5	30-50	30-50	50

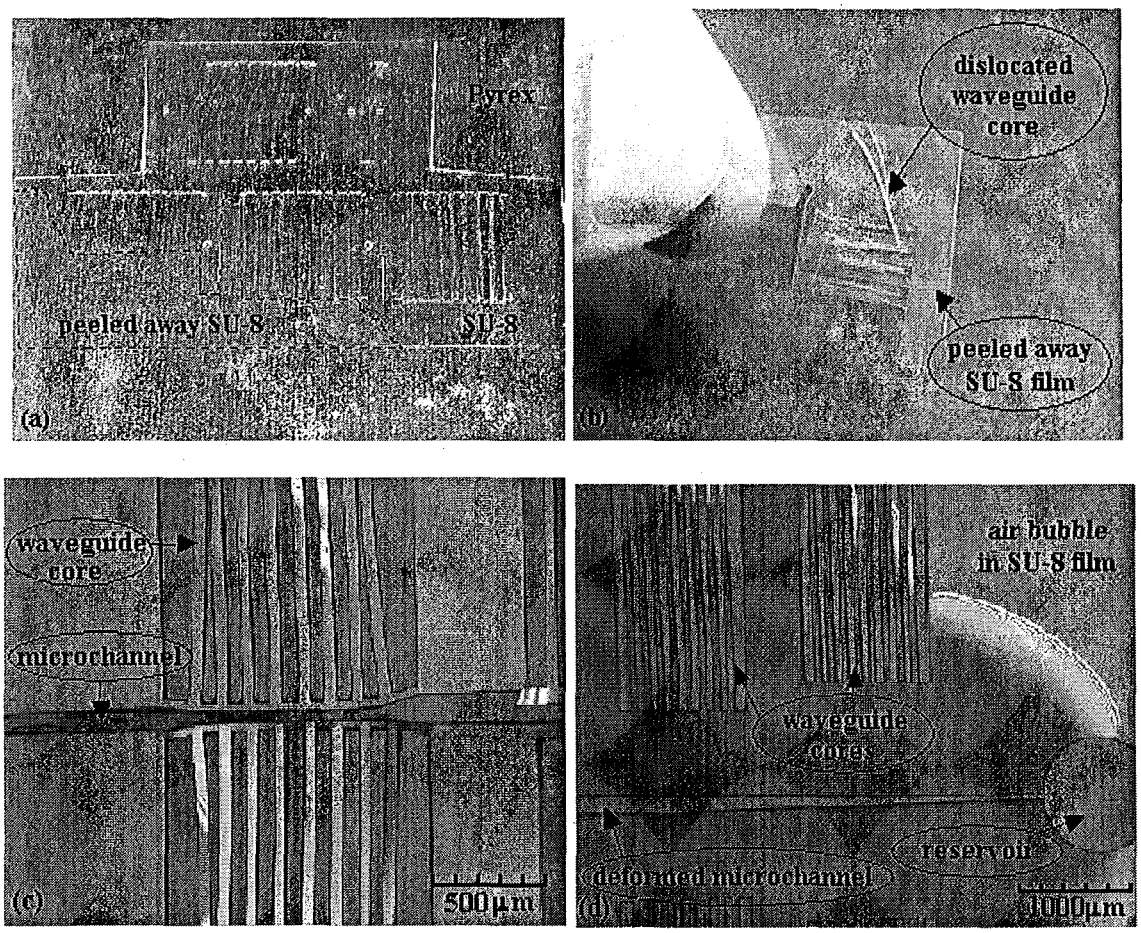

Figure 3.6: Slightly improved bonding obtained using standard processing conditions with surface modifiers of HMDS, GPTMS and Omnicoat showing (a) a device with a large section of SU-8 film peeled away from the Pyrex substrate, (b) a piece of the peeled away SU-8 film, (c) a device with deformed microchannels and waveguide cores and (d) a device with low residual material with a large air-bubble and deformed microchannel

Our next attempt was to introduce a chemical bond between SU-8 and glass using the coupling agent GPTMS as suggested by literature[71,72]. Two solutions were prepared for the application of GPTMS to the glass substrates as seen in table 3.3.

Table 3.3: Solutions necessary for the application of GPTMS on glass

Solution	Ethanol (ml)	GPTMS (g)	Water (g)	HCl (drops)
A	49	1	0	0
B	49	0	1	3

0.5ml of solution A was mixed with 0.5ml of solution B and shaken well for 2 to 3 minutes. The new solution was then spin coated on the surface of the glass substrate after baking at 265°C for 3 hours. Coated wafers were then heated to 100°C for 5 minutes and left to cool naturally. SU-8 processing using the standard conditions was performed next. As with HMDS, a small improvement to bonding was obtained, however it was not sufficient to prevent all air bubbles and structure displacement as seen in figures 3.6 (a), (b), (c) and (d). The results can be seen in table 3.2.

Our final attempt at surface modification utilized a product suggested by the SU-8 manufacturer called Omnicoat. The products primary function is to provide a thin layer that SU-8 can be processed on top of and the Omnicoat can later be dissolved using the appropriate solvent providing removal of an intact SU-8 film from the substrate. It has also been found that Omnicoat provides improved adhesion of SU-8 to glass substrates[73]. A thin layer of Omnicoat was spin coated on the glass substrate, after baking at 365°C for 3 hours, followed by a bake at 200°C for 1 min and natural cooldown to room temperature. SU-8 processing was performed normally utilizing the standard processing conditions. As with HMDS and GPTMS, slight improvements to bonding were obtained, however it was not sufficient to prevent all air bubbles and structure displacement as seen in figures 3.6 (a), (b), (c) and (d). The results can be seen in table 3.2.

The failure of the surface treatments in improving the bonding of SU-8 to glass suggested that there were other factors contributing to the poor bonding.

3.1.1.3 Bond Improvement Through Stress Reduction

Previous attempts at improved bonding of SU-8 on glass via process manipulation and surface modifications failed suggesting another factor is primarily responsible. In some cases, literature has suggested that stress management may be necessary in order to efficiently process SU-8, especially on glass substrates[74,75]. A high mismatch in the thermal expansion coefficients (CTE) of SU-8 (52ppm/°C) and glass (3.25ppm/°C) suggests stresses that may have been high enough to prevent the SU-8 film from effectively bonding to the glass and causing it to peel away during development. From this our next attempt investigated the use of an intermediate layer thicker than the layers used previously in surface modifications, that may be able to relax these stresses and allow for a strong interfacial bond. Using equations 3.1 and 3.2 below, the amount of stress in the SU-8 layer was estimated while employing intermediate layers of various thickness and shear moduli[76].

$$\tau_{max} = \frac{(\alpha_1 - \alpha_2)G\Delta T}{t_0 \kappa} \tanh\left(\frac{\kappa L}{2}\right) \tag{3.1}$$

In equation 1, τ_{max} is the maximum shear stress of an SU-8 layer with length, or wafer diameter, L. The coefficients α_1 and α_2 are the CTE values for SU-8 and Pyrex respectively while G denotes the shear modulus of the intermediate layer. ΔT is the maximum temperature difference and κ is determined using equation 3.2 below[76].

$$\kappa = \left(\frac{G}{t_0}\left(\frac{1}{E_1 t_1} + \frac{1}{E_2 t_2}\right)\right)^{\frac{1}{2}} \tag{3.2}$$

In equation 3.2, G remains the same as in equation 3.1, E_1 and E_2 are the Young's moduli of SU-8 and Pyrex respectively while t_0, t_1 and t_2 denote the thicknesses of the intermediate layer, the SU-8 layer and the glass substrate respectively[76]. The values of the variables are listed in table 3.4 and the length of the SU-8 layer was 4" or 0.10m. The maximum temperature difference was set at 85°C based on the baking step required during PDMS bonding to SU-8, ranging from 20°C to 100°C. This range also included the temperature change during the soft baking and post expose baking procedures where the wafers were ramped from room temperature (approximately 20°C) to 95°C.

Table 3.4: Properties of different device layers to be used in equations 1 and 2.

Property	Units	Intermediate Layer (SU-8 3000)	Patterened Layer (SU-8 2025)	Substrate (Pyrex)
Coefficient of thermal expansion	ppm/°C	52	52	3.25
Young's Modulus	GPa	3	3	64
Shear Modulus	GPa	1.6	NA	NA
thickness	m	Variable	2.70E-08	1.00E-03

Using the values obtained and plugging them into equations 3.1 and 3.2, a plot was developed for thicknesses ranging from 50nm to 3000nm, as seen in figure 3.7. From this plot, it is evident that the estimated maximum shear stress within the SU-8 layer is decreased with an increasing intermediate layer thickness. Maximum shear stress also decreases with decreasing shear modulus of the intermediate layer as expected.

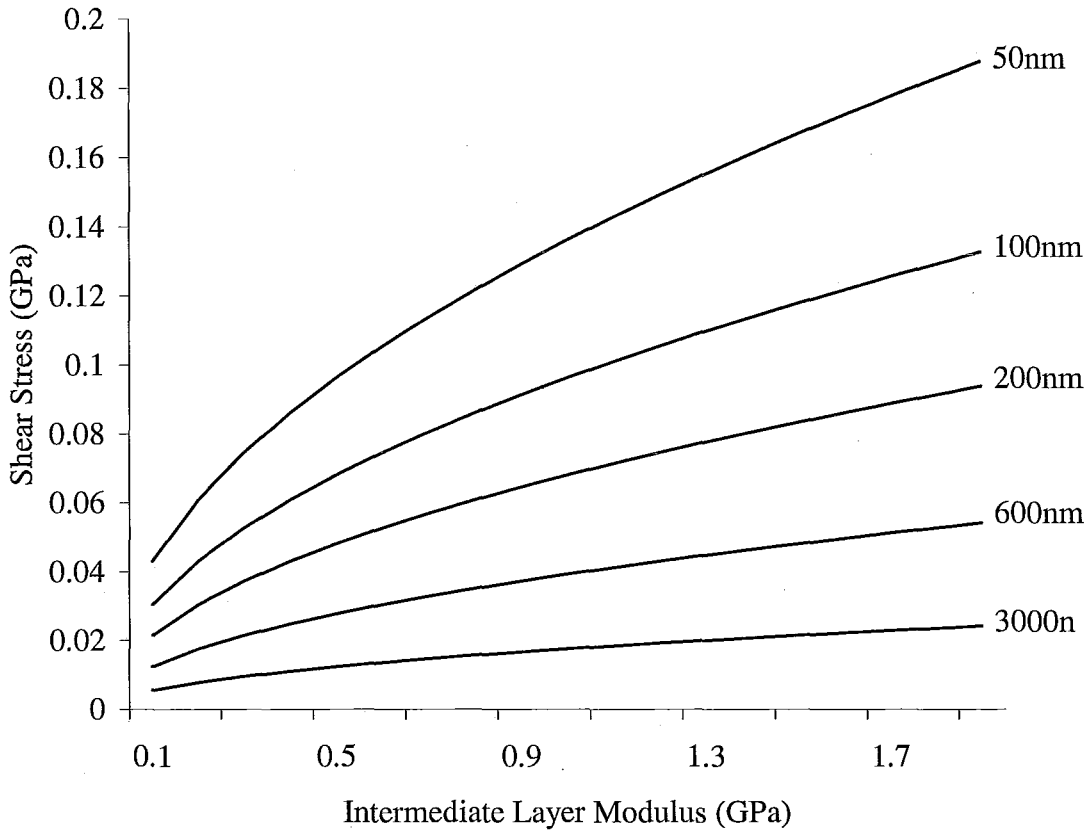

Figure 3.7: Theoretical maximum stress within the patterned SU-8 layer using different intermediate layer thicknesses over varying intermediate layer shear moduli calculated using equations 3.1 and 3.2.

Results suggest an inorganic polymer may be an effective material in reducing the stress effects. This is because organic polymers generally have smaller shear moduli than inorganic materials. Thus a suitable material would have a sufficiently low shear modulus, provide strong adhesion to both the glass substrate and an SU-8 layer as well as allow for adequate control of the layers thickness. Previously, it was suggested that SU-8 2002 could be used as a stress-reducing layer, and a 3μm layer was shown to work effectively[74]. From this, the specialty photoresist SU-8 3000 was chosen for the

intermediate layer, as this resist was specially developed to provide improved adhesion with glass while sacrificing the high aspect ratio of the SU-8 2000 series. SU-8 3000 also allows for thickness control similar to previous SU-8 materials and found to provide a strong chemical compatibility with the patterning SU-8 layer allowing for ease of processing. Using traditional processing, SU-8 3000 was unable to provide an intermediate layer thickness below about 5 microns. However, for an optically integrated microchip-based device, an intermediate layer with the same refractive index as the waveguide core material may allow light to leak out. Thus, the thickness of this layer must be kept as small as possible while still providing the necessary bonding improvement. To do this, SU-8 3000 was diluted to different weight percent concentrations using SU-8 developing solvent by weighing an amount of SU-8 in a small bottle and then determining and adding the appropriate amount of solvent. Shaking for about 5 minutes ensured the solution was well mixed and uniform enough for spin coating. In order to determine the layer thickness each dilution would provide, they were first processed on a silicon wafer. Silicon wafers were pretreated exactly as previously described for glass wafers. Diluted SU-8 3000 layers were soft baked for 1 minute at 65°C and 3 minutes at 95°C followed by a natural cool down before exposed to a UV dose of 185mJ/cm^2 and undergoing a final post expose bake, performed exactly as soft baking. This provided a solid uniform surface of SU-8, comparable to that on the glass wafers. The thickness of each layer was then determined using an ESM-300 elipsometer from J.A. Woollam CO. Inc. and recorded in table 3.5. Once the thickness of each dilution had been determined, the intermediate layers were processed identically to the

process described above, except on glass substrates. Next SU-8 2025 layers were processed on top of the cured intermediate layer using the standard processing conditions. After development, the degree of bonding of each device was evaluated qualitatively using the naked eye and microscopes based on the following parameters; percent of residual material remaining within the developed area, percent of the film that has lifted from the intermediate layer forming air bubbles, percent of structures displaced or misshapen and the percent of cracking found throughout the film. The results are summarized in table 3.5 below based upon at least 2 devices per layer.

Table 3.5: Evaluation of different intermediate layer thicknesses based upon the amount of residual material within the developed area and the bonding of the SU-8

			Bonding Before Post Processing Procedures		
Intermediate Layer Thickness (nm)	Amount of SU-8 3000 photoresist in SU-8 developer (wt%)	Residual Material (% of developed area)	Air bubbles (% of film)	Displaced Structures (%)	Cracking (% of film)
604	30	0-5	0	0	10
186	10	0-5	0	0	10
83	5	0-5	0	0	50
33	3	0-5	30	15	75
18	2	0-5	50	50	75
8	0.5	Complete Delamination of Patterned SU-8 Layer			

The percent of residual material remaining within developed regions was able to be kept sufficiently low in all devices due primarily to the low exposure dose and was observed in devices with all intermediate layer thicknesses. An intermediate layer of approximately 8nm was shown to provide no improvement, as the SU-8 film was completely removed from the glass substrate during development. Intermediate layer

thicknesses of approximately 18nm and 33nm provided an improvement, but still resulted in the formation of air bubbles in some regions and a number of displaced structures as seen in figures 3.8 (a) and (b) respectively.

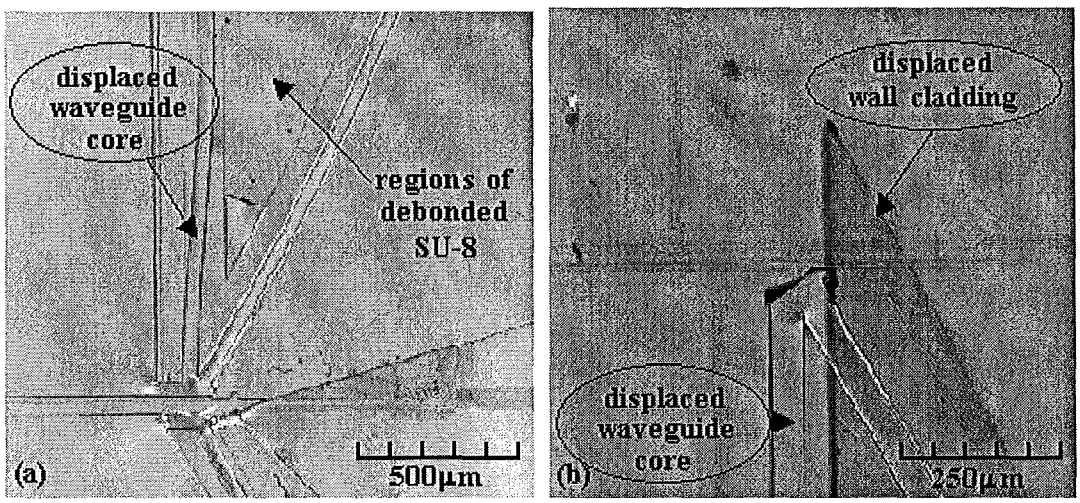

Figure 3.8: (a) cracks and dislocated waveguide cores around a microchannel with small regions of debonded SU-8 in a device fabricated with an 18nm intermediate layer and (b) waveguide cores and cladding wall region broken and pushed over top of a microchannel and lensing system, seen out of focus in the baground, on a device fabricated with a 33nm intermediate layer

In order to provide sufficient bonding with low residual material, an intermediate layer thickness of at least 80nm was required, however these devices still exhibited a high degree of stress fractures and cracking around structures, especially corners, as seen in figure 3.9.

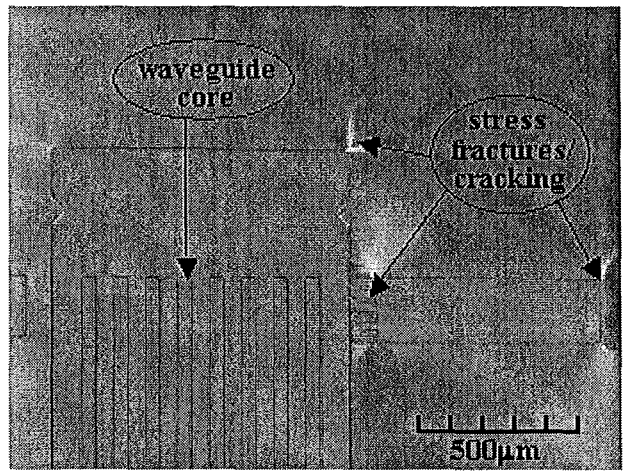

Figure 3.9: Device fabricated with an intermediate layer thickness of 80nm showing low residual material and sufficient bonding but a high degree of cracking and stress fractures, specifically at corners

A 186nm intermediate layer was found to not only provide low residual material and sufficient bonding throughout the film, but also greatly reduced the amount of cracking. Increasing the intermediate layer thickness to 604nm was found to provide no further improvement in the bonding or cracking, as it was found to be almost identical to devices constructed with a 186nm intermediate layer. Thus it was determined that the minimum intermediate layer thickness required to produce a quality photonic integrated microchip-based device was 186nm. Figure 3.10(a) shows a device with sufficient bonding and low residual material fabricated with an intermediate layer thickness of 600nm. A horizontal rectangular microchannel intersects vertical waveguides at the interrogation point of the device. Waveguides were 50µm wide, 27µm thick and straight waveguides were 1cm long. Microchannels were also 50µm wide and 27µm deep with length depending on the device design. An SEM image in figure 3.10(b) shows a diced curved waveguide end and demonstrates the sharp sidewalls and smooth surface of the device prior to sealing

obtained from the process. The dirt within the side air-cladding channels is from the rough dicing conditions discussed later and can be removed with pressure washing.

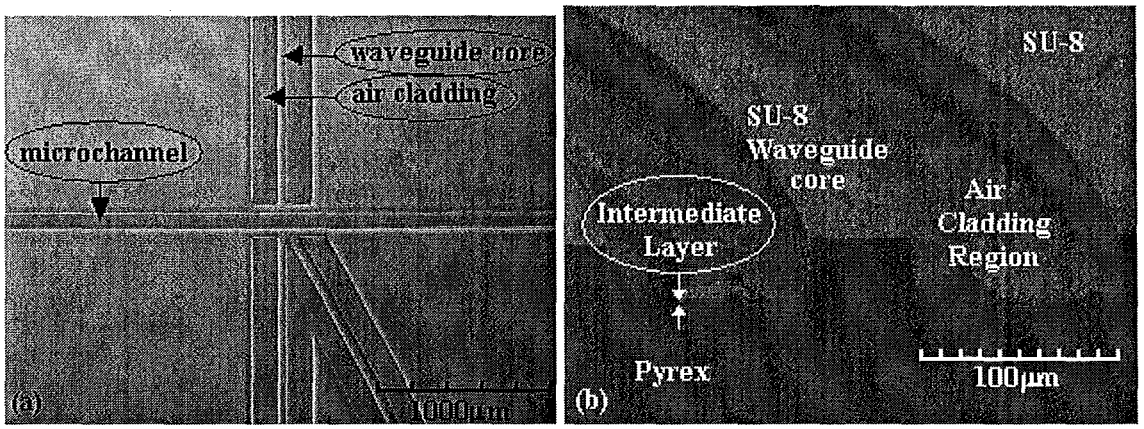

Figure 3.10: Devices fabricated using a 600nm intermediate layer (a) taken with a microscope showing a horizontal microchannel intersecting vertical waveguides with low residual material, strong bonding and low cracking and (b) an SEM image showing a diced curved waveguide end with sharp sidewalls.

As seen in figure 3.7 and table 3.5, a thicker intermediate layer provides better stress reduction and in turn better bonding. However, the intermediate layer chosen had the same refractive index (n=1.59 at 628nm) as the structural layer and hence the waveguide cores, thus light would be able to leak out through the intermediate layer. When fabricating a photonic integrated microchip-based flow cytometer, sensitivity of the device is highly dependent on the amount of light that can be collected. This problem suggested a thinner intermediate layer to keep these losses to a minimum while maintaining a thickness great enough to maintain effective bonding. The impact of the intermediate layer thickness on the performance of the device was tested using Rsoft's BeamPROP. Optical simulations were performed in which light was propagated down the length of a 1cm waveguide with a height of 27μm and a width of 50μm in the

presence of no intermediate layer, a 600nm intermediate layer and a 3000nm intermediate layer. Results of the simulation can be seen in figures 3.11 (a), (b) and (c) which denote light propagated down waveguides with no intermediate layer, a 600nm intermediate layer and a 3000nm intermediate layer respectively.

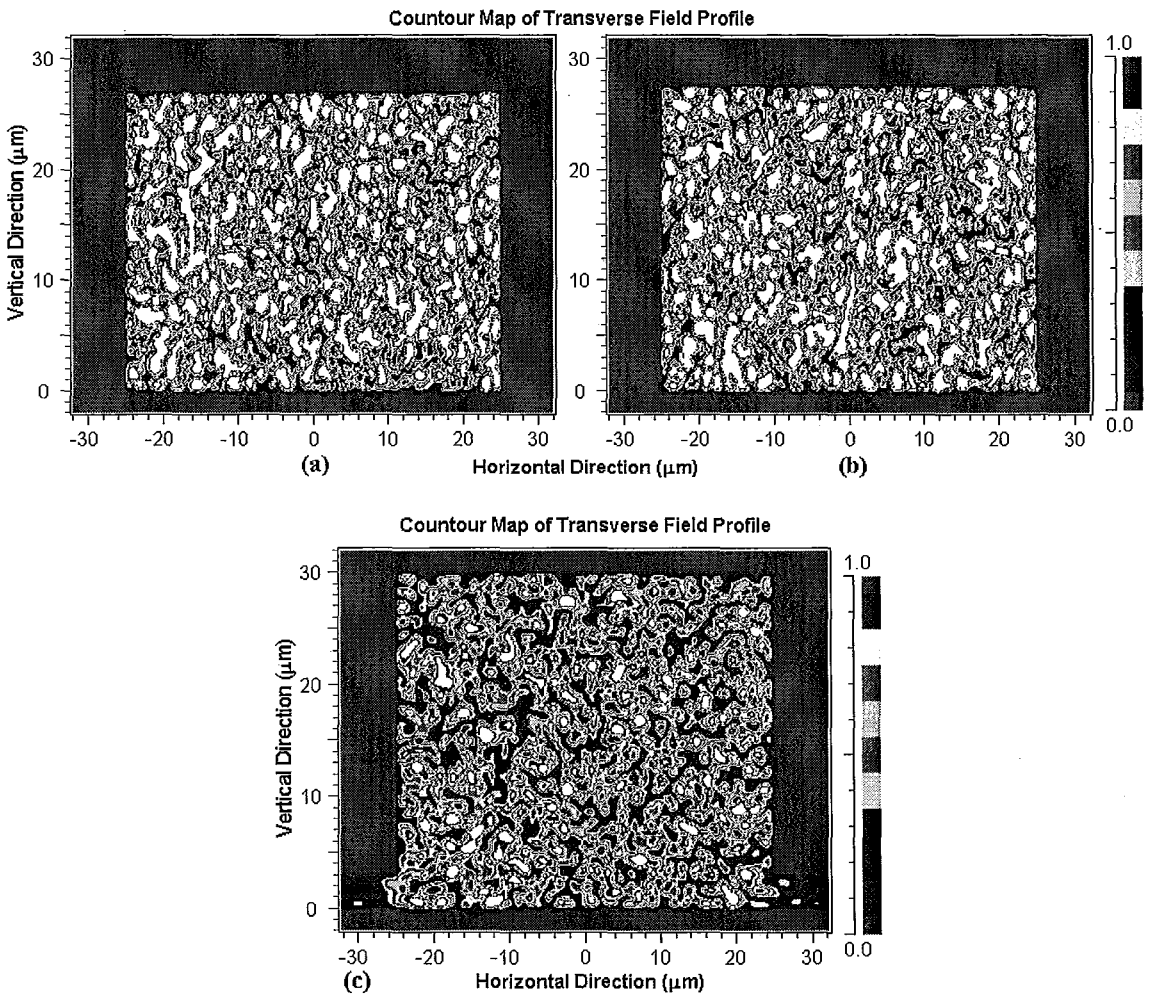

Figure 3.11: Simulated results showing relative power density of light at the end of a 1cm waveguide (a) without an intermediate layer, (b) with a 600nm intermediate layer and (c) with a 3000nm intermediate layer.

White regions denote areas of high power, 1 arbitrary unit, and decrease from there according to the power scale on the right of the figure. The overall power density was

further quantified in the graph of figure 3.12. A power density of 1 arbitrary units represents the power emitted from the end of an optical fiber used to couple the light into the waveguide. This optical fiber had a radius of 50μm, just like the one to be used for our device testing. Only about 0.50 arbitrary units were transferred directly from the larger fiber to the smaller waveguide, and further losses from that point were related to leaking light. With the waveguide without an intermediate layer as a benchmark, it can be seen that the power density remains relatively constant after coupling and oscillates around 0.43 arbitrary units. When the waveguide was simulated on top of a 600nm intermediate layer, which represents the thickest layer quality devices were fabricated with, there appears to be very little difference from a waveguide with no intermediate layer. Other than the small amounts of leaking light that can be seen in the bottom right and left corners of figure 3.11 (b), a 600nm layer appears to perform excellently, also with an oscillating power density around 0.43 arbitrary units. Conversely, when a 3000nm intermediate layer was used, the losses jumped dramatically. This can be seen in figure 3.11 (c) as there are very few white regions of high power density, and a large amount of light appears to have leaked out of the thick intermediate layer in the bottom left and right corners of the waveguide. Furthermore, the graph of figure 3.12 showed a steady decrease in the power density, dropping to about 0.23 arbitrary units by the time the light had propagated down the length of the waveguide. From the data obtained, a safe intermediate layer range for effective production of quality photonic integrated microchip-based flow cytometers can be determined. A minimum thickness of about 186nm is suggested for sufficient bonding with minimal residual material and cracking,

while a 600nm thickness is a safe upper limit where light leakage can be kept at an acceptably low level.

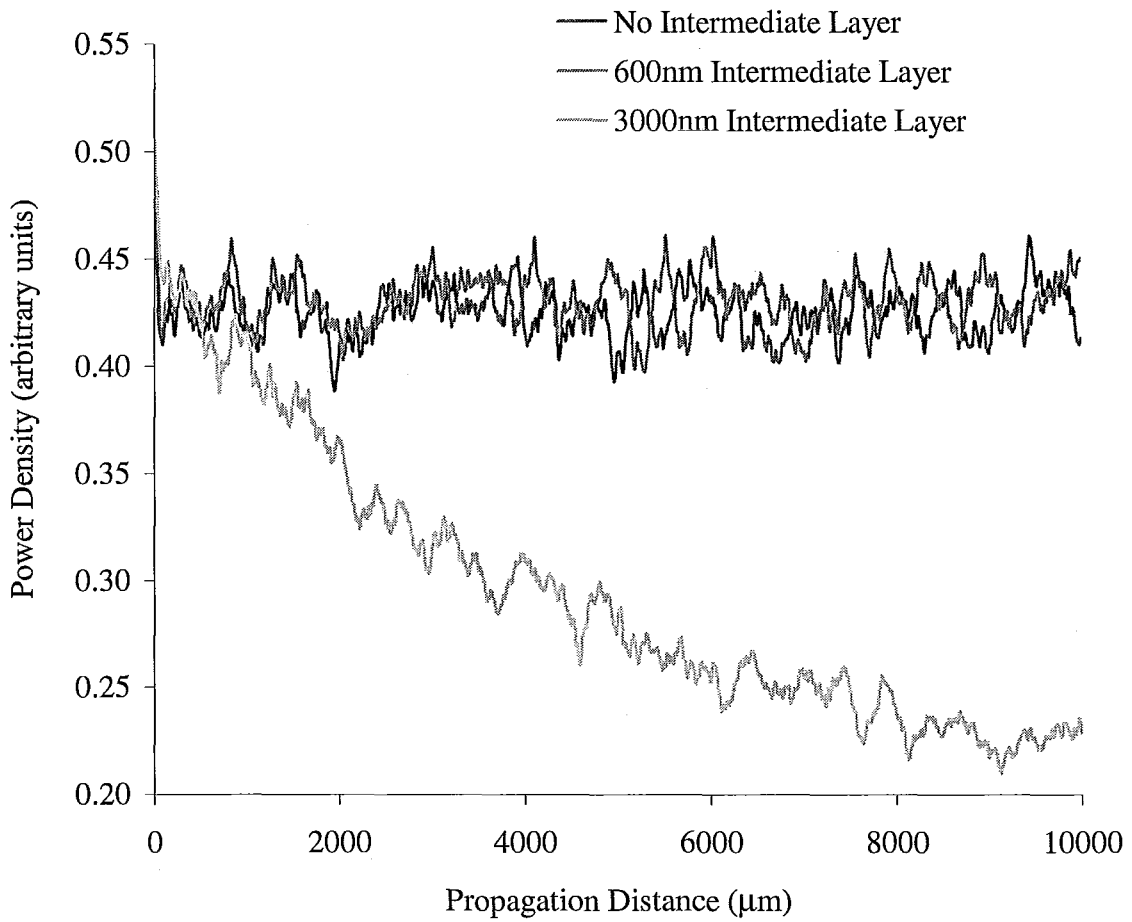

Figure 3.12: Plot of simulated relative power density through a 1 cm-long waveguide on glass without an intermediate layer, with a 600nm intermediate layer and with a 3000nm intermediate layer

3.1.2 Device Sealing

Sealing a microchip-based device serves a number of purposes depending on the devices function. Sealed microchannels allows for the application of pressure to provide high flow rates necessary in most applications. Furthermore, the sealing layer protects channels and components from the environment helping to prevent channel blockages from particles or adverse effects on any reactions or detecting taking place within the channels. Traditional requirements of a device seal include high mechanical strength and water tightness, biochemical and chemical resistance or compatibility, chemical inertness and compatibility with any detection requirements. Sealing must also avoid clogging channels and denaturing any components through temperature sensitivity or built in stresses causing distortions. Finally the sealing process must be robust to allow for easy and efficient alignment of specific components between the two layers[10]. One such process was previously outlined in figure 2.2 of section 2.2.3.

Our device specifically requires a mechanically strong watertight seal capable of allowing a sufficiently high pressure drop across the channel for pressure driven flow and sheath focusing, generally between 0.05 and 0.35 MPa. The sealing layer must also be transparent for optical testing and alignment purposes and must have a refractive index below that of the SU-8 waveguide cores, n=1.59 at 628nm. Finally, the sealing process itself must allow for a high level of alignment between the two layers primarily for fluidic connection. The elastomer PDMS was deemed adequate for the optical properties of the device with a refractive index of n=1.47 at 628nm, but a method to easily bond PDMS to SU-8 must be found. PDMS sealing layers may be easily fabricated via soft

lithography discussed previously. Surface-oxidation of the methyl groups on the PDMS surface to form silanol groups has been widely used to construct and seal various microchip-based devices via irreversible covalent siloxane bonds to surfaces such as another piece of plasma-oxidized PDMS, glass, silicon, silicon nitride polystyrene and polyethylene[10,77]. Plasma-oxidation of PDMS does not provide much time for alignment, approximately 30 seconds, because the silanol groups on the PDMS surface have a short shelf life. However, this method cannot be directly applied when using SU-8 because the SU-8 surface does not have the appropriate surface chemistry and cannot be similarly oxidized. Mogensen et al.[66] used a mechanical clamp to seal an SU-8 microchip-based device with PDMS, but this method was not deemed feasible for quality device production because of the bulky apparatus required. To solve this problem, we proposed creating a chemical bond between PDMS and SU-8 by introducing an amine group to the surface of PDMS and bonding it with residual epoxy molecules found on the surface of SU-8 via polyaddition reactions.

3.1.2.1 Mechanism

When SU-8 is processed using normal procedures without any hard baking, SU-8 experiences 57% or less of its total reaction leaving a sufficient amount of epoxy molecules unreacted on the surface[78]. Thus the main goal would be to provide a strong bond between the SU-8 epoxy groups and an acceptable sealing layer. Polyaddition reactions have been the most common method used for curing epoxy resins and could provide a sufficient reaction to produce a covalent bond between the SU-8 layer and a sealing layer. Most curing agents utilize an active hydrogen atom reacting with the active

carbon of the epoxy group forming a covalent bond and a hydroxyl group. This is traditionally performed using amine, acid, mercaptan, amide or phenol groups and the general reaction can be seen below where *X* is O, S or N*R* and *R*, R_1 and R_2 is an organic moiety[79].

$$R_1XH + (CHCH_2O_2)R_2 \rightarrow R_1XCH_2CH(OH)R_2$$

Thus the next step was to introduce an appropriate molecular group to the surface of the PDMS sealing layer in order to bond it to the residual SU-8 epoxy molecules. It has been shown that the molecule 3-aminopropyltrimethoxysilane (APTMS) may be bound to surface-oxidized PDMS in order to provide active amine groups for purposes such as DNA immobilization in immunoassays[80,81]. The methodology of this procedure is outlined below in figure 3.13.

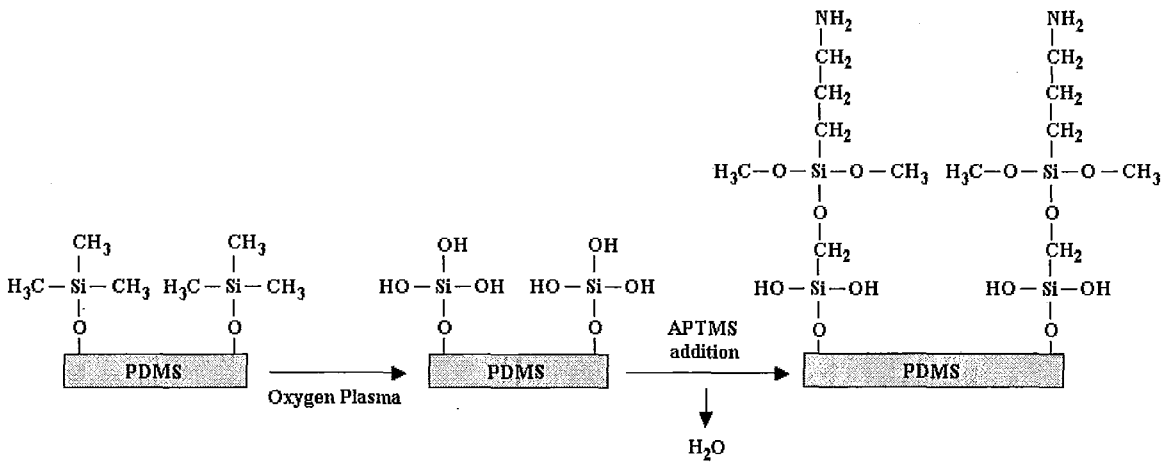

Figure 3.13: Reaction and bonding of APTMS to surface-oxidized PDMS

The presence of APTMS on the PDMS surface was confirmed by X-ray photoelectron spectroscopy (XPS) analysis as seen in the figure 3.14.

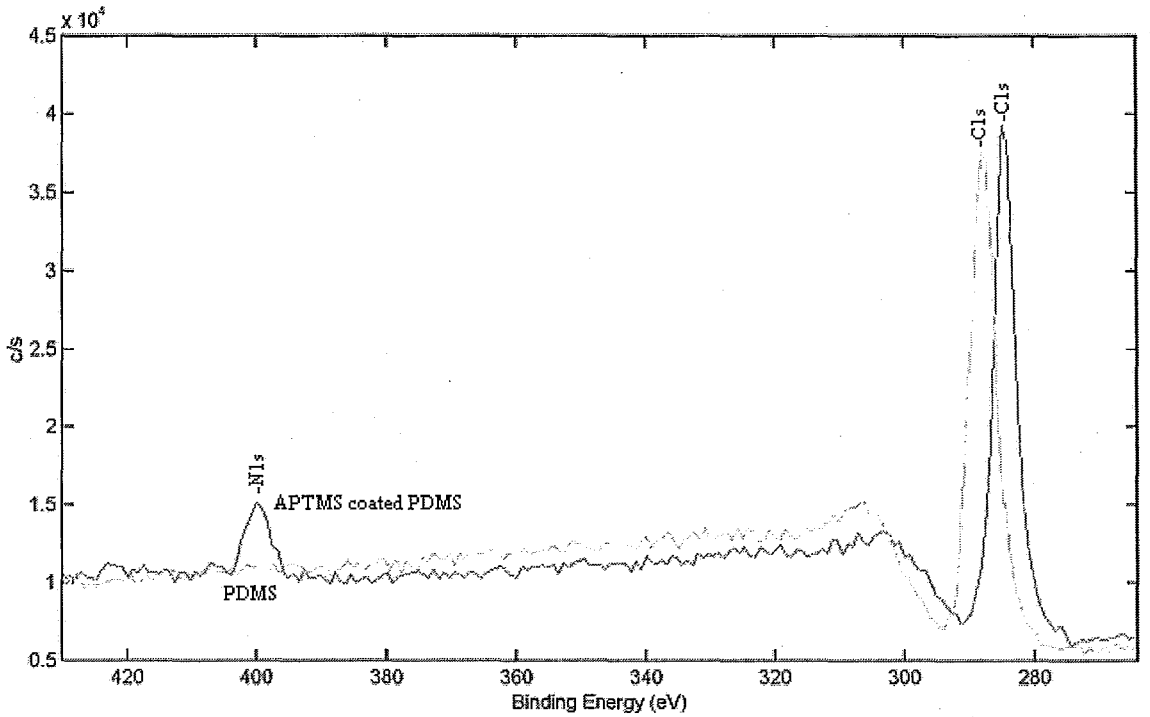

Figure 3.14: Confirmation of APTMS attachment to PDMS surface by XPS analysis, where the coated PDMS sample was heated to 100°C for 30 minutes and washed with ethanol

Silanol groups formed on the PDMS surface have a very short lifetime, as they have been shown to fall back into the structure to be replaced by traditional methyl groups[82]. Thus the APTMS must be applied quickly, within approximately 30-60 seconds of plasma treatment. This was a problem with traditional sealing using PDMS on glass wafers and others, as there was little time to align structures and no allowance for any reworking once contacted. Conversely, APTMS will remain on the PDMS surface for a longer period of time and the reaction with the residual epoxy molecules will not be formed until heated, thus complicated alignment can be reworked until the optimal alignment is obtained. The mechanism for bonding APTMS treated PDMS to SU-8 can be seen in figure 3.15 (a) and a bonded device can be seen in figure 3.15 (b).

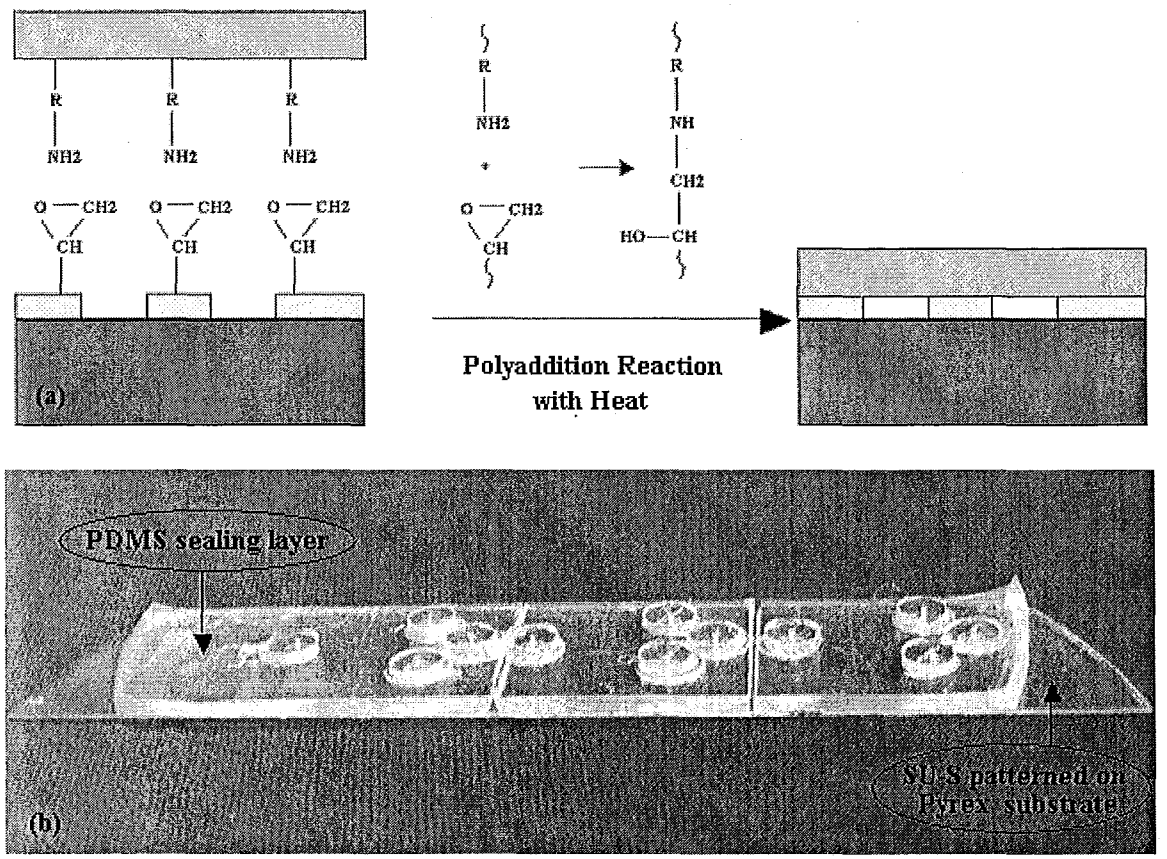

Figure 3.15: (a) diagram of the bonding of APTMS treated PDMS to residual epoxy molecules on the surface of the SU-8 layer and (b) a bonded device using the sealing process

3.1.2.2 Processing

After the mechanism was established and the theory proven to work, the next step was to determine the most effective conditions to use for processing. Initial tests determined the best solvent for the job. Literature suggested the use of ethanol, toluene and hexane as acceptable solvents for APTMS[83]. Each solvent was tested with three different weight percent concentrations of APTMS and the bond strength was determined by a scratch test. Scratch tests were performed by scratching the PDMS off of the SU-8

layer and determining if the bonding between the APTMS treated PDMS and SU-8 could be broken. This was determined visually by observing if the SU-8 layer had been reached and converting the remaining amount of PDMS to a percent of the bonded area to quantify the degree of bonding. At least three tests were performed for each solvent at each concentration and an average result was taken. Ethanol was the worst solvent and did not work at all at any of the concentrations used. In figure 3.16 (a) the outline of the APTMS treated PDMS can be seen as well as other residues within that region, but there is no PDMS remaining, which can be seen by the lack of any shiny surfaces when compared with figures 3.16 (b) and (c). Hexane performed much better than ethanol providing a much stronger bond that was similar at each concentration tested, however the degree of bonding was erratic causing a wide range for each concentration and never fully encompassing the whole bonding area. Figure 3.16 (b) shows the clear square of where the PDMS was placed, and a large amount of PDMS remains, as seen by the shiny reflections. However there are also some regions within this square where the PDMS has been removed, such as the bottom right corner of the square and near the top left corner. Toluene performed best as a solvent producing excellent bonds at every concentration and an example can be seen in figure 3.16 (c) where two separate squares of PDMS remain fully bonded after the scratch test as denoted by the shiny regions, and none of the SU-8 surface could be reached. Bonding results are summarized in table 3.6. In some cases, small corners of the toluene solvent samples were not bonded, resulting in the 95-100% result. This non-bonded area consistently occurred in regions where the sample was handled with tweezers during processing and was found to be non-existent when

extra care was taken to avoid any contact of the plasma-oxidized PDMS surface during processing. In most cases of device processing, any handling resulted in areas where bonding was not essential thus eliminating any problems. Furthermore, it was generally quite easy to avoid any surface contact eliminating the problem completely.

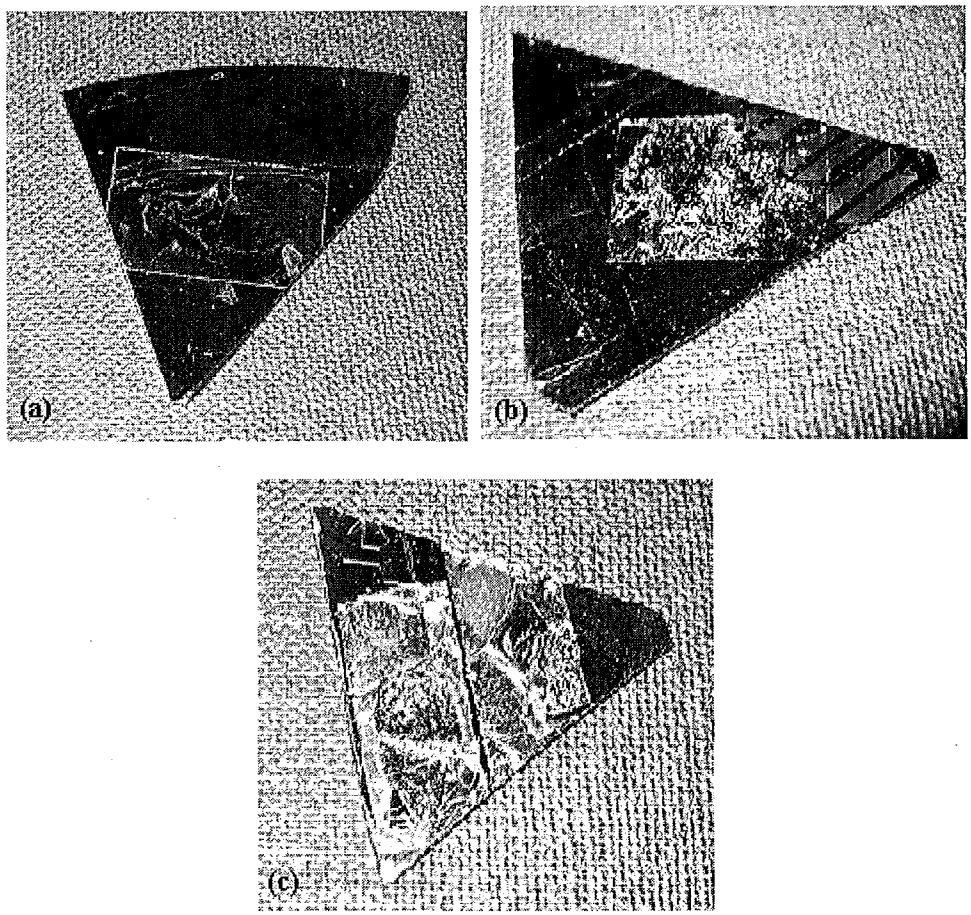

Figure 3.16: Scratch test results between SU-8 and PDMS treated with 1wt% APTMS in (a) ethanol solution (b) hexane solution and (c) toluene solution

Table 3.6: Average effect of solvent choice on the bonding of APTMS treated PDMS to SU-8 determined using the scratch test

Concentration (wt% APTMS)	Ethanol (% fracture in PDMS)	Hexane (% fracture in PDMS)	Toluene (% fracture in PDMS)
1	0	75-90	95-100
0.5	0	75-90	95-100
0.1	0	75-90	95-100

The next step was to determine the most effective weight percent concentration of APTMS in toluene. Building on the previous tests, two concentrations below 0.1wt% APTMS were also tested, 0.01wt% and 0.05wt%. At least three samples were prepared with each concentration and the average results from scratch tests were recorded in table 3.7 below. The lowest concentrations tested, 0.01wt% and 0.05wt%, provided a 0% fracture in the PDMS layer after performing the scratch test, resulting in no bonding at all. Thus it was determined that a minimum of 0.1wt% concentration of APTMS in toluene was required to provide strong, reproducible bonding to SU-8. For the remaining tests, the three concentrations providing strong reproducible bonding were used in case one began to fail under different conditions.

Table 3.7: Average effect of APTMS/toluene weight percent concentration on the bonding of APTMS treated PDMS to SU-8 using the scratch test

Concentration (wt% APTMS)	Bonding (% fracture in PDMS layer)
1	95-100
0.5	95-100
0.1	95-100
0.05	0
0.01	0

When coating PDMS with the APTMS/toluene solution, the PDMS layer swells with the solvent toluene causing deformation of the sealing layer. This presented a problem when a high level of alignment was required as in our device construction. Thus it was necessary to determine how long a coated layer of PDMS could be left, allowing the toluene to evaporate while maintaining strong bonding capabilities. To do this, PDMS samples were prepared, coated with different concentrations of APTMS in toluene, and had their surfaces dried off with an air stream before being left exposed to air for varying amounts of time. At least 3 samples were used for each test, and the average results are summarized in table 3.8. It was found that the samples could be left to dry for about 2 hours before experiencing any decreases in bonding. At the 4 hour period, some samples provided excellent bonding with the entire fracture within the PDMS layer, however some samples began to experience slight decreases in bonding. All samples left to dry for 1-4 days experienced greatly reduced bonding with very little fracture in the PDMS layer after the scratch test, and samples left for greater than 1 week, did not provide any significant bonding at all. It should be noted that a drying time of 1-2 minutes did not quite provide enough time for the PDMS to return to its normal structure, but due to the small size of the samples, did not pose a problem with bonding. It was observed that most PDMS samples required about 5-10 minutes to return to their regular shape, however this is dependent upon the size and shape of the PDMS layer and the amount of APTMS/toluene solution used.

Table 3.8: Average effect of drying time on the bonding of APTMS treated PDMS to SU-8, using the scratch test and 3 different concentrations of APTMS/toluene solutions

Drying Time	1wt% APTMS (% fracture in PDMS Layer)	0.5wt% APTMS (% fracture in PDMS Layer)	0.1wt% APTMS (% fracture in PDMS Layer)
1-2 min	95-100	95-100	95-100
30 min	95-100	95-100	95-100
1 hour	95-100	95-100	95-100
2 hours	95-100	95-100	95-100
4 hours	85-95	85-95	85-95
1 day	70-80	70-80	70-80
2 days	70-80	70-80	70-80
4 days	70-80	70-80	70-80
1 week	0	0	0
2 week	0	0	0

From these results a strong understanding of the processing conditions was obtained and further performance tests could be performed with confidence that each sample was initially well bonded.

3.1.2.3 Performance

Fabricated devices may require continuous flow, thus resulting in long exposure to fluids such as water. In order to ensure strong bonding throughout the testing procedures, it was necessary to determine if water had any effect on bonding. Several samples at varying APTMS/toluene weight percent concentrations were made and left to soak in water for up to a month with daily checks to ensure continued bonding. At least 3 samples were tested at each concentration and if any debonding was experienced, the scratch test was performed to determine an average percent fracture in the PDMS layer at that time. Results are summarized in table 3.9, and it can be seen that water appears to have little effect on the bonding strength at all of the concentrations tested with drying

times in air of up to 2 hours. Each of these samples lasted the full month and still provided a 95-100% fracture in the PDMS layer when the scratch test was performed. Samples tested with 4 hours of drying time in air began to show some decreased bonding. The 1wt% APTMS/toluene sample seemed to be unaffected by water, however the 0.5wt% and 0.1wt% APTMS/toluene samples showed decreased bonding, below the 85-95% determined from previous tests, after soaking in water for 1 month. These results suggest that water may have a small effect on bonding, but only on samples that were left to dry for over 2 hours, and thus were experiencing decreased bonding anyways. To avoid any question, a maximum drying time of about 2 hours should be imposed for device construction, which should provide more than enough time in all applications.

Table 3.9: Effect of water on the bonding of APTMS treated PDMS to SU-8, using the scratch test and three different concentrations of APTMS in toluene

Drying Time	1wt% APTMS		0.5wt% APTMS		0.1wt% APTMS	
	Length of Time Left in Water (days)	Percent Fracture in PDMS Layer	Length of Time Left in Water (days)	Percent Fracture in PDMS Layer	Length of Time Left in Water (days)	Percent Fracture in PDMS Layer
1-2 min	30	95-100	30	95-100	30	95-100
30 min	30	95-100	30	95-100	30	95-100
1 hour	30	95-100	30	95-100	30	95-100
2 hours	30	95-100	30	95-100	30	95-100
4 hours	30	85-95	30	75-85	30	75-85
1 day	<1	40-60	<1	25-40	<1	25-40
2 days	<1	0-10	<1	0-10	<1	0-10
4 days	<1	0-5	<1	0-5	<1	0-5

Pressure driven flow has been a popular method of moving fluids through microfluidic devices, especially microchip-based flow cytometers, as it is not hard to induce and control a pressure drop across a microfluidic channel. Thus the next step was

to ensure the sealing could withstand sufficiently high pressure drops for a wide range of pressure driven flow. To do this, PDMS molds with 16 channels ranging in width from 20-160μm with a depth of 17μm were created and bonded to an SU-8 coated Pyrex substrate. An example device can be seen in figure 3.17 below.

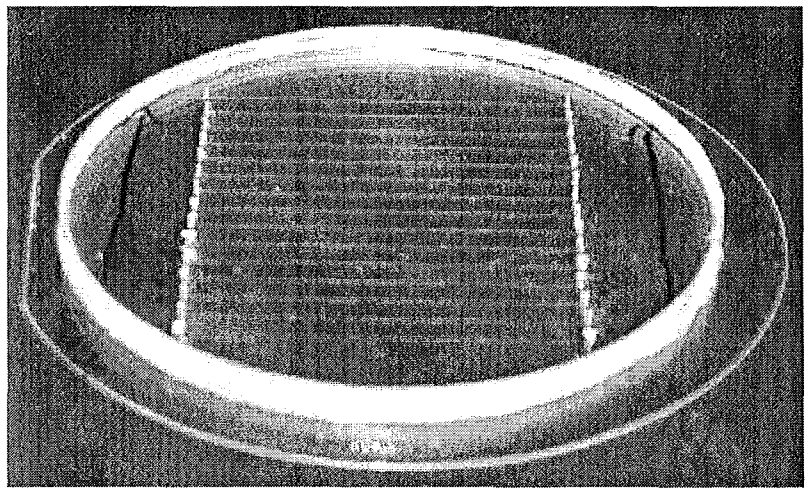

Figure 3.17: APTMS treated PDMS mold with 15 channels ranging from 20-160μm wide with a depth of 17μm bonded to an SU-8 layer on a Pyrex substrate to be used in pressure testing

This device was hooked up to the syringe pump by inserting the fluidic connecting pins into the punched wholes. A thickness of 3mm was used for the PDMS mold and thus buffer pieces of PDMS were not required. In order to convert the flow rate set by the syringe pump into a pressure measurement, the Hagen-Poiseuille equation was rearranged to solve for the pressure drop across the microchannel (ΔP(Pa)) and Dr was determined using the correlation below.

$$\Delta P = \frac{32Q\mu L}{(Dr)^2 wd} \tag{3.3}$$

$$Dr = \frac{2dw}{w+d} \tag{3.4}$$

In this equation, Q was the flow rate set by the syringe pump in μL/hr, μ was the dynamic viscosity of the liquid, water in this case (8.90×10^{-4} Pa·s), L was the length of the channel at 5cm, while w and d were the width, 20-160μm, and depth, 17μm, of the channel respectively. The flow rate through each channel was set, held for two minutes, and gradually increased until some part of the device failed. Summarized results of the tests can be found below in table 3.10.

Table 3.10: Results of pressure testing in 3 different devices with channels of varying width with the point of failure and maximum pressure reached in each case

	1wt% APTMS		0.5wt% APTMS		0.1wt% APTMS	
Channel Width (μm)	Failure Region	Max Pressure (MPa)	Failure Region	Max Pressure (MPa)	Failure Region	Max Pressure (MPa)
20	Inlet Seal	0.62	Inlet Seal	0.58	Inlet Seal	0.60
30	Inlet Seal	0.63	Inlet Seal	0.62	Inlet Seal	0.63
40	Inlet Seal	0.63	Inlet Seal	0.62	Inlet Seal	0.61
50	Inlet Seal	0.54	Inlet Seal	2.22	Inlet Seal	0.65
60	Inlet Seal	0.61	Inlet Seal	0.64	Inlet Seal	0.65
70	Inlet Seal	0.67	Inlet Seal	0.68	Inlet Seal	0.53
80	Inlet Seal	0.67	Inlet Seal	0.66	Inlet Seal	0.66
90	Inlet Seal	0.66	Inlet Seal	0.55	Inlet Seal	0.67
100	Inlet Seal	0.69	Inlet Seal	0.67	Inlet Seal	0.69
110	Inlet Seal	0.68	Inlet Seal	0.69	Inlet Seal	0.85
120	Inlet Seal	0.63	Inlet Seal	0.62	Inlet Seal	0.68
130	Inlet Seal	0.67	Inlet Seal	1.96	Inlet Seal	0.67
140	Inlet Seal	0.69	Inlet Seal	0.69	Inlet Seal	0.69
150	Inlet Seal	0.65	Inlet Seal	0.66	Inlet Seal	0.68
160	Inlet Seal	0.68	Inlet Seal	0.67	Inlet Seal	0.69

Average results were collected from 3 separate devices at each APTMS concentration. Results varied, except for the point of failure, which always appeared at the inlet

connection where the holes in the PDMS had been punched, as this was where the pressure was greatest. Some inlet seals were poorly punched and did not allow for any flow and thus were not included in the averages. From the channels that did provide flow, results suggested a very strong bond between the PDMS and SU-8 and that the punched holes were the weakest point of the device. Most of the inlet connections failed around 0.6-0.7MPa, but some channels managed to maintain a strong seal for pressures up to 2.2MPa before failing at the inlet seal. Furthermore, flow rates used for quality device testing were rarely required to rise above 1000μL/hr, which corresponded to a pressure of about 0.05MPa using our channel dimensions.

The next test was to check the reliability of the test devices. In this case, a flow rate corresponding to 0.5MPa was maintained for a period of 24 hours. It was found that bonding was quite reliable in all channels as they were able to maintain the continuous flow without encountering any failures.

On top of testing pressure in newly fabricated samples, the same pressure tests as described above were performed using testing channels that had been filled with water and soaked in a beaker for a period of 1 month to test the effects of aging. Results showed that there appeared to be no serious effect on the PDMS-SU-8 bond from soaking in water. Again all channels failed at the inlet seal and were able to withstand an average pressure of about 0.6-0.7MPa before failing at the inlet connection.

From the results obtained the bond established between PDMS and SU-8 using APTMS has been shown to be quite strong and robust. In all tests, pressure, reliability and aging, there was not one instance where the bonding between PDMS and SU-8

failed. Furthermore, all of the quality devices created for rigorous optical testing performed by collaborator Benjamin Watts have never experienced any failure in the bonded layer. Most devices last a number of weeks, depending on the type of testing and the amount of tests performed, with any failures occurring at the inlet and sometimes the outlet, seals. These seals can be temporarily fixed using some silicon adhesive around the fluidic connecting pins, but eventually fail again after further testing.

3.1.3 Device Packaging

Device packaging includes the procedures and connections required to make a device fully functional after all construction procedures are complete. These can include cutting or dicing of devices down to an appropriate size or to expose necessary regions, fluidic connections to introduce fluid to the channels and facilitate flow, electrical connections necessary for certain kinds of sensors or data collection, optical connections for light sensing and detecting and many others specific to each device. There were two main packaging steps required before our devices were fully functional and ready for testing. Step one was dicing, necessary to cut the devices to size and expose the waveguide ends for optical connections. Step two was to prepare the device for easy fluidic connections, where fluid could be easily introduced and pumped through the microchannels and swapped out for a different device as necessary. Each step will be discussed in the following sections.

3.1.3.1 Dicing

Dicing the devices was necessary primarily to expose the waveguide ends to allow for easy coupling of light via optical fibers or directly from the laser. The less

space between the two connections meant that there was less light lost as it was transferred from one medium to another. Reduced sizing also allowed the devices to be more manageable during testing. To further improve the optical coupling efficiency, the waveguide ends were polished after dicing using 1μm and 0.3μm polishing paper. Smoothing the surface like this helped lower scattering losses experienced during coupling and increased intensity within the channel as can be seen in figures 3.18 (a) and (b) below.

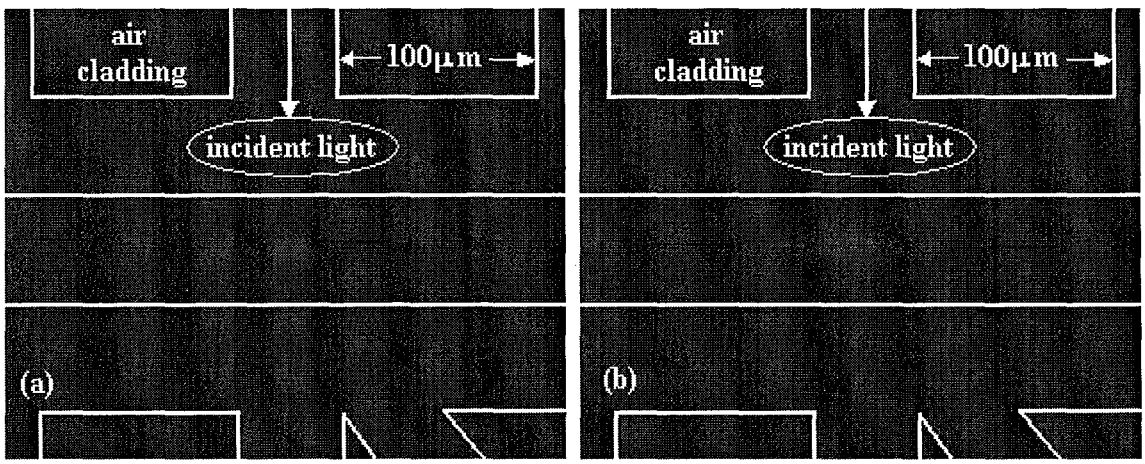

Figure 3.18: Fluorescence in device with sheath flow that (a) does not have a polished waveguide end and (b) has a polished waveguide end

Dicing was performed using a Precision Dicing System made by Kulicke & Soffa, Model 780 which is a wet process, using water to prevent glass particles from entering the air. Initial cuts were made along the designated lines on the wafers, however the process was found to be very harsh causing chipping of the SU-8 film, especially the fragile waveguide tips, as once cured SU-8 is a brittle material. The process also yielded a high amount of dirt and grit along the cut, which could provide problems during bonding of

the PDMS sealing layer and may affect the waveguide performance. Chipping and grit can be seen on a cut device in figure 3.19 below.

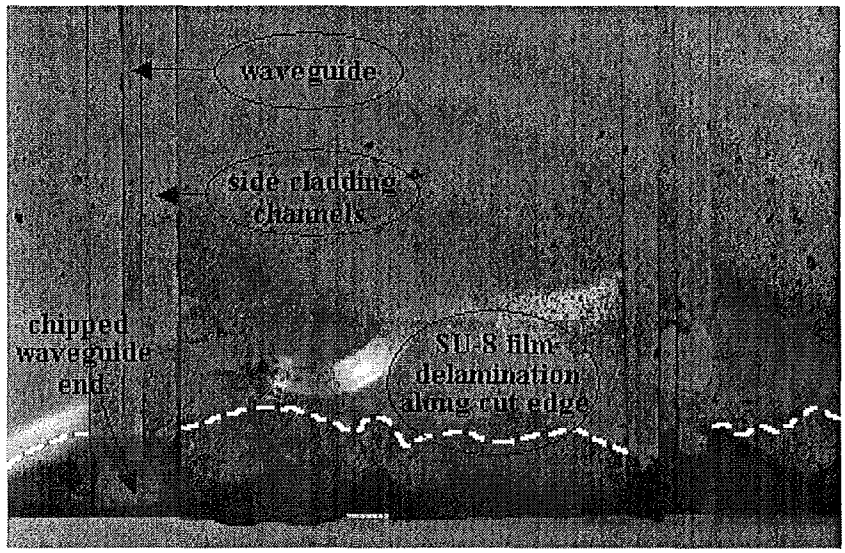

Figure 3.19: Chipping along diced end of a device and high degree of dirt and grit covering the edge of a device with no protection during dicing

Our first attempt to reduce this chipping and high levels of dirt and grit was to seal the device prior to dicing. This method proved to greatly reduce the amount of chipping in the SU-8 layer, however a new set of problems arose. Being an elastomer, the PDMS sealing layer did not cut well and was found to stick to the blade causing a very rough cut along the PDMS edge as seen in figure 3.20. In a few cases, the PDMS was found to rip away with a chunk of SU-8 still bonded to the PDMS. Furthermore, high amounts of dirt and grit became jammed up to about 1 mm within the open side cladding channels around the waveguide core and could not be removed.

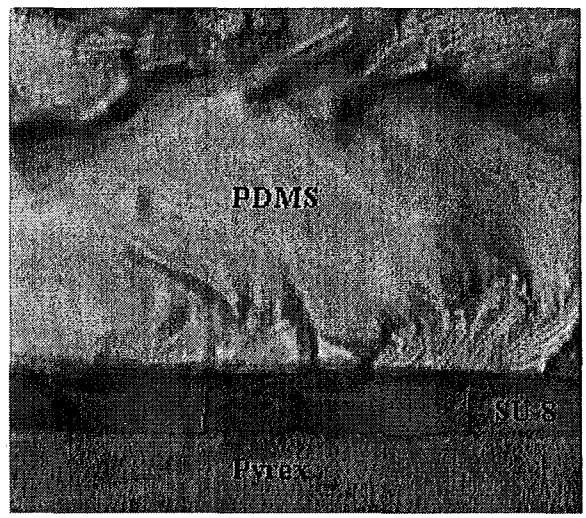

Figure 3.20: Rough PDMS after having been cut with the dicing saw with grit jammed in the side cladding channels

To eliminate the rough cutting with PDMS and grit lodged within the side cladding channels, it was decided to perform dicing with a reversibly bonded layer of PDMS covering the device. This way the PDMS layer could protect the SU-8 against chipping during dicing and be removed after, allowing for the device to be cleaned prior to sealing with a new PDMS layer so as much grit as possible could be removed as seen in figure 3.21 (a) and (b) below. The grit tended to be quite sticky and could not be removed completely in all cases, however the amount remaining did not interfere greatly with waveguide function. Almost all of the grit could be removed from the SU-8 surface ensuring it would not interfere with the bonding of the PDMS sealing layer.

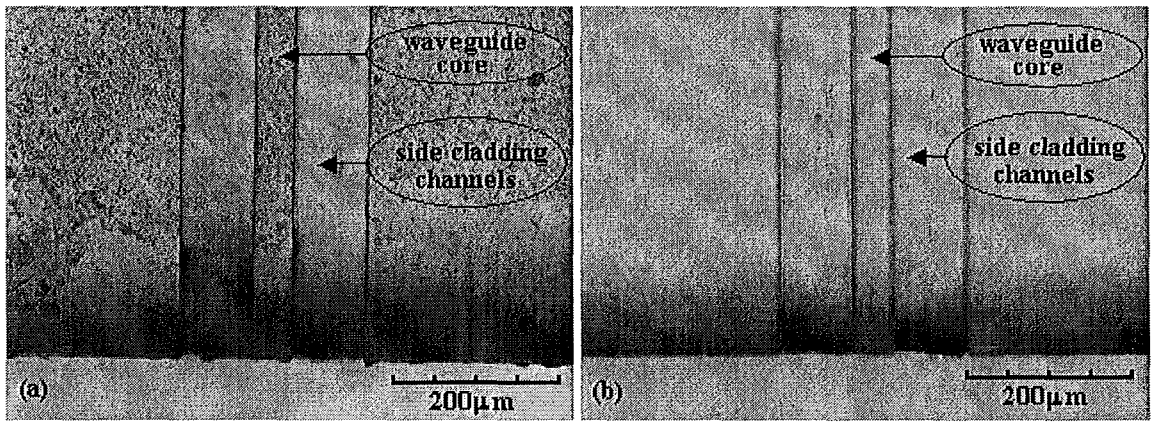

Figure 3.21: Diced device using a reversibly bonded PDMS cover (a) prior to cleaning and (b) after cleaning

Further evidence of the well constructed devices can be seen in figure 3.22 (a) where a length of device has been cut from the circular 4-inch wafer to expose the waveguide ends prior to sealing. In figure 3.22 (b) a side view of this device viewed under a microschope shows the sharp SU-8 edges of the waveguides and structure walls, as well as clean side-cladding channels.

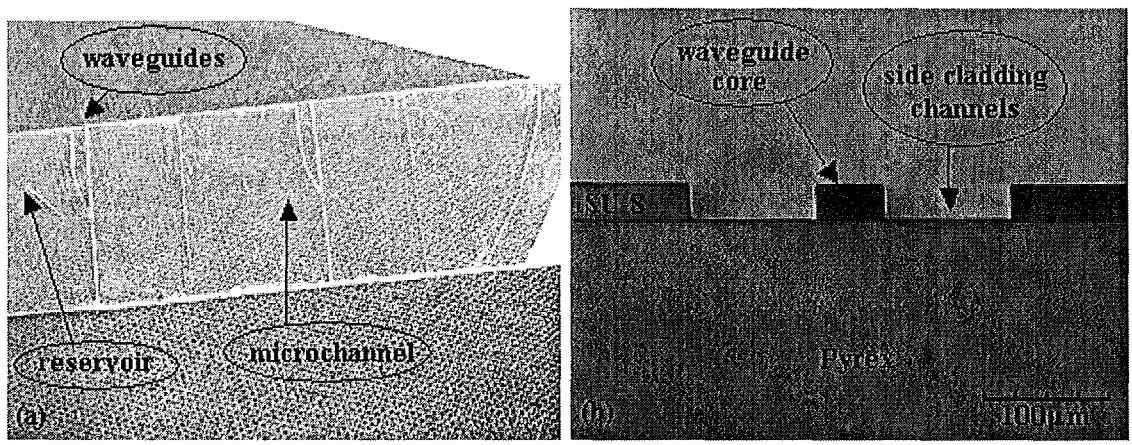

Figure 3.22: Figures of well cut low damage devices with no chipping prior to the bonding of a PDMS sealing layer (a) showing two designs on a strip cut from a 4 inch wafer taken with a camera and (b) showing a side view of a waveguide end after being cut and cleaned with low amounts of grit in the side cladding channels viewed under a microscope

After sealing the device with a new layer of PDMS, excess PDMS could be cut cleanly with a sharp cutting utensil such as a scalpel without affecting the waveguide as seen in figure 3.23. A large difference can be seen in the PDMS layer as opposed to that of figure 3.20.

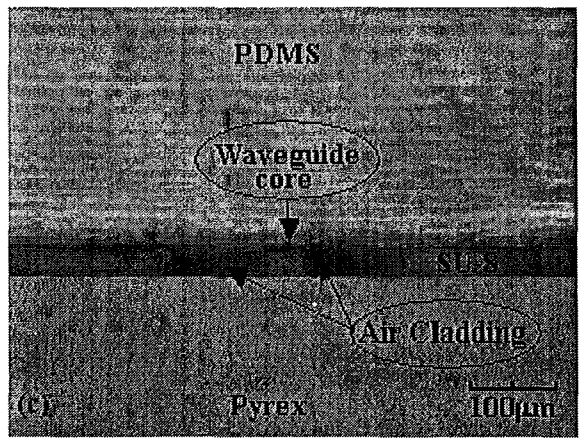

Figure 3.23: Cross-section of diced and sealed device showing an exposed waveguide end and cleanly cut PDMS sealing layer

It was found to be almost impossible to completely reduce the chipping of the SU-8 layer and waveguide cores during dicing, however the incidence of this chipping was greatly reduced. It was also found that the thickness of the intermediate layer used to fabricate the device had an effect on the amount of chipping of the SU-8 layer during dicing procedures and the results are summarized in table 3.13 below. As discussed previously, an intermediate layer thickness of approximately 80nm provided sufficient bonding but with a high degree of cracking prior to dicing, however a high degree of chipping of the SU-8 layer was experienced after dicing. Our lower thickness of at least 186nm was determined to be the minimum thickness to provide low chipping during

dicing and thus produce the highest quality devices. A 600nm intermediate layer was also tested but showed no further improvement.

Table 3.11: Analysis of SU-8 layer bonding during post processing procedures with intermediate layer thicknesses that provided sufficient bonding and low residual material before post processing procedures

		Bonding Before Post Processing Procedures			Bonding After Post Processing Procedures	
Intermediate Layer Thickness (nm)	Residual Material (% of developed area)	Air bubbles (% of film)	Displaced Structures (%)	Cracking (% of film)	Chipping of SU-8 Along Cut (%)	Waveguide ends Damaged (%)
604	0-5	0	0	10	10	0-10
186	0-5	0	0	10	10	0-10
83	0-5	0	0	50	50	50-70

3.1.3.2 Fluidic Connections

Pressure driven flow using a syringe pump was chosen to drive our fluid because several different streams could be connected and controlled separately, as required to provide sheath flow. A syringe would be filled with an appropriate fluid and connected to a rubber tube with a metal connector pin at the other end for connection with the microchip-based device. From this, it was necessary to punch wholes in the PMDS sealing layer prior to bonding with the SU-8 so that the pins could be effectively inserted. Furthermore, the holes needed to be punched in the precise pattern such that they would line up with the small reservoirs fabricated in the SU-8 layer, 1mm in diameter. To make the process easier, the PDMS sealing layer was molded on a silicon master with 3mm diameter reservoirs that could easily be aligned over the SU-8 reservoirs to provide more room for error while punching the holes. It was determined that in order to provide the most efficient optical collections, that the PDMS sealing layer should be as thin as

possible, yet thick enough to allow for a sufficiently large amount of pressure driven flow within the channels. A thickness of 1mm was determined to be acceptable for both conditions. However, this thickness wasn't large enough to insert the connector pins for the reservoir without the pressure forcing them out. In solution to this, about 1mm thick buffer pieces of PDMS were precisely cut and bonded using a silicon adhesive to the PDMS surface over the reservoirs in order to provide a thick layer for the pins to be inserted to for an effective seal while maintaining the thin 1mm thickness in the optical interrogation area. The buffer layers can be seen on a completed device in figure 3.15 (b).

3.2 Device Performance

The following evaluation of device performance provides a small sample of the rigorous testing performed on the quality fabricated devices in order to demonstrate their ability to achieve and perform to the standards outlined by Benjamin Watts. A more detailed report of device testing will be completed in the PhD thesis of Benjamin Watts. As previously discussed, the use of integrated on-chip waveguides imposed stringent requirements on materials selection as the refractive indices of all cladding layers were required to be lower than that of the waveguide core. Thus, many of the main device materials needed to perform two functions, as seen in table 3.14.

Table 3.12: Summary of each materials use in device construction and function as well as their refractive indices.

Material	Device Component	Refractive Index @ 628nm
SU-8 2025	structural layer & waveguide core	1.59
PDMS	sealing layer & uppercladding	1.47
Pyrex	substrate & undercladding	1.45
Air	sidecladding	1.00
SU-8 3000	intermediate layer	1.59

Not only did all materials need to provide acceptable cladding, but they also needed to serve a dual purpose as a strong robust material capable of undergoing rigorous testing. SU-8 2025 was required to act as a strong, inert structural layer for microchannel walls and other device structures while at the same time effectively propagating light to the interrogation point. Furthermore, to help limit scattering losses, fabricated structures required sharp edges as demonstrated in figure 3.10 (b) and 3.22 (b). PDMS had to provide a strong seal for the microchannels, while allowing easy packaging for fluidic connections and to provide an uppercladding layer for the waveguide core. Pyrex needed to provide a strong surface on which to support the device and act as an undercladding layer for the waveguides. Air was easily implemented as sidecladding by fabricating open microchannels around the waveguide core. Lastly the SU-8 3000 intermediate layer was necessary to improve SU-8 2025 bonding to Pyrex but needed to be thin enough not to affect optical function as described above in section 3.1.1.3. These materials produced a powerful multimode waveguide capable of transporting a high number of photons, very

useful for obtaining a strong S/N ratio in microchip-based flow cytometers. All of these components came together to produce a quality photonic integrated microchip-based device as can be seen in figure 3.24 below with the excitation of a fluorescent dye in the microchannel. Devices were also capable of producing sheath flow with fluorescence within the microchannels as seen previously in figures 3.18 (a) and (b).

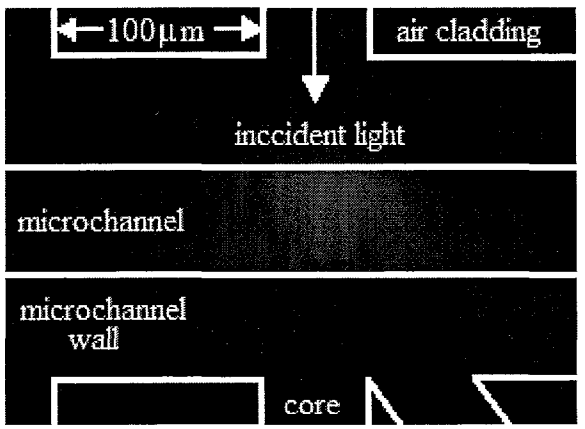

Figure 3.24: Excited fluorescent dye in microchannel excited with a 628nm HeNe laser coupled into the on-chip waveguide seen through a 660nm bandpass filter with the device structures having been drawn on for perspective

Further optical designs by Benjamin Watts focused on integrating lensing systems in the same structural plane as the waveguides and microfluidic channels. These lensing systems would be used to focus light down to different vertical spot sizes in the centre of the microchannel to increase the intensity of light the particles would pass through, thus increasing the number of photons interacting with the cells for a higher S/N ratio. In order to effectively implement these lensing systems, structures needed to be small and compact to fabricate as much as possible on a small surface area, providing better device functionality. Devices were successfully fabricated with structure widths as small as

15μm in some areas and spot sizes as small as 4.5μm were achieved using the developed process described above. Figure 3.25 (a) and (b) show various lens systems used to achieve spot sizes of 35μm and 50μm respectively. As the light moves from one medium to the next (SU-8 to air) the light is refracted and focused. Figures 3.26 shows light from a fabricated waveguide and lens system focused down to about 10μm within the centre of the microchannel.

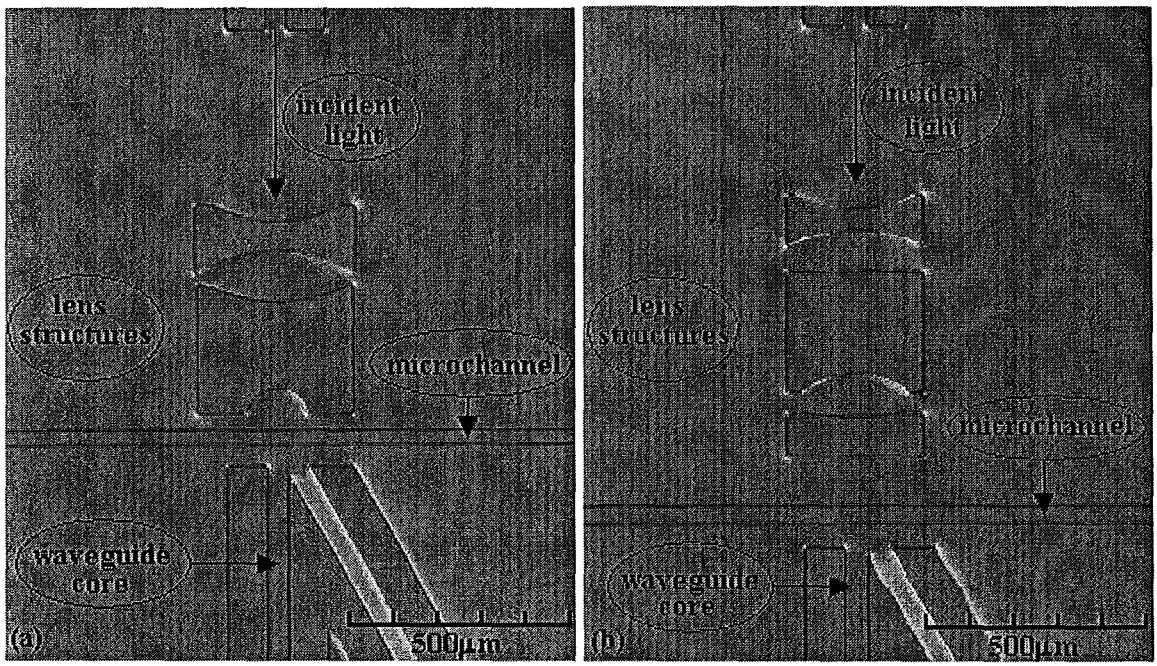

Figure 3.25: Lens systems implemented to achieve a spot size in the middle of the microchannel of (a) 35μm and (b) 50μm

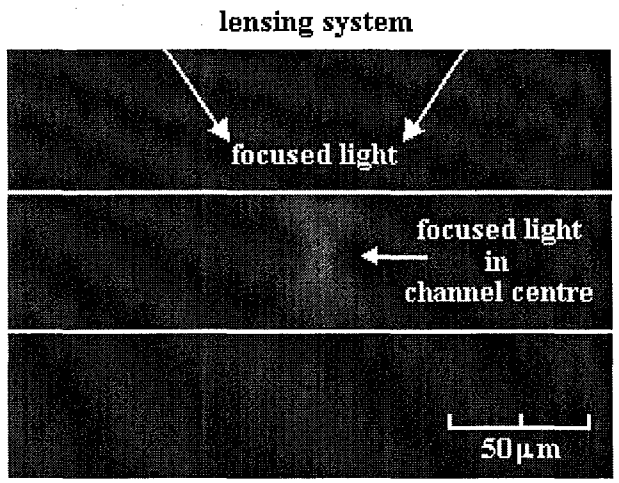

Figure 3.26: Beam focusing down to about 10μm width at the centre of the microchannel

The ability to achieve small compact designs allowed for easier device fabrication, as 10 different devices could be fit on a single four-inch wafer and fabricated simultaneously as seen on the photomask in figure 2.3 (a). Also of note are the curved waveguides in figure 2.3 (b) which were made possible by the highly multimodal characteristics of the waveguides achieved with the relatively high refractive index differences between the core and cladding materials. The highly multimodal signal capable with the fabricated waveguides also provides potential for the collection of a high percentage area of the emitted spherical light, generally side scatter or fluorescent light. Current flow cytometers are capable of collecting around 4% of this spherical area. Optical simulations performed by collaborator Benjamin Watts using the materials used in device construction suggest the potential for collection of 10% of this light, while theoretical calculations suggest that the current design is capable of collecting 3%. All of these specially designed devices can be fabricated using the processes developed in this work.

4 CONCLUSION

The purpose of this study was to develop an effective process for fabricating photonic integrated microchip-based flow cytometers in a planar one shot process based upon optical designs and simulations performed by collaborator Benjamin Watts. Three main areas of processing were focused upon in the study; waveguide and open microfluidic channel fabrication, device sealing and device packaging. An effective procedure to achieve the research objectives was developed and implemented to create quality devices.

4.1 Achievements

An effective method for the easy and reproducible fabrication of quality microchip-based flow cytometers was developed after overcoming technical processing problems. Poor bonding of SU-8 to Pyrex substrates was the main problem facing the fabrication of the devices structural layer. Manipulation of the SU-8 manufacturers processing conditions, mainly the baking times and temperatures and the exposure dose, was found to provide minimal improvement. Any significant increase in bonding resulted in high residual material between device structures that could not be removed. The most effective processing conditions were determined to be a low exposure dose around 225mJ/cm^2, to prevent any residual material formation, and slow heating and cooling at rates of 50°C/hr and 20°C/hr respectively to reduce stresses from thermal expansion mismatches. Surface treatments were utilized to improve chemical bonding between the two materials, and although they provided small improvements to bonding, they were unable to allow for consistent bonding throughout the device. The solution

was to implement a polymer intermediate layer capable of reducing the stresses involved while still being compatible with SU-8 and Pyrex to provide a chemical linkage between the two materials. Specialty SU-8 3000 was determined acceptable and a rough range of 186-600nm was determined to provide good bonding and low residual material using the effective processing conditions previously determined. Unfortunately the intermediate layer had the same refractive index as the structural layer, and thus could allow light to leak out of the waveguide. However, it was shown that the intermediate layer was thin enough such that the optical performance of the device was barely affected.

Irreversible sealing of SU-8 devices with PDMS has not previously been reported, and is an important development for microchip-based devices providing an easy, cheap, efficient and strong method of sealing. In this study we provide an overview of the process conditions and the bond strength as used with microfluidic devices. Residual epoxy molecules were determined to be present on the surface of the SU-8 structural layer, and the most common way to provide a linkage with epoxy molecules was via a polyaddition reaction. Amine groups are commonly used in this reaction for this purpose, and it has previously been shown that the molecule APTMS could be bound to the surface of oxygen treated PDMS sealing layers and the amine groups could subsequently bond with the residual epoxies producing strong covalent bonding. Toluene was determined to be the most acceptable solvent for the process and a concentration of 0.1wt% APTMS was shown to be the lowest concentration for effective bonding. Concentrations of 0.5wt% and 1wt% APTMS in toluene were also tested and provided almost identical results. The process was shown to allow for 2 hours of drying in air for

solvent evaporation and alignment of the sealing layer before the bonding strength began to decrease. Samples were able to last submerged in water for at least 1 month without showing any signs of bond degradation. Testing pressures in the microfluidic channels was unable to break the bond between SU-8 and APTMS treated PDMS as all failures occurred at the inlet fluidic connection in the PDMS layer with most occurring around 0.6-0.7MPa. Some channels maintained a strong inlet seal with pressures up to 2.2MPa within the channels. Further aging tests of 1 month were unable to degrade the bonding and quality microchip-based devices could be easily and reproducibly sealed using this method.

During the rough post processing dicing procedures, it was determined that a layer of PDMS helped reduce chipping of the SU-8 structural layer, and protected it from excessive grit. It was determined that a reversibly bound PDMS layer was more acceptable for the process as it could be removed and the structural layer cleaned prior to device sealing. Furthermore, the minimum intermediate layer thickness of 186nm was shown effective for the rough dicing conditions and the final rough range of 186-600nm for the intermediate layer remained effective in fabricating quality microchip-based flow cytometers.

These procedures allowed for the production of quality devices based upon the optical designs and simulations of collaborator Benjamin Watts. Devices were compact and robust, capable of transporting high powered multimodal light and exciting fluorescence within the microchannels. Furthermore, lensing systems were integrated in the same plane as the waveguides and microchannels, allowing for beam focusing, down

to 4.5μm within the centre of the channel, greatly increasing the intensity at the interrogation point to help provide a high S/N ratio.

4.2 Recommendations

In this study, many problems were experienced with the initial processing to bond SU-8 on Pyrex. The exposure machine necessary for use with four-inch wafers was an older model and may not have been ideally suited for SU-8 processing. More specialized aligners for use with SU-8, generally allowing for a maximum wafer size of three inches, may have provided better processing results, specifically helping to reduce residual material and increasing structure aspect ratios. As design complexity increases and higher functionality is required, it is suggested that higher quality equipment is employed to obtain the small structures and high aspect ratios required.

One obstacle that needed to be overcome in our processing were the rough dicing conditions of the dicing saw available. A dicing process inducing less stress on fabricated wafers could greatly reduce chipping of the SU-8 layer and eliminate much of the dirt and grit. The dirt and grit was especially cumbersome as it was not always possible to remove all of it, resulting in channel clogging rendering some devices useless.

Another area where device improvements could be made is that of the fluidic connections, currently the weakest point during pressure driven flow. For the purposes of this study, the fluidic connections were robust enough to allow for sufficient testing, but as device designs change, a higher pressure flow may be required. Thus a more reliable inlet seal would be necessary. One method to do this may be to permanently attach a fluidic connecting pin to the device via adhesive, strengthening the point of weakness and

attach and remove the fluidic connection at a stronger point, further from the device. However one must be careful to avoid any interference with the interrogation zone for optical analysis.

Ultimately, the success of microchip-based flow cytometers lies in successfully integrating all components, including flow cells, light sources, optics, detectors and electronics and even sorters. Some groups have attempted to achieve this, but with unusable S/N ratios. Here we've focused on improving the interaction of optics with the flow cell in an attempt to provide multiple detection and high S/N ratios. Improvement of the optical design and further testing is necessary to achieve these goals, and is continued by collaborator Benjamin Watts. The processes developed here provide a strong understanding of the processing required allowing for improved optical design to move forward smoothly. Furthermore, these processes can be applied to many other microchip-based devices aiding many others in furthering their research goals.

5 RERENCES

[1] Whitesides GM, "The origins and future of microfluidics", 2006, *Nature*, **442**, 368-373

[2] Fiorini GS, Chiu DT, "Disposable microfluidic devices: fabrication, function, and application", 2005, *BioTechniques*, **38**, 429-446

[3] Verpoote E, De Rooij NF, "Microfluidics Meets MEMS", 2003, *Proceedings of the IEEE*, **91**, NO. 6, 930-953

[4] Sia SK, Whitesides GM, "Microfluidic devices fabricated in poly(dimethylsiloxane) for biological studies", 2003, *Electrophoresis*, **24**, 3563-3576

[5] Terry SC, Jerman JH, Angell JB, "A gas chromatographic air analyzer fabricated on silicon wafer", 1979, *IEEE Trans Electron Devices*, **26**, 1880-1886

[6] Manz A, Graber N, Widmer HM, "Miniaturized total chemical analysis systems: A novel concept for chemical sensing", 1990, *Sensors and Actuators*, **vol. B1**, 244-248

[7] Manz A, Harrison JD, Verpoote EMJ, Fettinger JC, Paulus A, Ludi H, Widmer HM, "Planar chips technology for miniaturization and integration of separation techniques into monitoring systems-Capillary electrophoresis on a chip," 1992, *Journal of Chromatography*, **593**, 253-258

[8] Jacobson SC, Hergenroder R, Koutny LB, Ramsey JM, "High-speed separations on a microchip," 1994, *Analytical Chemistry,* **66**, 1114-1118

[9] Becker H, Gartner C, "Polymer microfabrication technologies for microfluidic systems," 2008, *Analytical and Bioanalytical Chemistry,* **390**, 89-111

[10] Velten T, Ruf HH, Barrow D, Aspragathos N, Lazarou P, Jung E, Malek CK, Richter M, Kruckow J, Wackerle M, "Packaging of Bio-MEMS: Strategies, Technologies, and Applications," 2005, *IEEE Transactions on Advanced Packaging*, **28**, 533-546

[11] Reyes DR, Iossifidis D, Auroux P-A, Manz A, "Micro Total Analysis Systems. 1. Introduction, Theory and Technology", 2002, *Analytical Chemistry*, **74**, 2623-2636

[12] Kelly JJ, Philipsen HGG, "Anisotropy in the wet-etching of semiconductors", 2005, *Current Opinion in Solid State and Materials Science*, **9**, 84-90

[13] Pearton SJ, Ren F, "Science of dry etching of III-V materials", 1994, *Journal of Materials Science: Materials in Electronics,* **5**, 1-12

[14] Becker H, Locascio LE, "Polymer microfluidic devices", 2002, *Talanta*, **56**, 267-287

[15] Xia Y, Whitesides GM, "Soft Lithography", 1998, *Annual Review of Material Science*, **28**, 153-184

[16] Niklaus F, Stemme G, Lu J-Q, Gutmann RJ, "Adhesive wafer bonding", 2006, *Journal of Applied Physics,* **99**, 031101-1 – 031101-28

[17] Tsao C-W, DeVoe DL, "Bonding of thermoplastic polymer microfluidics", 2008, *Microfluidics and Nanofluidics*, **6**, 1-16

[18] Beebe DJ, Mensing GA, Walker GM, "Physics and Applications of Microfluidics in Biology", 2002, *Annual Review of Biomedical Engineering*, **4**, 261-286

[19] Seong GH, Crooks RM, "Efficient Mixing and Reactions within Microfluidic Channels Using Microbead-Supported Catalysts", 2002, *Journal of the American Chemical Society*, **124**, 13360-13361

[20] de Mello A, "On-chip chromatography: the last twenty years", 2002, *Lab-on-a-chip*, **2**, 48N-54N

[21] Harris CM, "Shrinking the LC Landscape", 2003, *Analytical Chemistry*, **75**, 64A-69A

[22] Wu D, Qin J, Lin B, "Electrophoretic separations on microfluidic chips", 2008, *Journal of Chromatography A*, **1184**, 542-559

[23] Sassa F, Morimoto K, Satoh W, Suzuki H, "Electrochemical techniques for microfluidic applications", 2008, *Electrophoresis*, **29**, 1787-1800

[24] Haswell SJ, Skelton V, "Chemical and biochemical microreactors", 2000, *Trends in Analytical Chemistry,* **19**, 389-395

[25] Jensen KF, "Microreaction engineering – is small better?", 2001, *Chemical Engineering Science*, **56**, 293-303

[26] Erickson D, Li D, "Integrated microfluidic devices", 2004, *Analytica Chemica Acta*, **507**, 11-26

[27] Liu J, Enzelberger M, Quake S, "A nanoliter rotary device for polymerase chain reaction", 2002, *Electrophoresis*, **23**, 1531-1536

[28] Lagally ET, Medintz I, Mathies RA, "Single-Molecule DNA Amplification and Analysis in an Integrated Microfluidic Device", 2001, *Analytical Chemistry*, **73**, 565-570

[29] Cokelt GR, Soave R, Pugh G, Rathbun L, "Fabrication of in-vitro microvascular blood-flow systems by photolithography", 1993, *Microvascular Research*, **46**, 394-400

[30] Gifford SC, Frank MG, Derganc J, Gabel C, Austin RH, Yoshida T, Bitensky MW, "Parallel microchannel-based measurements of individual erythrocyte areas and volumes", 2003, Biophysics Journal, **84**, 623-633

[31] Shapiro HM, "Practical Flow Cytometry: 4th edition", 2003, Wiley-Liss, Hoboken, NJ

[32] Gucker FT Jr, O'Konski CT, Pickard HB, Pitts JN Jr, "A photoelectronic counter for colloidal particles", 1947, *Journal of the American Chemical Society*, **69**, 2422-2431

[33] Crossland-Taylor PJ, "A Device for Counting Small Particles Suspended in a Fluid through a Tube",1953, *Nature*, **171**, 37-38

[34] Coulter WH, "High Speed Automatic Blood Cell Counter and Cell Size Analyzer", 1956, *Proceedings of the National Electronics Conference*, **12**, 1034-1042

[35] Herzenberg LA, Parks D, Sahaf B, Perez O, Roederer M, Herzenberg LA, "The History and Future of the Fluorescence Activated Cell Sorter and Flow Cytometry: A View from Stanford",2002, *Clinical Chemistry*, **48**, 1819-1827

[36] Godin J, Chen C-H, Cho SH, Qiao W, Tsai F, Lo Y-H, "Microfluidics and photonics for Bio-System-on-a-Chip: A review of advancements in technology towards a microfluidic flow cytometry chip", 2008, *Journal of Biophotonics*, **1**, No. 5, 355-376

[37] Invitrogen, "http://probes.invitrogen.com/resources/education/tutorials/4Intro_Flow/player.html", accessed March 22, 2008

[38] Baumgarth N, Roederer M, "A practical approach to multicolor flow cytometry for immunophenotyping", 2000, *Journal of Immunological Methods*, **243**, 77-97

[39] Tung JW, Heydari K, Tirouvanziam R, Sahaf B, Parks DR, Herzenberg LA, Herzenberg LA, "Modern Flow Cytometry: A Practical Approach", 2007, *Clinics in Laboratory Medicine,* **27**:453-468

[40] Ateya DA, Erickson JS, Howell PB Jr., Hilliard LR, Golden JP, Ligler FS, "The good, the bad, and the tiny: a review of microflow cytometry", 2008, *Analytical and Bioanalytical Chemistry,* **391**, 1485-1498

[41] Eyal S, Quake SR, "Velocity-independent microfluidic flow cytometry", 2002, *Electrophoresis,* **23**, 2653-2657

[42] Jacobson SC, Ramsey JM, "Electrokinetic Focusing in Microfabricated Channel Structures", 1997, *Analytical Chemistry*, **69**, 3213-3217

[43] Knight, JB, Vishwanath A, Brody JP, Austin RH, "Hydrodynamic Focusing on a Silicon Chip: Mixing Nanoliters in Microseconds", 1998, *Physical Review Letters*, **80**, No.17, 3863-3866

[44] Lee GB, Chang C-C, Huang S-B, Yang R-J, "The hydrodynamic focusing effect inside rectangular microchannels", 2006, *Journal of Micromechanics and Microengineering*, **16**, 1024-1032

[45] Wolff A, Perch-Nielsen IR, Larsen UD, Friis P, Goranovic G, Poulsen CR, Kutter JP, Telleman P, "Integrating advanced functionality in a microfabricated high-throughput fluorescent-activated cell sorter", 2003, *Lab on a Chip*, **3**, 22-27

[46] Chang C-C, Huang Z-X, Yang R-J, "Three-dimensional hydrodynamic focusing in two-layer polydimethyldiloxane (PDMS) microchannels", 2007, *Journal of Micromechanics and Microengineering*, **17**, 1479-1486

[47] Mao X, Waldeisen JR, Huan TJ, " "Microfluidic drifiting"- implementing three-dimensional hydrodynamic focusing with a single-layer planar microfluidic device", 2007, *Lab on a Chip*, **7**, 1260-1262

[48] Novak L, Neuzil P, Pipper J, Zhang Y, Lee S, "An integrated fluorescence detection system for lab-on-a-chip applications", 2007, *Lab-on-a-chip*, **7**, 27-29

[49] Balslev S, Jorgensen AM, Bilenberg B, Mogensen KB, Snakenborg D, Geschke O, Kutter JP, Kristensen A, "Lab-on-a-chip with integrated optical transducers", 2006, *Lab-on-a-chip*, **6**, 213-217

[50] Kuo J-N, Hsieh C-C, Yang S-Y, Lee G-B, "An SU-8 microlens array fabricated by soft replica molding for cell counting applications", 2007, *Journal of Micromechanics and Microengineering,* **17**, 693-699

[51] Fu J-L, Fang Q, Zhang T, Jin X-H, Fang Z-L, "Laser-Induced Fluorescence Detection System for Microfluidic Chips Based on an Orthogonal Optical Arrangement", 2006, *Analytical Chemistry*, **78**, 3827-3834

[52] Hong K-S, Wang J, Sharonov A, Chandra D, Aizenberg J, Yang S, "Tunable microfluidic optical devices with an integrated microlens array", 2006, *Journal of Micromechanics and Microengineering*, **16**, 1660-1666

[53] Shapiro HM, Hercer M, "Flow Cytometers Using Optical Waveguides in Place of Lenses for Specimen Illumination and Light Collection", 1986, *Cytometry*, **7**, 221-223

[54] Wang Z, El-Ali J, Engelund M, Gotsaed T, Perch-Nielsen IR, Mogensen KB, Snakenborg D, Kutter JP, Wolff A, "Measurements of scattered light on a microchip flow cytometer with integrated polymer based optical elements", 2004, *Lab on a Chip*, **4**, 372-377

[55] Lien V, Zhao K, Berdichevsky Y, Lo Y-H, "High-Sensitivity Cytometric Detection Using Fluidic-Photonic Integrated Circuits With Array Waveguides", 2005, *IEEE Journal of Selected Topics in Quantum Electronics*, **11**, 827-834

[56] Irawan R, Tjin SC, Fang X, Fu CY, "Integration of optical fiber light guide, fluorescence detection system, and multichannel disposable microfluidic chip", 2007, *Biomedical Microdevices,* **9**, 413-419

[57] Hubner J, Mogensen KB, Jorgensen AM, Friis P, Telleman P, Kutter JP, "Integrated optical measurement system for fluorescence spectroscopy in microfluidic channels", 2000, *Review of Scientific Instruments*, **72**, 229-233

[58] Tung Y-C, Zhang M, Lin C-T, Kurabayashi K, Skerlos SJ, "PDMS-based opto-fluidic micro flow cytometer with two-color multi-angle fluorescence detection capability using PIN photodiodes", 2004, *Sensors and Actuators B*, **98**, 356-367

[59] Camou S, Fujita H, Fujii T, "PDMS 2D optical lens integrated with microfluidic channels: principle and characterization", 2003, *Lab on a Chip*, **3**, 40-45

[60] Byun I, Kim W, Park S, "A micro flow cell cytometry based on MEMS technologies using silicon and optical fibers", **2003**, *Journal of Materials Science*, **38**, 4603-4605

[61] Chabinyc ML, Chiu DT, McDonald JC, Stroock AD, Christian JF, Karger AM, Whitesides GM, "An Integrated Fluorescence Detection System in Poly(dimethylsiloxane) for Microfluidic Applications", 2001, *Analytical Chemistry*, **73**, 4491-4498

[62] Keiser G "Optical Fiber Communications", 2000, Third Edition, The McGraw Hill Companies, Inc., USA, 32-24

[63] Lien V, Berdichevsky Y, Lo T-H, "A Prealigned Process of Integrating Optical Waveguides With Microfluidic Devices", 2004, *IEEE Photonics Technology Letters*, **16**, No. 6, 1525-1527

[64] Bliss CL, McMullin JN, Backhouse CJ, "Rapid fabrication of a microfluidic device with integrated optical waveguides for DNA fragment analysis", 2007, *Lab on a Chip*, **7**, 1280-1287

[65] Wolfe BD, Conroy RS, Garstecki P, Mayers BT, Fischbach MA, Paul KE, Prentiss M, Whitesides GM, "Dynamic control of liquid-core/liquid-cladding optical waveguides", 2004, *Proceedings of the National Academy of Sciences*, **101,** 12434-12438

[66] Mogensen KB, El-Ali J, Wolff A, Kutter JP, "Integration of polymer waveguides for optical detection in microfabricated chemical analysis systems", 2003, *Applied Optics*, **42**, No. 19, 4072-4079

[67] Fleger M, Neyer A, "PDMS microfluidic chip with integrated waveguides for optical detection", 2006, *Microelectronic Engineering*, **83**, 1291-1293

[68] Seo J, Lee LP, "Disposable integrated microfluidics with self-aligned planar microlenses", 2004, *Sensors and Actuators B*, **99**, 615-622

[69] Bilenberg B, Nielsen T, Clausen B, Kristensen A, "PMMA to SU-8 bonding for polymer based lab-on-a-chip systems with integrated optics", 2004, *Journal of Micromechanics and Microengineering,* **14**, 814-818

[70] Campo A, Greiner C, "SU-8: a photoresist for high-aspect-ratio and 3D submicron lithography", 2007, *Journal of Micromechanics and Microengineering,* **17**, R81-R95

[71] Rahimi A, Gharazi S, Ershad-Langroudi A, Ghasemi D, "Synthesis and Characterization of Hydrophilic Nanocomposite Coating on Glass Substrate", 2006, *Journal of Applied Polymer Science,* **102**, 5322-5329

[72] Carlier J, Chuda K, Arscott S, Thomy V, Verbeke B, Coqueret X, Camart J C, Duron C, Tabourier P, "High pressure-resistant SU-8 microchannels for monolithic porous structure integration", 2006, *Journal of Micromechanics and Microengineering,* **16**, 2211-2219

[73] Microchem Corporation, "OmniCoat", 2008, Newton, Massachusetts, www.microchem.com, accessed September 23, 2008

[74] Carlier J, Arscott S, Thomy V, Fourrier J C, Caron F, Camart J C, Druon C, Tabourier P, "Integrated microfluidics based on mult-layered SU-8 for mass spectrometry analysis", 2004, *Journal of Micromechanics and Microengineering,* **14**, 619-624

[75] Agirregabiria M, Blanco FJ, Berganzo J, Arroyo MT, Fullaondo A, Mayora K, Ruano-Lopez JM, "Fabrication of SU-8 multilayer microstructures based on successive CMOS compatible adhesive bonding and releasing steps", 2005, *Lab on a Chip,* **5** 545-552

[76] Schmidt WF "Mechanical Design Considerations" In. Brown WD (ed) "Advanced Electronic Packaging: With Emphasis on Multichip Modules", 1999, IEEE Press, New York, 241-245

[77] Ng JMK, Gitlin I, Stroock AD, Whitesides GM, "Components for integrated poly(dimethylsiloxane) microfluidic systems", 2002, *Electrophoresis*, **23**, 3463-3473

[78] Zhang Z, Zhao P, Xiao G, "The fabrication of polymer microfluidic devices using a solid-to-solid interfacial polyaddition", 2009, *Polymer*, **50**, 5358-5361

[79] Tanaka Y, Sauer RS in "Epoxy Resins: Chemistry and Technology", 1988, ed. By May CA, Marcek Dekker, Inc., New York, 285

[80] Zammatteo N, Jeanmart L, Hamels S, Courtois S, Louette P, Hevesi L, Remacle J, "Comparison between Different Strategies of Covalent Attachment of DNA to Glass Surfaces to Build DNA Microarrays", 2000, *Analytical Biochemistry,* **280**, 143-150

[81] Sui G, Wang J, Lee C-C, Lu W, Lee SP, Leyton JV, Wu AM, Tseng H-R, "Solution-Phase Surface Modification in Intact Poly(dimethylsiloxane) Microfluidic Channels", 2006, *Analytical Chemistry*, **78**, 5543-5551

[82] Kuznetsov AY, Bagryansky VA, Petrov AK, "The surface relaxation of glow discharge-treated silicone polymer", 1995, *Journal of Applied Polymer Science*, **57**, 201-207

[83] Chauhan AK, Aswal DK, Koiry SP, Gupta SK, Yakhmi JV, Surgers C, Guerin D, Lenfant S, Vuillaume D, "Self-assembly of the 3-aminopropyltrimethoxysilane multilayers on Si and hysteretic current-voltage characteristics", 2008, *Applied Physics A*, 90, 581-589